

Analyzing the Evolution of Graphs and Texts

A Dissertation presented

by

Xingzhi Guo

to

The Graduate School

in Partial Fulfillment of the

Requirements

for the Degree of

Doctor of Philosophy

in

Computer Science

Stony Brook University

May 2023

Stony Brook University

The Graduate School

Xingzhi Guo

We, the dissertation committee for the above candidate for the

Doctor of Philosophy degree, hereby recommend

acceptance of this dissertation

Steven S. Skiena

Distinguished Teaching Professor, Department of Computer Science, Stony Brook University

Nick Nikiforakis

Associate Professor, Department of Computer Science, Stony Brook University

Paul Fodor

Associate Professor of Practice, Department of Computer Science, Stony Brook University

Jason J. Jones

Associate Professor, Department of Sociology, Stony Brook University

This dissertation is accepted by the Graduate School

Celia Marshik

Dean of the Graduate School

Abstract of the Dissertation

Analyzing the Evolution of Graphs and Texts

by

Xingzhi Guo

Doctor of Philosophy

in

Computer Science

Stony Brook University

2023

With the recent advance of representation learning algorithms on graphs (e.g., DeepWalk/GraphSage) and natural languages (e.g., Word2Vec/BERT), the state-of-the-art models can even achieve human-level performance over many downstream tasks, particularly for the task of node and sentence classification. However, most algorithms focus on large-scale models for static graphs and text corpus without considering the inherent dynamic characteristics or discovering the reasons behind the changes.

This dissertation aims to efficiently model the dynamics in graphs (such as social networks and citation graphs) and understand the changes in texts (specifically news titles and personal biographies). To achieve this goal, we utilize the renowned Personalized PageRank algorithm to create effective dynamic network embeddings for evolving graphs. Our proposed approaches significantly improve the running time and accuracy for both detecting network abnormal intruders and discovering entity meaning shifts over large-scale dynamic graphs. For text changes, we analyze the post-publication changes in news titles to understand the intents behind the edits and discuss the potential impact of titles changes from information integrity perspective. Moreover, we investigate self-presented occupational identities in Twitter users' biographies over five years, investigating job prestige and demographics effects in how people disclose jobs, quantifying over-represented jobs and their transitions over time.

Contents

1	Introduction	1
1.1	Word and Graph Embeddings	1
1.1.1	Word Embeddings: Represent words by vectors	1
1.1.2	Graph Embeddings: Represent vertices by vectors	3
1.1.3	Our Motivations	3
1.2	Subset Node Embeddings over Dynamic Graphs	4
1.3	Local Anomaly Detection over Dynamic Graphs	5
1.4	Efficient PPR-based GNN over Dynamic Graphs	6
1.5	Analysis of News Title Changes	6
1.6	Analysis of Biography Changes	7
1.7	List of Publications and Submissions	8
2	Personalized PageRank	10
2.1	Notations	11
2.2	Personalized PageRank Formulation	12
2.3	Approximate PPR using Forward Push Algorithm	13
2.4	Approximate PPR as ℓ_1 Regularized Optimization	14
2.5	Incrementally Maintain PPR	15
3	Subset Node Embeddings over Dynamic Graph	17
3.1	Introduction	18
3.2	Related Work	19
3.3	Preliminaries	21
3.3.1	Dynamic graph model and its embedding	21
3.4	Proposed method	22
3.4.1	Dynamic graph embedding for single batch	22
3.4.2	DYNAMICPPE	26
3.4.3	Complexity analysis	27

3.5	Experiments	27
3.5.1	Datasets	27
3.5.2	Node Classification Task	28
3.5.3	Change Detection	32
3.6	Discussion and Conclusion	34
3.7	Appendix	35
3.7.1	Proof of lemmas	35
3.7.2	Heuristic method: Commute	36
3.7.3	Details of data preprocessing	37
3.7.4	Details of parameter settings	38
3.7.5	Visualizations of Embeddings	38
4	Subset Node Anomaly Detection over Dynamic Graph	41
4.1	Introduction	41
4.2	Related Work	44
4.3	Forward Local Push Algorithm over Weighted Graphs	45
4.4	Problem formulation	46
4.5	The Proposed Framework	47
4.5.1	Maintenance of Dynamic PPVs	48
4.5.2	Anomaly Tracking Framework: DYNANOM	50
4.6	Experiments	53
4.6.1	Datasets	54
4.6.2	Baseline Methods	55
4.6.3	Exp1: Node-level Anomaly Localization	55
4.6.4	Exp2: Graph-level Anomaly Detection	58
4.6.5	Case Study: Localize Changes in Person’s Life over Real World Graph	59
4.7	Discussion and Conclusion	60
4.8	Appendix	61
4.8.1	Proof of Weighted Dynamic Push	61
4.8.2	Proof of Time Complexity	63
4.8.3	Timelines of real world graphs	64
4.8.4	Hyper-parameter Settings	64
4.8.5	Experiment Details	64
5	Efficient Contextual Node Representation Learning over Dy- namic Graphs	67
5.1	Introduction	67

5.2	Related Work	70
5.3	Preliminaries	72
	5.3.1 Message Passing as Approx. Propagation	72
	5.3.2 Calculate PPR as ℓ_1 Regularized Optimization	74
5.4	Problem Definition	74
5.5	Proposed Framework	75
	5.5.1 Maintain PPR in the lens of Optimization	75
	5.5.2 PPR-based Contextual Node Representation and Positional Encodings	76
5.6	Experiments	80
	5.6.1 Experiment Configurations	81
	5.6.2 Efficiency Experiments	82
	5.6.3 Accuracy and Robustness Experiments	84
	5.6.4 Discussions and Future Works	86
5.7	Conclusion	87
5.8	Appendix	87
	5.8.1 Formulate Quadratic Objective from Forward Push	87
	5.8.2 PPV maintenance on dynamic graphs	89
	5.8.3 Dimension Reduction using Random Projection	90
	5.8.4 Experiment Details and Reproducibility	90
	5.8.5 Infrastructure	90
	5.8.6 PPR Implementation	90
	5.8.7 Neural Model Configurations	91
	5.8.8 Reproducibility	91
	5.8.9 Edge event sampling	91
	5.8.10 Extra results	92
6	Post-publication Modification in News Outlets	93
6.1	Introduction	93
6.2	Related Work	95
6.3	Dataset Preparation	96
	6.3.1 News Publisher Identification	96
	6.3.2 Data Collection Infrastructure	97
6.4	Post-Publication Headline Changes	98
	6.4.1 Headline Change Magnitude	99
	6.4.2 Categorization of News Title Changes	103
	6.4.3 News Propagation over Twitter	107
6.5	Conclusion	109

6.6	Discussion	110
6.7	Appendix	111
7	Information and Evolution of Personal Biographies	115
7.1	Introduction	115
7.2	Background and Related Work	118
7.3	Biography Dataset Collection and Pre-processing	119
7.4	Ethical Considerations	122
7.5	Occupations in Twitter Bios	124
	7.5.1 Over/Under-represented Occupations in Twitter Biographies	125
	7.5.2 Social Approval and Demographics in Occupational Identity Establishment	127
7.6	Occupational Identity Evolution	130
	7.6.1 Minor Edits in Biographies	133
	7.6.2 Transitions Between Occupational Identities	133
	7.6.3 Case Study: Transitions in/out Occupational Identities Space amid COVID-19	137
7.7	Conclusions and Future Work	139
7.8	Appendix	140
8	Conclusion and Future Work	145
9	Bibliography	147

Chapter 1

Introduction

1.1 Representation Learning for Languages and Graphs

Modern machine learning techniques rely heavily on dense numerical vectors. Predictive and clustering algorithms, including Support Vector Machines and deep neural networks, operate on low-dimensional vectors that typically range from 60 to 512 dimensions. While image classification models naturally use dense matrices of pixels to represent images, discrete symbols, such as English words and graph vertices, present a more challenging problem. Unlike images that can be directly digitized by camera sensors, languages and graphs are constructed from discrete symbols, which makes it difficult to directly capture using low-dimensional vectors.

In recent years, there has been significant progress in the field of natural language processing (NLP) and graph representation learning, which involves learning meaningful and low-dimensional dense vector representations of words and vertices. These vector representations are useful for a variety of NLP tasks as well as graph tasks, such as sentiment analysis, text summarization, node classification and link prediction. We briefly introduce the two seminal works in word and node embeddings as follows.

1.1.1 Word Embeddings: Represent words by vectors

The advent of Word2Vec[116] has brought about significant advancements in artificial intelligence, specifically in the area of language embeddings or word embeddings. Word embeddings involve assigning a discrete symbolic unit (such

as an English word) to a low-dimensional space that typically ranges from 60 to 300 dimensions. The aim is to ensure that vectors that are closely located in this space share similar semantic meanings.

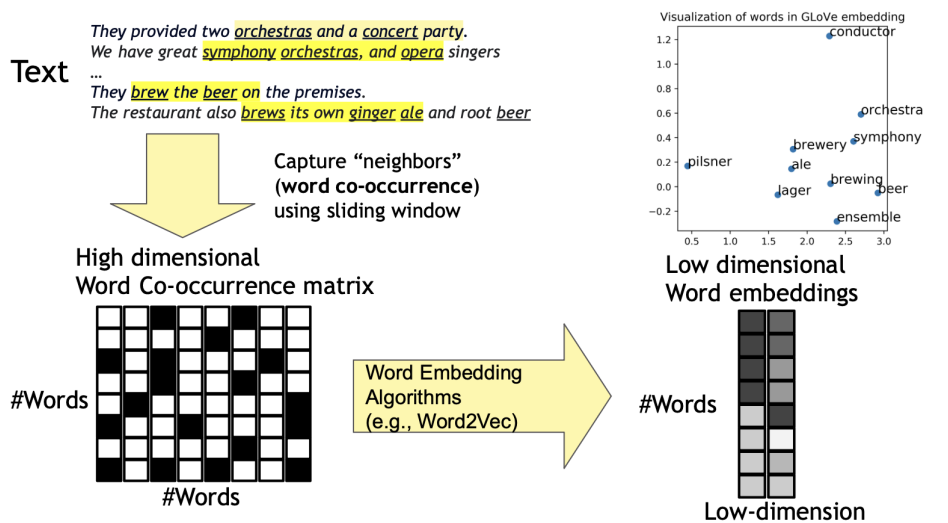


Figure 1.1: The illustration of word embedding algorithms.

Word embeddings preserve the human-sense of lexical meaning within the low-dimensional vector. This property makes them useful for many downstream NLP tasks, such as sentiment classification and textual entailment prediction, which can be tackled with human-level performance. This is particularly true after pre-training large language models such as BERT or GPT.

Word embeddings can be formulated in two stages, as illustrated in Figure 1.1. The first stage, used in Word2Vec, involves counting which words are near or co-occurred with the center word within a fixed context length (e.g., 5 words from its left and right). The resulting co-occurrence matrix is large, with a size square of the vocabulary, and sparse. In the second stage, several self-supervised tasks are created to pre-train the neural network, leading to the low-dimensional word vectors for predicting context words given the center word (Skip-gram) or vice versa (Continuous bag-of-words). In practice, these word embeddings demonstrate superior performance for a wide range of NLP tasks, from word similarity measurement to sentence sentiment classification.

1.1.2 Graph Embeddings: Represent vertices by vectors

Network or graph embeddings are a concept that is similar to word embeddings. It involves representing discrete vertices using low-dimensional vectors. The seminal network embedding algorithm, DeepWalk [126], proposed a wise problem formulation that converted a graph into node sequences path by random walk, thereby leading the graph learning community into the deep learning era.

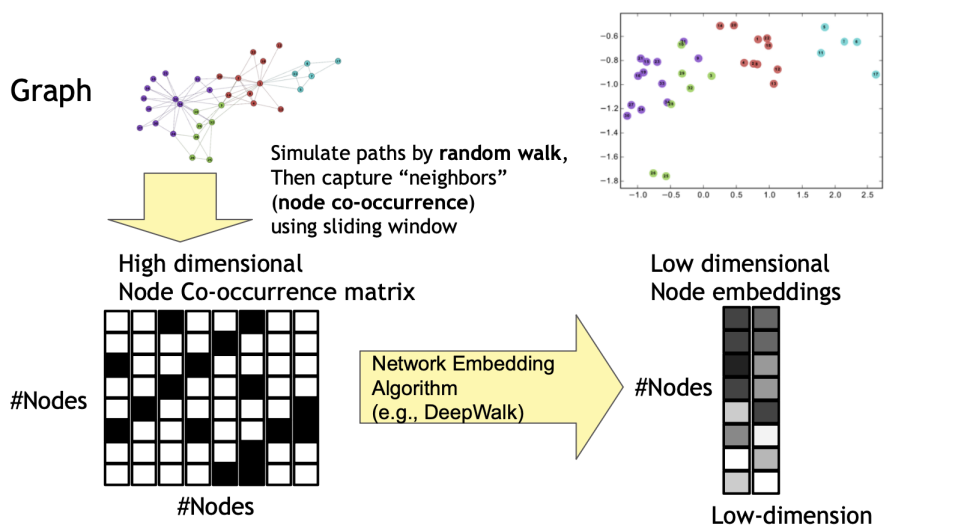


Figure 1.2: The illustration of network embeddings.

As illustrated in Figure 1.2, DeepWalk utilizes random walk starting from each vertex to sample paths, where each path ends with a fixed walk length (e.g., 80 vertices) and simulates "sentences" consisting of vertices. Afterwards, the same processes are applied as in Word2Vec with context length and self-supervised pre-training. The resulting node embeddings are practically useful for many graph tasks, such as node classification and missing link prediction.

1.1.3 Our Motivations

The aforementioned graph algorithms only focus on static graphs, while real-world graphs are highly dynamic, with structural changes occurring over time. For instance, Wikipedia volunteers tirelessly update Wiki articles, as well as hyperlinks, to reflect the latest events that happen every day. However, most network

embedding algorithms were designed for static graphs and cannot efficiently adapt to the dynamic graph’s changing structure.

Moreover, real-world graphs are usually massive, with millions of nodes, while real-world applications often focus on a few thousand nodes for clustering or prediction. Most embedding algorithms, such as DeepWalk, have to calculate whole embeddings but only use a small subset of them, which is computationally inefficient or even prohibited given the graph’s large scale. Based on these two observations, we are motivated to propose three efficient graph learning frameworks, specifically for dynamic subset node embeddings.

Meanwhile, we are interested in understanding the expected and unexpected changes in texts. For example, we have monitored news headlines on major U.S. news outlets and discovered post-publication headline changes. Moreover, we have analyzed the changes in Twitter user biographies over six years to study the evolution of self-identity over time. Unlike conventional NLP tasks that predict labels given benchmarks, our aim is to utilize the latest NLP techniques to gain societal insights by examining text changes.

In the following sections, we introduce our proposed dynamic graph embedding algorithms, their extensions for graph anomaly detection applications, and an efficient graph neural network framework. Additionally, we present our studies on changing text in online news headlines and personal biographies.

1.2 Subset Node Embeddings over Dynamic Graph

Dynamic graph representation learning is a task to learn node embeddings over dynamic networks, and has many important applications, including knowledge graphs, citation networks to social networks. Graphs of this type are usually large-scale but only a small subset of vertices are related in downstream tasks. Current methods are too expensive to this setting as the complexity is at best linear-dependent on both the number of nodes and edges.

In Chapter 3 , we propose a new method, namely Dynamic Personalized PageRank Embedding (DYNAMICPPE) for learning a target subset of node representations over large-scale dynamic networks. Based on recent advances in local node embedding and a novel computation of dynamic personalized PageRank vector (PPV), DYNAMICPPE has two key ingredients: 1) the per-PPV complexity is $\mathcal{O}(m\bar{d}/\epsilon)$ where m, \bar{d} , and ϵ are the number of edges received, average degree, global precision error respectively. Thus, the per-edge event update of a single node is only dependent on \bar{d} in average; and 2) by using these high quality PPVs

and hash kernels, the learned embeddings have properties of both locality and global consistency. These two make it possible to capture the evolution of graph structure effectively. Experimental results demonstrate both the effectiveness and efficiency of the proposed method over large-scale dynamic networks. We apply DYNAMICPPE to capture the embedding change of Chinese cities in the Wikipedia graph during this ongoing COVID-19 pandemic ¹. Our results show that these representations successfully encode the dynamics of the Wikipedia graph.

1.3 Subset Node Anomaly Detection over Dynamic Graph

Tracking a targeted subset of nodes in an evolving graph is important for many real-world applications. Existing methods typically focus on identifying anomalous edges or finding anomaly graph snapshots in a stream way. However, edge-oriented methods cannot quantify how individual nodes change over time while others need to maintain representations of the whole graph all time, thus computationally inefficient.

Chapter 4 proposes DYNANOM, an efficient framework to quantify the changes and localize per-node anomalies over large dynamic weighted-graphs. Thanks to recent advances in dynamic representation learning based on Personalized PageRank, DYNANOM is 1) *efficient*: the time complexity is linear to the number of edge events and independent on node size of the input graph; 2) *effective*: DYNANOM can successfully track topological changes reflecting real-world anomaly; 3) *flexible*: different type of anomaly score functions can be defined for various applications. Experiments demonstrate these properties on both benchmark graph datasets and a new large real-world dynamic graph. Specifically, an instantiation method based on DYNANOM achieves the accuracy of 0.5425 compared with 0.2790, the best baseline, on the task of node-level anomaly localization while running 2.3 times faster than the baseline. We present a real-world case study and further demonstrate the usability of DYNANOM for anomaly discovery over large-scale graphs.

¹https://en.wikipedia.org/wiki/COVID-19_pandemic

1.4 Efficient Contextual Node Representation Learning over Dynamic Graphs

Real-world graphs grow rapidly with edge and vertex insertions over time, motivating the problem of efficiently maintaining robust node representation over evolving graphs. Recent efficient GNNs are designed to decouple recursive message passing from the learning process, and favor Personalized PageRank (PPR) as the underlying feature propagation mechanism. However, most PPR-based GNNs are designed for static graphs, and efficient PPR maintenance remains as an open problem. Further, there is surprisingly little theoretical justification for the choice of PPR, despite its impressive empirical performance.

In Chapter 5, we are inspired by the recent PPR formulation as an explicit ℓ_1 -regularized optimization problem and propose a unified dynamic graph learning framework based on sparse node-wise attention. We also present a set of desired properties to justify the choice of PPR in STOA GNNs, and serves as the guideline for future node attention designs. Meanwhile, we take advantage of the PPR-equivalent optimization formulation and employ the proximal gradient method (ISTA) to improve the efficiency of PPR-based GNNs by 2-5 times. Finally, we instantiate a simple-yet-effective model (GOPPE) with robust positional encodings by maximizing PPR previously used as attention. The model performs comparably to or better than the STOA baselines and greatly outperforms when the initial node attributes are noisy during graph evolution, demonstrating the effectiveness and robustness of GOPPE.

1.5 Post-publication Modification in News Headlines

Digital media (including websites and online social networks) facilitate the broadcasting of news via flexible and personalized channels. Unlike conventional newspapers which become “read-only” upon publication, online news sources are free to arbitrarily modify news headlines *after* their initial release. The motivation, frequency, and effect of post-publication headline changes are largely unknown, with no offline equivalent from where researchers can draw parallels.

In Chapter 6, we collect and analyze over 41K pairs of altered news headlines by tracking ~ 411 K articles from major US news agencies over a six month period (March to September 2021), identifying that 7.5% articles have at least one

post-publication headline edit with a wide range of types, from minor updates, to complete rewrites. We characterize the frequency with which headlines are modified and whether certain outlets are more likely to be engaging in post-publication headline changes than others. We discover that 49.7% of changes go beyond minor spelling or grammar corrections, with 23.13% of those resulting in drastically disparate information conveyed to readers. Finally, to better understand the interaction between post-publication headline edits and social media, we conduct a temporal analysis of news popularity on Twitter. We find that an effective headline post-publication edit should occur within the first ten hours after the initial release to ensure that the previous, potentially misleading, information does not fully propagate over the social network.

1.6 Information and Evolution of Personal Biographies

Occupational identity concerns the self-image of an individual’s affinities and socioeconomic class, and directs how a person should behave in certain ways. Understanding the establishment of occupational identity is important to study work-related behaviors. However, large-scale quantitative studies of occupational identity are difficult to perform due to its indirect observable nature. But profile biographies on social media contain concise yet rich descriptions about self-identity. Analysis of these self-descriptions provides powerful insights concerning how people see themselves and how they change over time.

In this paper, we present and analyze a longitudinal corpus recording the self-authored public biographies of 51.18 million Twitter users as they evolve over a six-year period from 2015-2021. In particular, we investigate the demographics and social approval (e.g., job prestige and salary) effects in how people self-disclose occupational identities, quantifying over-represented occupations as well as the occupational transitions w.r.t. job prestige over time. We show that males are more likely to define themselves by their occupations than females do, and that self-reported jobs and job transitions are biased toward more prestigious occupations. We also present an intriguing case study about how self-reported jobs changed amid COVID-19 and the subsequent "*Great Resignation*" trend with the latest full year data in 2022. These results demonstrate that social media biographies are a rich source of data for quantitative social science studies, allowing unobtrusive observation of the intersections and transitions obtained in online self-presentation.

1.7 List of Publications and Submissions

Published

1. Giorgian Borca-Tasciuc, **Xingzhi Guo**, Stanley Bak, and Steven Skiena. "Provable Fairness for Neural Network Models using Formal Verification", *European Workshop on Algorithmic Fairness (EWAFA 2023)*, Extended abstract [24].
2. Zhuoyi Lin, Lei Feng, **Xingzhi Guo**, Rui Yin, Chee Keong Kwoh, and Chi Xu. COMET: Convolutional Dimension Interaction for Deep Matrix Factorization. In, *ACM Transactions on Intelligent Systems and Technology (TIST), 2023* [108]
3. **Xingzhi Guo**, Baojian Zhou, and Steven Skiena. Subset Node Anomaly Tracking over Large Dynamic Graphs. In *Proceedings of the 28th ACM SIGKDD Conference on Knowledge Discovery & Data Mining (KDD '22)*., New York, NY, USA.[73]
4. **Xingzhi Guo**, Brian Kondracki, Nick Nikiforakis, and Steven Skiena. 2022. Verba Volant, Scripta Volant: Understanding Post-publication Title Changes in News Outlets. In *Proceedings of the ACM Web Conference 2022 (WWW '22)*. ACM, New York, NY, USA. [71]
5. Syed Fahad Sultan, **Xingzhi Guo**, and Steven Skiena. 2022. Low-dimensional genotype embeddings for predictive models. In *Proceedings of the 13th ACM International Conference on Bioinformatics, Computational Biology and Health Informatics (BCB '22)*, ACM, New York, NY, USA, Article 52. [154]
6. **Xingzhi Guo**, Baojian Zhou, and Steven Skiena. 2021. Subset Node Representation Learning over Large Dynamic Graphs. In *Proceedings of the 27th ACM SIGKDD Conference on Knowledge Discovery & Data Mining (KDD '21)*. ACM, New York, NY, USA. [29]
7. K. Gillespie, I. C. Konstantakopoulos, **X. Guo**, V. T. Vasudevan and A. Sethy, "Improving Device Directedness Classification of Utterances With Semantic Lexical Features," *ICASSP 2020 - 2020 IEEE International Conference on Acoustics, Speech and Signal Processing (ICASSP)*, 2020. [56]

In Submission

1. **Xingzhi Guo**, Baojian Zhou, and Steven Skiena. Efficient Contextual Node Representation Learning over Dynamic Graphs.
2. Zhen Chen, **Xingzhi Guo**, Baojian Zhou, Deqing Yang, and Steven Skiena, Accelerating Personalized PageRank Vector Computation. [29]
3. **Xingzhi Guo**, Dakota Handzlik, Jason J. Jones, and Steven Skiena. Biographies and Their Evolution: Occupational Identities over Twitter.[74]
4. **Xingzhi Guo** and Steven Skiena. Hierarchies over Vector Space: Orienting Word and Graph Embeddings. [67]
5. **Xingzhi Guo**, Baojian Zhou, Haochen Chen, Sergiy Verstyuk, and Steven Skiena. Why Do Embedding Spaces Look as They do?

Chapter 2

Personalized PageRank

Personalized PageRank (PPR) [123] is a renowned algorithm that forms the foundation of the proposed algorithms in this thesis. In this section, we present the standard notations and preliminaries to provide an overview of the recent advancements and the current state-of-the-art PPR research.

PageRank is an algorithm used to measure the centrality of nodes in a graph. This algorithm was developed by Google to measure the importance of web pages and to improve their search engine results. The PageRank of a node is calculated by measuring the probability of landing on that node during a random walk on the graph. Figure 2.1 illustrates an example of PageRank in the left subfigure where node 1 is the most important nodes of high PageRank value.

Personalized PageRank is an extension of the PageRank algorithm that is used to measure the importance of nodes in a graph relative to a particular starting node. In other words, it measures the centrality of nodes in an "ego net" around a starting node. An ego net is a sub-graph that consists of a focal node (the starting node) and its neighbors. To calculate PPR, one starts with a random walk on the graph, beginning at the focal node (or starting node). However, to prevent the walk from getting away from the local area, the algorithm also includes a probability of randomly jumping back to the starting node. This ensures that the algorithm explores the entire graph while still focusing on the ego net around the starting node. Likewise, the PPR value of a node is calculated by measuring the probability of landing on that node during this modified random walk.

In Figure 2.1 (right), we illustrate the PPR values given the starting node is node 7. Compare to PageRank, although the graph structure is the same, The PPR values are significantly different from PageRank as it favors the nodes around the starting node 7.

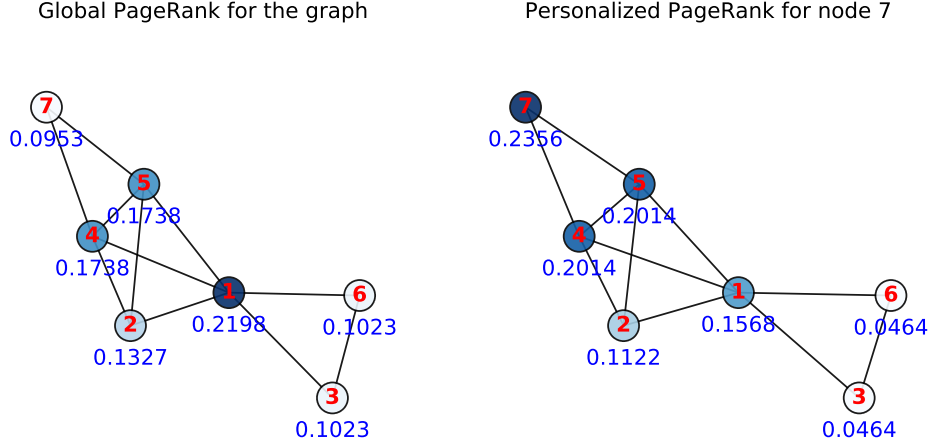


Figure 2.1: The example of global PageRank (Left) and Personalized PageRank for node 7 (Right). Their PageRank values are below the nodes and colored blue. Personalized PageRank measures the neighbor importance given one starting node, while Global PageRank measures the overall importance of nodes.

Typically, PPR can be solved analytically using linear algebra and power iteration method. However, these algorithms can be computationally expensive on large graphs. Therefore, various approximation techniques have been developed to compute the PPR more efficiently. These techniques include using a algorithmic local forward push operations to approximate PPR and utilizing numerical optimization techniques to solve a PPR-equivalent optimization problem. In the subsequent sections, we will present a formal discussion of the PPR definition and its approximation methods.

2.1 Notations

We use bold capitalized letter (e.g. \mathbf{A} and \mathbf{X}) to represent matrices and bold lower letters for vectors (e.g., \mathbf{a} and \mathbf{x}). Let $\mathcal{G}(\mathcal{V}, \mathcal{E}, \mathcal{W}, \mathbf{X})$ be a directed weighted-graph where $\mathcal{V} = \{1, 2, \dots, n\}$ is the node set, $\mathcal{E} \subseteq \mathcal{V} \times \mathcal{V}$ is the set of edges, and \mathcal{W} is corresponding edge weights of \mathcal{E} . If presented, $\mathbf{X} \in \mathbb{R}^{d \times |\mathcal{V}|}$ is the nodes' d -dim raw attributes or features. For each node v , $\text{Nei}_{out}(v)$ stands for out-neighbors of v . For all $v \in \mathcal{V}$, the generalized out-degree vector of \mathcal{V} is \mathbf{d} where v -th entry $d(v) \triangleq \sum_{u \in \text{Nei}(v)} w_{(v,u)}$ and $w_{(v,u)}$ could be the weight of edge (v,u) in graph \mathcal{G} .

The generalized degree matrix is then denoted as $\mathbf{D} := \text{diag}(\mathbf{d})$ and the adjacency matrix is written as \mathbf{A} with $\mathbf{A}(u,v) = w_{(u,v)}$. To simplify our notation, we use $d(i)$ or d_i to denote the degree of node i . Let $\mathbf{P} = \mathbf{D}^{-1}\mathbf{A}$ be the random walk matrix and then $\mathbf{P}^\top = \mathbf{A}^\top \mathbf{D}^{-1}$ is the column stochastic matrix.

2.2 Personalized PageRank Formulation

As a measure of the relative importance among nodes, Personalized PageRank (PPR), a generalized version of original PageRank [123], plays an important role in many graph mining tasks. In this thesis, most proposed algorithms are built on PPR. Specifically, the Personalized PageRank vector (PPV) of a node s in \mathcal{G} is defined as the following:

Definition 1 (Personalized PageRank Vector (PPV)). *Given a graph $\mathcal{G}(\mathcal{V}, \mathcal{E}, \mathcal{W})$ with $|\mathcal{V}| = n$ and $|\mathcal{E}| = m$. Define the lazy random walk transition matrix $\mathbf{P} \triangleq (1-\beta)\mathbf{D}^{-1}\mathbf{A} + \beta\mathbf{I}_n$, $\beta \in [0,1)$ where \mathbf{D} is the generalized degree matrix and \mathbf{A} is the adjacency matrix of \mathcal{G} .¹ Given teleport probability $\alpha \in [0,1)$ and the source node s , the Personalized PageRank vector of s is defined as:*

$$\boldsymbol{\pi}_{\alpha,s} = (1-\alpha)\mathbf{P}^\top \boldsymbol{\pi}_{\alpha,s} + \alpha\mathbf{1}_s, \quad (2.1)$$

where the teleport probability α is a small constant (e.g. $\alpha = .15$), and $\mathbf{1}_s$ is an indicator vector of node s , that is, s -th entry is 1, 0 otherwise. We simply denote PPV of s as $\boldsymbol{\pi}_s$.

Clearly, $\boldsymbol{\pi}_s$ can be calculated in a closed form, i.e., $\boldsymbol{\pi}_s = \alpha(\mathbf{I}_n - (1-\alpha)\mathbf{P}^\top)^{-1}\mathbf{1}_s$ but with time complexity $\mathcal{O}(n^3)$. The most commonly used method is *Power Iteration* [123], which approximates $\boldsymbol{\pi}_s$ iteratively: $\boldsymbol{\pi}_s^{(t)} = (1-\alpha)\mathbf{P}^\top \boldsymbol{\pi}_s^{(t-1)} + \alpha\mathbf{1}_s$. After $t = \lceil \log_{1-\alpha} \epsilon \rceil$ iterations, one can achieve $\|\boldsymbol{\pi}_s - \boldsymbol{\pi}_s^{(t)}\|_1 \leq \epsilon$. Hence, the overall time complexity of power iteration is $\mathcal{O}(m \log_{1-\alpha} \epsilon)$ with $\mathcal{O}(m)$ memory requirement. However, the per-iteration of the power iteration needs to access the whole graph which is time-consuming. Even worse, it is unclear how one can efficiently use power-iteration to obtain an updated $\boldsymbol{\pi}_s$ from \mathcal{G}_t to \mathcal{G}_{t+1} . Other types of PPR can be found in [172, 176, 182] and references therein.

¹Our PPV is defined based on the lazy random walk transition matrix. This definition is equivalent to the one using $\mathbf{D}^{-1}\mathbf{A}$ but with a different parameter α . Without loss of generality, we use $\beta=0$ throughout the paper.

2.3 Approximate PPR using Forward Push Algorithm

forward push algorithm [9], a.k.a. the bookmark-coloring algorithm [15], approximates $\pi_s(v)$ locally via an approximate $p_s(v)$. The key idea is to maintain solution vector \mathbf{p}_s and a residual vector \mathbf{r}_s (at the initial $\mathbf{r}_s = \mathbf{1}_s, \mathbf{p}_s = \mathbf{0}$).

Algorithm 1 FORWARDLOCALPUSH [194]

```

1: Input:  $\mathbf{p}_s, \mathbf{r}_s, \mathcal{G}, \epsilon, \beta = 0$ 
2: while  $\exists u, r_s(u) > \epsilon d(u)$  do
3:   PUSH( $u$ )
4: while  $\exists u, r_s(u) < -\epsilon d(u)$  do
5:   PUSH( $u$ )
6: return  $(\mathbf{p}_s, \mathbf{r}_s)$ 
7: procedure PUSH( $u$ )
8:    $p_s(u) += \alpha r_s(u)$ 
9:   for  $v \in \text{Nei}(u)$  do
10:     $r_s(v) += (1 - \alpha)r_s(u)(1 - \beta)/d(u)$ 
11:     $r_s(u) = (1 - \alpha)r_s(u)\beta$ 

```

Algorithm 1 is a generalization from Andersen et al. [9] and there are several variants of forward push [9, 15, 111], which are dependent on how β is chosen (we assume $\beta = 0$). The essential idea of forward push is that, at each PUSH step, the frontier node u transforms her α residual probability $r_s(u)$ into estimation probability $p_s(u)$ and then pushes the rest residual to its neighbors. The algorithm repeats this push operation until all residuals are small enough². Methods based on local push operations have the following invariant property.

Lemma 2 (Invariant property [83]). *FORWARDLOCALPUSH has the following invariant property*

$$\pi_s(u) = p_s(u) + \sum_{v \in V} r_s(v) \pi_v(u), \forall u \in \mathcal{V}. \quad (2.2)$$

²There are two implementation of forward push depends on how frontier is selected. One is to use a first-in-first-out (FIFO) queue [57] to maintain the frontiers while the other one maintains nodes using a priority queue is used [15] so that the operation cost is $\mathcal{O}(1/\epsilon\alpha)$ instead of $\mathcal{O}(\log n/\epsilon\alpha)$.

The local push algorithm can guarantee that the each entry of the estimation vector $p_s(v)$ is very close to the true value $\pi_s(v)$. We state this property as in the following

Lemma 3 (Approximation error and time complexity [9, 194]). *Given any graph $\mathcal{G}(\mathcal{V}, \mathcal{E})$ with $\mathbf{p}_s = \mathbf{0}, \mathbf{r}_s = \mathbf{1}_s$ and a constant ϵ , the run time for FORWARDLOCAL-PUSH is at most $\frac{1 - \|\mathbf{r}_s\|_1}{\alpha \epsilon}$ and the estimation error of $\pi_s(v)$ for each node v is at most ϵ , i.e. $|p_s(v) - \pi_s(v)|/d(v) \leq \epsilon$.*

2.4 Approximate PPR as ℓ_1 Regularized Optimization

Interestingly, recent research [51, 52] discovered that Algorithm 1 is equivalent to the Coordinate Descent algorithm, which solves an explicit optimization problem. Furthermore, with the specific termination condition, a ℓ_1 -regularized quadratic objective function has been proposed as the alternative PPR formulation (Lemma 4).

Lemma 4 (Variational Formulation of Personalized PageRank). *Solving PPR in Equ.2.1 is equivalent to solving the following ℓ_1 -regularized quadratic objective function where the PPR vector $\boldsymbol{\pi} := \mathbf{D}^{1/2} \mathbf{x}^*$:*

$$\mathbf{x}^* = \underset{\mathbf{x}}{\operatorname{argmin}} f(\mathbf{x}) := \underbrace{\frac{1}{2} \mathbf{x}^\top \mathbf{W} \mathbf{x} + \mathbf{x}^\top \mathbf{b}}_{g(\mathbf{x})} + \underbrace{\epsilon \|\mathbf{D}^{1/2} \mathbf{x}\|_1}_{h(\mathbf{x})}, \text{ where} \quad (2.3)$$

$$\mathbf{W} = \mathbf{D}^{-1/2} (\mathbf{D} - (1 - \alpha) \mathbf{A}) \mathbf{D}^{-1/2}, \mathbf{b} = -\alpha \mathbf{D}^{-1/2} \mathbf{e}_s$$

We present the proof details in Appendix 5.8.1.

Lemma 4 provides a unique perspective to understand PPR and tackle it with intensively studied optimization methods for the ℓ_1 -regularization problem, specifically proximal gradient methods such as ISTA and FISTA.

ISTA Solver for PPR: Equ.2.3 has the composition of a smooth function $g(\mathbf{x})$ and a non-smooth function $h(\mathbf{x})$, Note that

$$\nabla^2 g(\mathbf{x}) = \mathbf{W} = \alpha \mathbf{I}_n + (1 - \alpha) \underbrace{(\mathbf{I}_n - \mathbf{D}^{-1/2} \mathbf{A} \mathbf{D}^{-1/2})}_{\text{Normalized Laplacian of } \lambda_{max} \leq 2},$$

where λ_{max} is the largest eigenvalue. With $\|\nabla^2 g(\mathbf{x})\|_2 \leq 2 - \alpha$, let $\eta = \frac{1}{2 - \alpha}$, one can convert the original optimization problem (Equ.2.3) into proximal form using the second-order approximation:

$$\mathbf{x}^{(k+1)} = \text{PROX}_{h(\cdot)}(\mathbf{x}^{(k)} - \eta \nabla_i f(\mathbf{x}^{(k)})), \text{ where}$$

$$\text{PROX}_{h(\cdot)}(\mathbf{z}) = \underset{\mathbf{x}}{\text{argmin}} \frac{1}{2\eta} \|\mathbf{x} - \mathbf{z}\|_2^2 + h(\mathbf{x})$$

To this end, we can apply the Proximal Gradient Descent algorithm, specifically ISTA (Algorithm 2) to solve this well-defined PPR-equivalent ℓ_1 -regularized optimization problem.

Algorithm 2 ISTA SOLVER FOR PPR-EQUIVALENT OPTIMIZATION

- 1: **Input:** $k=0, \mathbf{x}^{(0)} = \mathbf{0}, \mathcal{G}, \epsilon, \alpha$
- 2: $\nabla f(\mathbf{x}^{(0)}) = -\alpha \mathbf{D}^{-1/2} \mathbf{e}_s$
- 3: $\eta = \frac{1}{2 - \alpha}$
- 4: **while** $\mathbf{x}^{(k)}$ has not converged yet **do**
- 5: $\mathbf{z}^{(k)}(i) := \mathbf{x}^{(k)}(i) - \eta \nabla_i f(\mathbf{x}^{(k)})$
- 6: $\mathbf{x}^{(k+1)}(i) = \text{PROX}_{h(\cdot)}(\mathbf{z}^{(k)}(i))$ can be solved analytically:

$$\mathbf{x}^{(k+1)}(i) = \begin{cases} \mathbf{z}^k(i) - \epsilon' d(i)^{1/2}, & \text{if } \mathbf{z}^k(i) > \epsilon d(i)^{1/2} \\ 0, & \text{if } \|\mathbf{z}^k(i)\|_1 \leq \epsilon' d(i)^{1/2} \\ \mathbf{z}^k(i) + \epsilon' d(i)^{1/2}, & \text{if } \mathbf{z}^k(i) < -\epsilon d(i)^{1/2} \end{cases}$$

- 7: **return** $(\mathbf{x}^{(k)}, \nabla f(\mathbf{x}^{(k)}))$
 - 8: //Note that PPR vector $\boldsymbol{\pi} = \mathbf{D}^{1/2} \mathbf{x}^{(k)}, \mathbf{r} = \mathbf{D}^{1/2} \nabla f(\mathbf{x}^{(k)})$
-

2.5 Incrementally Maintain PPR

For a dynamic graph, the graph snapshot at time t is denoted as $\mathcal{G}^t(\mathcal{V}^t, \mathcal{E}^t, \mathcal{W}^t, \mathbf{X}^{(t)})$. The notation (subscript for time t) are used for other graph attributes. For instance, if there is no ambiguity, the degree of a node u can be denoted as $d_u^{(t)}$ or $d^t u$.

To maintain the PPVs (PPR Vectors) for a dynamic graph, the naive approach is to recalculate the PPVs from scratch. However, this approach comes at the cost of a significant computational budget. Interestingly, Zhang et al. [194] proposed

a novel updating strategy for calculating dynamic PPVs. Given a new edge $e_{u,v}$ with $d^{t+1}(u) = d^t(u) + 1$ at time $t+1$, the PPR adjustments are :

$$\boldsymbol{\pi}^{t+1}(u) = \boldsymbol{\pi}^t(u) * \frac{d^t(u)+1}{d^t(u)}, \quad \boldsymbol{r}^{t+1}(u) = \boldsymbol{r}^t(u) - \frac{\boldsymbol{\pi}^t(u)}{\alpha d^t(u)}, \quad \boldsymbol{r}^{t+1}(v) = \boldsymbol{r}^t(v) + \frac{1-\alpha}{\alpha} \frac{\boldsymbol{\pi}^t(u)}{d^t(u)}$$

However, the original update of per-edge event strategy proposed in [194] is not suitable for batch update between graph snapshots. Guo et al. [66] propose to use a batch strategy, which is more practical in real-world scenario where there is a sequence of edge events between two consecutive snapshots. This motivates us to develop a new algorithms for dynamic PPVs and then use these PPVs to obtain high quality dynamic embedding vectors. In Chapter 3, 4, 5 we present our efficient algorithms that build upon the key preliminaries discussed above.

Chapter 3

Subset Node

Embeddings over Dynamic Graph ¹

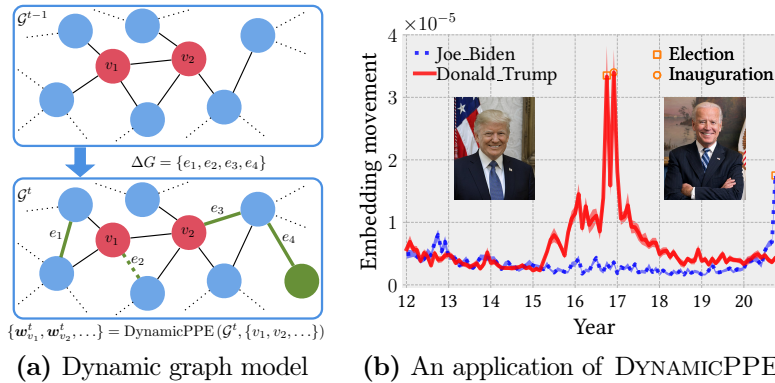


Figure 3.1: (a) The model of dynamic network in two consecutive snapshots. (b) An application of DYNAMICPPE to keep track embedding movements of interesting Wikipedia articles (vertices). We learn embeddings of two presidents of the United States on the whole English Wikipedia graph from 2012 monthly, which cumulatively involves 6.2M articles (nodes) and 170M internal links (edges). The *embedding movement* between two time points is defined as $1 - \cos(\mathbf{w}_v^t, \mathbf{w}_v^{t+1})$ where $\cos(\cdot, \cdot)$ is the cosine similarity. The significant embedding movements may reflect big social status changes of Donald_Trump and Joe_Biden ²in this dynamic Wikipedia graph.

¹Xingzhi Guo, Baojian Zhou, and Steven Skiena. 2021. Subset Node Representation Learning over Large Dynamic Graphs. In *Proceedings of the 27th ACM SIGKDD Conference on Knowledge Discovery & Data Mining (KDD '21)*. Association for Computing Machinery, New York, NY, USA, 516–526. <https://doi.org/10.1145/3447548.3467393> [70]

3.1 Introduction

Graph node representation learning aims to represent nodes from graph structure data into lower dimensional vectors and has received much attention in recent years [65, 78, 79, 102, 126, 140, 159]. Effective methods have been successfully applied to many real-world applications where graphs are large-scale and static [188]. However, networks such as social networks [14], knowledge graphs [90, 174, 175, 175], and citation networks [36] are usually time-evolving where edges and nodes are inserted or deleted over time. Computing representations of all vertices over time is prohibitively expensive because only a small subset of nodes may be interesting in a particular application. Therefore, it is important and technical challenging to efficiently learn dynamic embeddings for these large-scale dynamic networks under this typical use case.

Specifically, we study the following dynamic embedding problem: We are given a subset $S = \{v_1, v_2, \dots, v_k\}$ and an initial graph \mathcal{G}^t with $t=0$. Between time t and $t+1$, there are edge events of insertions and/or deletions. The task is to design an algorithm to learn embeddings for k nodes with time complexity independent on the number of nodes n per time t where $k \ll n$. This problem setting is both technically challenging and practically important. For example, in the English Wikipedia graph, one needs focus only on embedding movements of articles related to political leaders, a tiny portion of the whole Wikipedia. Current dynamic embedding methods [45, 120, 200, 205, 207] are not applicable to this large-scale problem setting due to the lack of efficiency. More specifically, current methods have the *dependence issue* where one must learn all embedding vectors. This dependence issue leads to per-embedding update is linear-dependent on n , which is inefficient when graphs are large-scale. This obstacle motivates us to develop a new method.

In this paper, we propose a dynamic personalized PageRank embedding (DYNAMICPPE) method for learning a subset of node representations over large-sale dynamic networks. DYNAMICPPE is based on an effective approach to compute dynamic PPVs [194]. There are two challenges of using Zhang et al. [194] directly: 1) the quality of dynamic PPVs depends critically on precision parameter ϵ , which unfortunately is unknown under the dynamic setting; and 2) The update of per-edge event strategy is not suitable for batch update between graph snapshots. To resolve these two difficulties, first, we adaptively update ϵ so that the *estimation error* is independent of n, m , thus obtaining high-quality PPVs. Yet previous work

²Two English Wikipedia articles are accessible at https://en.wikipedia.org/wiki/Donald_Trump and https://en.wikipedia.org/wiki/Joe_Biden.

does not give an estimation error guarantee. We prove that the time complexity is only dependent on \bar{d} . Second, we incorporate a batch update strategy inspired from [66] to avoid frequent per-edge update. Therefore, the total run time to keep track of k nodes for given snapshots is $\mathcal{O}(k\bar{d}m)$. Since real-world graphs have the sparsity property $\bar{d} \ll n$, it significantly improves the efficiency compared with previous methods. Inspired by *InstantEmbedding* [128] for static graph, we use hash kernels to project dynamic PPVs into embedding space. Figure 3.1 shows an example of successfully applying DYNAMICPPE to study the dynamics of social status in the English Wikipedia graph. To summarize, our contributions are:

1. We propose a new algorithm DYNAMICPPE, which is based on the recent advances of local network embedding on static graph and a novel computation of dynamic PPVs. DYNAMICPPE effectively learns PPVs and then projects them into embedding space using hash kernels.
2. DYNAMICPPE adaptively updates the precision parameter ϵ so that PPVs always have a provable estimation error guarantee. In our subset problem setting, we prove that the time and space complexity are all linear to the number of edges m but independent on the number of nodes n , thus significantly improving the efficiency.
3. Node classification results demonstrate the effectiveness and efficiency of the proposed. We compile three large-scale datasets to validate our method. As an application, we showcase that learned embeddings can be used to detect the changes of Chinese cities during this ongoing COVID-19 pandemic articles on a large-scale English Wikipedia.

The rest of this paper is organized as follows: In Section 5.2, we give the overview of current dynamic embedding methods. The problem definition and preliminaries are in Section 3.3. We present our proposed method in Section 3.4. Experimental results are reported in Section 4.6. The discussion and conclusion will be presented in Section 6.5. Our code and created datasets are accessible at <https://github.com/zjlxgz/DynamicPPE>.

3.2 Related Work

There are two main categories of works for learning embeddings from the dynamic graph structure data. The first type is focusing on capturing the evolution of

dynamics of graph structure [205]. The second type is focusing on both dynamics of graph structure and features that lie in these graph data [160]. In this paper, we focus on the first type and give an overview of related works. Due to the large amount of work in this area, some related works may not be included, one can find more related works in a survey [96] and references therein.

Dynamic latent space models The dynamic embedding models had been initially explored by using latent space model [82]. The dynamic latent space model of a network makes an assumption that each node is associated with an d -dimensional vector and distance between two vectors should be small if there is an edge between these two nodes [143, 144]. Works of these assume that the distance between two consecutive embeddings should be small. The proposed dynamic models were applied to different applications [81, 145]. Their methods are not scalable from the fact that the time complexity of initial position estimation is at least $\mathcal{O}(n^2)$ even if the per-node update is $\log(n)$.

Incremental SVD and random walk based methods Zhang et al. [201] proposed TIMERS that is an incremental SVD-based method. To prevent the error accumulation, TIMERS properly set the restart time so that the accumulated error can be reduced. Nguyen et al. [120] proposed continuous-time dynamic network embeddings, namely CTDNE. The key idea of CTDNE is that instead of using general random walks as DeepWalk [126], it uses temporal random walks containing a sequence of edges in order. Similarly, the work of Du et al. [45] was also based on the idea of DeepWalk. These methods have time complexity dependent on n for per-snapshot update. Zhou et al. [205] proposed to learn dynamic embeddings by modeling the triadic closure to capture the dynamics.

Graph neural network methods Trivedi et al. [160] designed a dynamic node representation model, namely DYREP, as modeling a latent mediation process where it leverages the changes of node between the node’s social interactions and its neighborhoods. More specifically, DYREP contains a temporal attention layer to capture the interactions of neighbors. Zang and Wang [192] proposed a neural network model to learn embeddings by solving a differential equation with ReLU as its activation function. [105] presents a dynamic embedding, a recurrent neural network method, to learn the interactions between users and items. However, these methods either need to have features as input or cannot be applied to large-scale dynamic graph. Kumar et al. [105] proposed an algorithm to learn the trajectory of the dynamic embedding for temporal interaction networks. Since the learning task is different from ours, one can find more details in their paper.

3.3 Preliminaries

Notations for dynamic graphs We use $[n]$ to denote a ground set $[n] := \{0, 1, \dots, n-1\}$. The graph snapshot at time t is denoted as $\mathcal{G}^t(\mathcal{V}^t, \mathcal{E}^t)$. More specifically, the embedding vector for node v at time t denoted as $\mathbf{w}_v^t \in \mathbb{R}^d$ and d is the embedding dimension. The i -th entry of \mathbf{w}_v^t is $w_v^t(i) \in \mathbb{R}$. The embedding of node v for all T snapshots is written as $\mathbf{W}_v = [\mathbf{w}_v^1, \mathbf{w}_v^2, \dots, \mathbf{w}_v^T]^\top$. We use n_t and m_t as the number of nodes and edges in \mathcal{G}^t which we simply use n and m if time t is clear in the context.

Given the graph snapshot \mathcal{G}^t and a specific node v , the personalized PageRank vector (PPV) is an n -dimensional vector $\boldsymbol{\pi}_v^t \in \mathbb{R}^n$ and the corresponding i -th entry is $\pi_v^t(i)$. We use $\mathbf{p}_v^t \in \mathbb{R}^n$ to stand for a calculated PPV obtained from a specific algorithm. Similarly, the corresponding i -th entry is $p_v^t(i)$. The teleport probability of the PageRank is denoted as α . The *estimation error* of an embedding vector is the difference between true embedding \mathbf{w}_v^t and the estimated embedding $\hat{\mathbf{w}}_v^t$, is measure by $\|\cdot\|_1 := \sum_{i=1}^n |w_v^t(i) - \hat{w}_v^t(i)|$.

3.3.1 Dynamic graph model and its embedding

Given any initial graph (could be an empty graph), the corresponding dynamic graph model describes how the graph structure evolves over time. We first define the dynamic graph model, which is based on Kazemi and Goel [96].

Definition 5 (Simple dynamic graph model [96]). *A simple dynamic graph model is defined as an ordered of snapshots $\mathcal{G}^0, \mathcal{G}^1, \mathcal{G}^2, \dots, \mathcal{G}^T$ where \mathcal{G}^0 is the initial graph. The difference of graph \mathcal{G}^t at time $t=1, 2, \dots, T$ is $\Delta \mathcal{G}^t(\Delta \mathcal{V}^t, \Delta \mathcal{E}^t) := \mathcal{G}^t \setminus \mathcal{G}^{t-1}$ with $\Delta \mathcal{V}^t := \mathcal{V}^t \setminus \mathcal{V}^{t-1}$ and $\Delta \mathcal{E}^t := \mathcal{E}^t \setminus \mathcal{E}^{t-1}$. Equivalently, $\Delta \mathcal{G}^t$ corresponds to a sequence of edge events as the following*

$$\Delta \mathcal{G}^t = \{e_1^t, e_2^t, \dots, e_{m'}^t\}, \quad (3.1)$$

where each edge event e_i^t has two types: insertion or deletion, i.e., $e_i^t = (u, v, \text{event})$ where $\text{event} \in \{\text{Insert}, \text{Delete}\}$ ³.

The above model captures the evolution of a real-world graph naturally where the structure evolution can be treated as a sequence of edge events occurred in this graph. To simplify our analysis, we assume that the graph is undirected. Based on this, we define the subset dynamic representation problem as the following.

³The node insertion can be treated as inserting a new edge and then delete it and node deletion is a sequence of deleting its edges.

Definition 6 (Subset dynamic network embedding problem). *Given a dynamic network model $\{\mathcal{G}^0, \mathcal{G}^1, \mathcal{G}^2, \dots, \mathcal{G}^T\}$ define in Definition 5 and a subset of target nodes $S = \{v_1, v_2, \dots, v_k\}$, the subset dynamic network embedding problem is to learn dynamic embeddings of T snapshots for all k nodes S where $k \ll n$. That is, given any node $v \in S$, the goal is to learn embedding matrix for each node $v \in S$, i.e.*

$$\mathbf{W}_v := [\mathbf{w}_v^1, \mathbf{w}_v^2, \dots, \mathbf{w}_v^T]^\top \text{ where } \mathbf{w}_v^t \in \mathbb{R}^d \text{ and } v \in S. \quad (3.2)$$

3.4 Proposed method

To obtain dynamic embedding vectors, the general idea is to obtain dynamic PPVs and then project these PPVs into embedding space by using two kernel functions [128, 177]. In this section, we present our proposed method DYNAMICPPE where it contains two main components: 1) an adaptive precision strategy to control the estimation error of PPVs. We then prove that the time complexity of this dynamic strategy is still independent on n . With this quality guarantee, learned PPVs will be used as proximity vectors and be "projected" into lower dimensional space based on ideas of *Verse* [161] and *InstantEmbedding* [128]. We first show how can we get high quality PPVs and then present how use PPVs to obtain dynamic embeddings. Finally, we give the complexity analysis.

3.4.1 Dynamic graph embedding for single batch

For each batch update ΔG^t , the key idea is to dynamically maintain PPVs where the algorithm updates the estimate from \mathbf{p}_v^{t-1} to \mathbf{p}_v^t and its residuals from \mathbf{r}_v^{t-1} to \mathbf{r}_v^t . Our method is inspired from Guo et al. [66] where they proposed to update a personalized contribution vector by using the local reverse push⁴. The proposed dynamic single node embedding, DYNAMICSNE is illustrated in Algorithm 3. It takes an update batch $\Delta \mathcal{G}^t$ (a sequence of edge events), a target node s with a precision ϵ^t , estimation vector of s and residual vector as inputs. It then obtains an updated embedding vector of s by the following three steps: 1) It first updates the estimate vector \mathbf{p}_s^t and \mathbf{r}_s^t from Line 2 to Line 9; 2) It then calls the forward local push method to obtain the updated estimations, \mathbf{p}_s^t ; 3) We then use the hash kernel projection

⁴One should notice that, for undirected graph, PPVs can be calculated by using the invariant property from the contribution vectors. However, the invariant property does not hold for directed graph. It means that one cannot use reverse local push to get a personalized PageRank vector directly. In this sense, using forward push algorithm is more general for our problem setting.

step to get an updated embedding. This projection step is from *InstantEmbedding* where two universal hash functions are defined as $h_d: \mathbb{N} \rightarrow [d]$ and $h_{\text{sgn}}: \mathbb{N} \rightarrow \{\pm 1\}$ ⁵. Then the hash kernel based on these two hash functions is defined as $H_{h_{\text{sgn}}, h_d}(\mathbf{x}): \mathbb{R}^n \rightarrow \mathbb{R}^d$ where each entity i is $\sum_{j \in h_d^{-1}(i)} x_j h_{\text{sgn}}(j)$. Different from random projection used in RandNE [200] and FastRP [28], hash functions has $\mathcal{O}(1)$ memory cost while random projection based method has $\mathcal{O}(dn)$ if the Gaussian matrix is used. Furthermore, hash kernel keeps unbiased estimator for the inner product [177].

In the rest of this section, we show that the time complexity is $\mathcal{O}(m\bar{d}/\epsilon)$ in average and the estimation error of learned PPVs measure by $\|\cdot\|_1$ can also be bounded. Our proof is based on the following lemma which follows from Guo et al. [66], Zhang et al. [194].

Lemma 7. *Given current graph \mathcal{G}^t and an update batch $\Delta\mathcal{G}^t$, the total run time of the dynamic single node embedding, DYNAMICSNE for obtaining embedding \mathbf{w}_s^t is bounded by the following*

$$T_t \leq \frac{\|\mathbf{r}_s^{t-1}\|_1 - \|\mathbf{r}_s^t\|_1}{\alpha\epsilon^t} + \sum_{u \in \Delta\mathcal{G}^t} \frac{2-\alpha}{\alpha} \frac{p_s^{t-1}(u)}{d(u)} \quad (3.3)$$

Proof. We first make an assumption that there is only one edge update (u, v, event) in $\Delta\mathcal{G}^t$, then based Lemma 14 of [195], the run time of per-edge update is at most:

$$\frac{\|\mathbf{r}_s^{t-1}\|_1 - \|\mathbf{r}_s^t\|_1}{\alpha\epsilon^t} + \frac{\Delta_t(s)}{\alpha\epsilon^t}, \quad (3.4)$$

where $\Delta_t(s) = \frac{2-\alpha}{\alpha} \frac{p_s^{t-1}(u)}{d(u)}$. Suppose there are k edge events in $\Delta\mathcal{G}^t$. We still obtain a similar bound, by the fact that forward push algorithm has monotonicity property: the entries of estimates $p_s^t(v)$ only increase when it pushes positive residuals (Line 2 and 3 of Algorithm 1). Similarly, estimates $p_s^t(v)$ only decrease when it pushes negative residuals (Line 4 and 5 of Algorithm 1). In other words, the amount of work for per-edge update is not less than the amount of work for per-batch update. Similar idea is also used in [66]. \square

⁵For example, in our implementation, we use MurmurHash <https://github.com/aappleby/smhasher>

Algorithm 3 DYNAMICSNE($\mathcal{G}^t, \Delta\mathcal{G}^t, s, \mathbf{p}_s^{t-1}, \mathbf{r}_s^{t-1}, \epsilon^t, \alpha$)

- 1: **Input:** graph $\mathcal{G}^t, \Delta\mathcal{G}^t$, target node s , precision ϵ , teleport α
 - 2: **for** $(u, v, \text{op}) \in \Delta\mathcal{G}^t$ **do**
 - 3: **if** $\text{op} == \text{INSERT}(u, v)$ **then**
 - 4: $\Delta_p = p_s^{t-1}(u) / (d(u)^t - 1)$
 - 5: **if** $\text{op} == \text{DELETE}(u, v)$ **then**
 - 6: $\Delta_p = -p_s^{t-1}(u) / (d(u)^t + 1)$
 - 7: $p_s^{t-1}(u) \leftarrow p_s^{t-1}(u) + \Delta_p$
 - 8: $r_s^{t-1}(u) \leftarrow r_s^{t-1}(u) - \Delta_p / \alpha$
 - 9: $r_s^{t-1}(v) \leftarrow r_s^{t-1}(v) + \Delta_p / \alpha - \Delta_p$
 - 10: $\mathbf{p}_s^t = \text{FORWARDPUSH}(\mathbf{p}_s^{t-1}, \mathbf{r}_s^{t-1}, \mathcal{G}^t, \epsilon^t, \alpha)$
 - 11: $\mathbf{w}_s^t = \mathbf{0}$
 - 12: **for** $i \in \{v : p_s^t(v) \neq 0, v \in \mathcal{V}^t\}$ **do**
 - 13: $w_s^t(h_d(i)) += h_{\text{sgn}}(i) \max(\log(p_s^t(i)n^t), 0)$
-

Theorem 8. *Given any graph snapshot \mathcal{G}^t and an update batch $\Delta\mathcal{G}^t$ where there are m_t edge events and suppose the precision parameter is ϵ^t and teleport probability is α , DYNAMICSNE runs in $\mathcal{O}(m_t/\alpha^2 + m_t \bar{d}^t / (\epsilon\alpha^2) + m_t / (\epsilon\alpha))$ with $\epsilon^t = \epsilon / m_t$*

Proof. Based lemma 7, the proof directly follows from Theorem 12 of [195]. \square

The above theorem has an important difference from the previous one [194]. We require that the precision parameter will be small enough so that $\|\mathbf{p}_s^t - \boldsymbol{\pi}_s^t\|_1$ can be bound (will be discussed later). As we did the experiments in Figure 3.2, the fixed epsilon will make the embedding vector bad. We propose to use a dynamic precision parameter, where $\epsilon^t \sim \mathcal{O}(\epsilon / m_t)$, so that the ℓ_1 -norm can be properly bounded. Interestingly, this high precision parameter strategy will not cause too high time complexity cost from $\mathcal{O}(m/\alpha^2)$ to $\mathcal{O}(m\bar{d}/(\epsilon\alpha^2))$. The bounded estimation error is presented in the following theorem.

Theorem 9 (Estimation error). *Given any node s , define the estimation error of PPVs learned from DYNAMICSNE at time t as $\|\mathbf{p}_s^t - \boldsymbol{\pi}_s^t\|_1$, if we are given the precision parameter $\epsilon^t = \epsilon / m_t$, the estimation error can be bounded by the following*

$$\|\mathbf{p}_s^t - \boldsymbol{\pi}_s^t\|_1 \leq \epsilon, \quad (3.5)$$

where we require $\epsilon \leq 2$ ⁶ and ϵ is a global precision parameter of DYNAMICPPE independent on m_t and n_t .

Proof. Notice that for any node u , by Lemma 3, we have the following inequality

$$|p_s^t(u) - \pi_s^t(u)| \leq \epsilon d^t(u).$$

Summing all these inequalities over all nodes u , we have

$$\begin{aligned} \|\mathbf{p}_s^t - \boldsymbol{\pi}_s^t\|_1 &= \sum_{u \in \mathcal{V}^t} |p_s^t(u) - \pi_s^t(u)| \\ &\leq \sum_{u \in \mathcal{V}^t} \epsilon^t d^t(u) = \epsilon^t m_t = \frac{\epsilon}{m_t} m_t = \epsilon. \end{aligned}$$

□

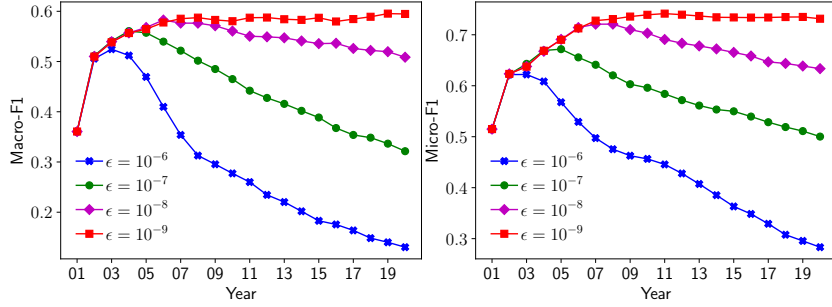


Figure 3.2: ϵ as a function of year for the task of node classification on the English Wikipedia graph. Each line corresponds to a fixed precision strategy of DYNAMICSNE. Clearly, when the precision parameter ϵ decreases, the performance of node classification improves.

The above theorem gives estimation error guarantee of \mathbf{p}_s^t , which is critically important for learning high quality embeddings. First of all, the dynamic precision strategy is inevitable because the precision is unknown parameter for dynamic graph where the number of nodes and edges could increase dramatically over time. To demonstrate this issue, we conduct an experiments on the English Wikipedia graph where we learn embeddings over years and validate these embeddings by using node classification task. As shown in Figure 3.2, when we use the fixed

⁶By noticing that $\|\mathbf{p}_s^t - \boldsymbol{\pi}_s^t\|_1 \leq \|\mathbf{p}_s^t\|_1 + \|\boldsymbol{\pi}_s^t\|_1 \leq 2$, any precision parameter larger than 2 will be meaningless.

parameter, the performance of node classification is getting worse when the graph is getting bigger. This is mainly due to the lower quality of PPVs. Fortunately, the adaptive precision parameter ϵ/m_t does not make the run time increase dramatically. It only depends on the average degree \bar{d}^t . In practice, we found $\epsilon=0.1$ are sufficient for learning effective embeddings.

3.4.2 DYNAMICPPE

Our finally algorithm DYNAMICPPE is presented in Algorithm 4. At every beginning, estimators \mathbf{p}_s^t are set to be zero vectors and residual vectors \mathbf{r}_s^t are set to be unit vectors with mass all on one entry (Line 4). The algorithm then call the procedure DYNAMICSNE with an empty batch as input to get initial PPVs for all target nodes ⁷ (Line 5). From Line 6 to Line 9, at each snapshot t , it gets an update batch $\Delta\mathcal{G}^t$ at Line 7 and then calls DYNAMICSNE to obtain the updated embeddings for every node v .

Algorithm 4 DYNAMICPPE($\mathcal{G}_0, S, \epsilon, \alpha$)

- 1: **Input:** initial graph \mathcal{G}^0 , target set S , global precision ϵ , teleport probability α
 - 2: $t=0$
 - 3: **for** $s \in S := \{v_1, v_2, \dots, v_k\}$ **do**
 - 4: $\mathbf{p}_s^t = \mathbf{0}, \mathbf{r}_s^t = \mathbf{1}_s$
 - 5: DYNAMICSNE($\mathcal{G}^0, \emptyset, s, \mathbf{p}_s^t, \mathbf{r}_s^t, 1/m_0, \alpha$)
 - 6: **for** $t \in \{1, 2, \dots, T\}$ **do**
 - 7: read a sequence of edge events $\Delta\mathcal{G}^t := \mathcal{G}^t \setminus \mathcal{G}^{t-1}$
 - 8: **for** $s \in S := \{v_1, v_2, \dots, v_k\}$ **do**
 - 9: $\mathbf{w}_s^t = \text{DYNAMICSNE}(\mathcal{G}^t, \Delta\mathcal{G}^t, s, \mathbf{p}_s^{t-1}, \mathbf{r}_s^{t-1}, \epsilon/m_t, \alpha)$
 - 10: **return** $\mathbf{W}_s^t = [\mathbf{w}_s^1, \mathbf{w}_s^2, \dots, \mathbf{w}_s^T], \forall s \in S$.
-

Based on our analysis, DYNAMICPPE is an dynamic version of *InstantEmbedding*. Therefore, DYNAMICPPE has two key properties observed in [128]: *locality* and *global consistency*. The embedding quality is guaranteed from the fact that *InstantEmbedding* implicitly factorizes the proximity matrix based on PPVs [161].

⁷For the situation that some nodes of S has not appeared in \mathcal{G}^t yet, it checks every batch update until all nodes are initialized.

3.4.3 Complexity analysis

Time complexity The overall time complexity of DYNAMICPPE is the k times of the run time of DYNAMICSNE. We summarize the time complexity of DYNAMICPPE as in the following theorem

Theorem 10. *The time complexity of DYNAMICPPE for learning a subset of k nodes is $\mathcal{O}(k\frac{m_t}{\alpha^2} + k\frac{m_t d^t}{\alpha^2} + \frac{m_t}{\epsilon} + kT\min\{n, \frac{m}{\epsilon\alpha}\})$*

Proof. We follow Theorem 8 and summarize all run time together to get the final time complexity. \square

Space complexity The overall space complexity has two parts: 1) $\mathcal{O}(m)$ to store the graph structure information; and 2) the storage of keeping nonzeros of \mathbf{p}_s^t and \mathbf{r}_s^t . From the fact that local push operation [9], the number of nonzeros in \mathbf{p}_s^t is at most $\frac{1}{\epsilon\alpha}$. Thus, the total storage for saving these vectors are $\mathcal{O}(k\min\{n, \frac{m}{\epsilon\alpha}\})$. Therefore, the total space complexity is $\mathcal{O}(m + k\min(n, \frac{m}{\epsilon\alpha}))$.

Implementation Since learning the dynamic node embedding for any node v is independent with each other, DYNAMICPPE is are easy to parallel. Our current implementation can take advantage of multi-cores and compute the embeddings of S in parallel.

3.5 Experiments

To demonstrate the effectiveness and efficiency of DYNAMICPPE, in this section, we first conduct experiments on several small and large scale real-world dynamic graphs on the task of node classification, followed by a case study about changes of Chinese cities in Wikipedia graph during the COVID-19 pandemic.

3.5.1 Datasets

We compile the following three real-world dynamic graphs, more details can be found in Appendix 3.7.3.

Enwiki20 English Wikipedia Network We collect the internal Wikipedia Links (WikiLinks) of English Wikipedia from the beginning of Wikipedia, January 11th, 2001, to December 31, 2020 ⁸. The internal links are extracted using a regular expression proposed in [39]. During the entire period, we collection 6,151,779 valid

⁸We collect the data from the dump <https://dumps.wikimedia.org/enwiki/20210101/>

articles⁹. We generated the WikiLink graphs only containing edge insertion events. We keep all the edges existing before Dec. 31 2020, and sort the edge insertion order by the creation time. There are 6,216,199 nodes and 177,862,656 edges during the entire period. Each node either has one label (*Food, Person, Place,...*) or no label.

Patent (US Patent Graph) The citation network of US patent[77] contains 2,738,011 nodes with 13,960,811 citations range from year 1963 to 1999. For any two patents u and v , there is an edge (u,v) if the patent u cites patent v . Each patent belongs to six different types of patent categories. We extract a small weakly-connected component of 46,753 nodes and 425,732 edges with timestamp, called *Patent-small*.

Coauthor We extracted the co-authorship network from the Microsoft Academic Graph [151] dumped on September 21, 2019. We collect the papers with less than six coauthors, keeping those who has more than 10 publications, then build undirected edges between each coauthor with a timestamp of the publication date. In addition, we gather temporal label (e.g.: *Computer Science, Art, ...*) of authors based on their publication’s field of study. Specifically we assign the label of an author to be the field of study where s/he published the most up to that date. The original graph contains 4,894,639 authors and 26,894,397 edges ranging from year 1800 to 2019. We also sampled a small connected component containing 49,767 nodes and 755,446 edges with timestamp, called *Coauthor-small*.

Academic The co-authorship network is from the academic network [155, 205] where it contains 51,060 nodes and 794,552 edges. The nodes are generated from 1980 to 2015. According to the node classification setting in Zhou et al. [205], each node has either one binary label or no label.

3.5.2 Node Classification Task

Experimental settings We evaluate embedding quality on binary classification for Academic graph (as same as in [205]), while using multi-class classification for other tasks. We use balanced logistic regression with ℓ_2 penalty in on-vs-rest setting, and report the Macro-F1 and Macro-AUC (ROC) from 5 repeated trials with 10% training ratio on the labeled nodes in each snapshot, excluding dangling nodes. Between each snapshot, we insert new edges and keep the previous edges.

We conduct the experiments on the aforementioned small and large scale graph. In small scale graphs, we calculate the embeddings of all nodes and compare our proposed method (**DynPPE.**) against other state-of-the-art models from

⁹A valid Wikipedia article must be in the 0 namespace

three categories¹⁰. 1) Random walk based static graph embeddings (**Deepwalk**¹¹ [126], **Node2Vec**¹² [65]); 2) Random Projection-based embedding method which supports online update: **RandNE**¹³ [200]; 3) Dynamic graph embedding method: **DynamicTriad (DynTri.)**¹⁴ [205] which models the dynamics of the graph and optimized on link prediction.

Table 3.1: Node classification task on the *Academic*, *Patent Small*, *Coauthor Small* graph on the final snapshot

		Academic		Patent Small		Coauthor Small	
		F1	AUC	F1	AUC	F1	AUC
$d=128$							
Static method	Node2Vec	0.833	0.975	0.648	0.917	0.477	0.955
	Deepwalk	0.834	0.975	0.650	0.919	0.476	0.950
Dynamic method	DynTri.	0.817	0.969	0.560	0.866	0.435	0.943
	RandNE	0.587	0.867	0.428	0.756	0.337	0.830
	DynPPE.	0.808	0.962	0.630	0.911	0.448	0.951
$d=512$							
Static method	Node2Vec	0.841	0.975	0.677	0.931	0.486	0.955
	Deepwalk	0.842	0.975	0.680	0.931	0.495	0.955
Dynamic method	DynTri.	0.811	0.965	0.659	0.915	0.492	0.952
	RandNE	0.722	0.942	0.560	0.858	0.493	0.895
	DynPPE.	0.842	0.973	0.682	0.934	0.509	0.958

Table 3.1 shows the classification results on the final snapshot. When we restrict the dimension to be 128, we observe that static methods outperform all dynamic methods. However, the static methods independently model each snapshot and the running time grows with number of snapshots, regardless of the number of edge changes. In addition, our proposed method (DynPPE.) outperforms other dynamic baselines, except that in the *academic* graph, where DynTri. is slightly better. However, their CPU time is 13 times more than ours as shown in Table 3.2. According to the Johnson-Lindenstrauss lemma[40, 91], we suspect that the poor result of RandNE is partially caused by the dimension size. As we increase the dimension to 512, we see a great performance improvement of

¹⁰Appendix 3.7.4 shows the hyper-parameter settings of baseline methods

¹¹<https://pypi.org/project/deepwalk/>

¹²<https://github.com/aditya-grover/node2vec>

¹³<https://github.com/ZW-ZHANG/RandNE/tree/master/Python>

¹⁴<https://github.com/luckiezhou/DynamicTriad>

¹⁵We ran static graph embedding methods over a set of sampled snapshots and estimate the total CPU time for all snapshots.

Table 3.2: Total CPU time for small graphs (in second). RandNE-I is with orthogonal projection, the performance is slightly better, but the running time is significantly increased. RandNE-II is without orthogonal projection.

	Academic	Patent Small	Coauthor Small
Deepwalk ¹⁵	498,211.75	181,865.56	211,684.86
Node2vec	4,584,618.79	2,031,090.75	1,660,984.42
DynTri.	247,237.55	117,993.36	108,279.4
RandNE-I	12,732.64	9,637.15	8,436.79
RandNE-II	1,583.08	9,208.03	177.89
DynPPE.	18,419.10	3,651.59	21,323.74

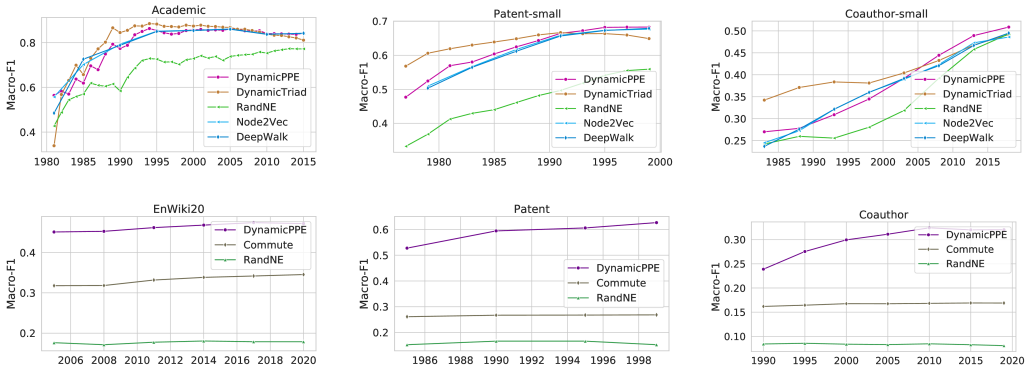


Figure 3.3: Macro-F1 scores of node classification as a function of time. The results of the small and large graphs are on the first and second row respectively (dim=512). Our proposed methods achieves the best performance on the last snapshot when all edges arrived and performance curve matches to the static methods as the graph becomes more and more complete.

RandNE. Also, our proposed method takes the same advantage, and outperform all others baselines in F1-score. Specifically, the increase of dimension makes hash projection step (Line 12-13 in Algorithm 3) retain more information and yield better embeddings. We attach the visualization of embeddings in Appendix.3.7.5.

The first row in the Figure 3.3 shows the F1-scores in each snapshot when the dimension is 512. We observe that in the earlier snapshots where many edges are not arrived, the performance of DynamicTriad [205] is better. One possible reason is that it models the dynamics of the graph, thus the node feature is more

robust to the "missing" of the future links. While other methods, including ours, focus on an online feature updates incurred by the edge changes without explicitly modeling the temporal dynamics of a graph. Meanwhile, the performance curve of our method matches to the static methods, demonstrating the embedding quality of the intermediate snapshots is comparable to the state-of-the-art.

Table 3.2 shows the CPU time of each method (Dim=512). As we expected, static methods is very expensive as they calculate embeddings for each snapshot individually. Although our method is not blazingly fast compared to RandNE, it has a good trade-off between running time and embedding quality, especially without much hyper-parameter tuning. Most importantly, it can be easily parallelized by distributing the calculation of each node to clusters.

We also conduct experiment on large scale graphs (*EnWiki20*, *Patent*, *Coauthor*). We keep track of the vertices in a subset containing $|S| = 3,000$ nodes randomly selected from the first snapshot in each dataset, and similarly evaluate the quality of the embeddings of each snapshot on the node classification task. Due to scale of the graph, we compare our method against **RandNE** [200] and an fast heuristic **Algorithm 5**. Our method can calculate the embeddings for a subset of useful nodes only, while other methods have to calculate the embeddings of all nodes, which is not necessary under our scenario detailed in Sec. 7.6.3. The second row in Figure 3.3 shows that our proposed method has the best performance.

Table 3.3: Total CPU time for large graphs (in second)

	Enwiki20	Patent	Coauthor
Commute	6,702.1	639.94	1,340.74
RandNE-II	47,992.81	6,524.04	20,771.19
DynPPE.	1,538,215.88	139,222.01	411,708.9
DynPPE (Per-node)	512.73	46.407	137.236

Table 3.3 shows the total CPU time of each method (Dim=512). Although total CPU time of our proposed method seems to be the greatest, the average CPU time for one node (as shown in row 4) is significantly smaller. This benefits a lot of downstream applications where only a subset of nodes are interesting to people in a large dynamic graph. For example, if we want to monitor the weekly embedding changes of a single node (e.g., the city of Wuhan, China) in English Wikipedia network from year 2020 to 2021, we can have the results in roughly 8.5 minutes. Meanwhile, other baselines have to calculate the embeddings of all

nodes, and this expensive calculation may become the bottleneck in a downstream application with real-time constraints. To demonstrate the usefulness of our method, we conduct a case study in the following subsection.

3.5.3 Change Detection

Thanks to the contributors timely maintaining Wikipedia, we believe that the evolution of the Wikipedia graph reflects how the real world is going on. We assume that when the structure of a node greatly changes, there must be underlying interesting events or anomalies. Since the structural changes can be well-captured by graph embedding, we use our proposed method to investigate whether anomalies happened to the Chinese cities during the COVID-19 pandemic (from Jan. 2020 to Dec. 2020).

Changes of major Chinese Cities We target nine Chinese major cities (*Shanghai, Guangzhou, Nanjing, Beijing, Tianjin, **Wuhan**, Shenzhen, Chengdu, Chongqing*) and keep track of the embeddings in a 10-day time window. From our prior knowledge, we expect that *Wuhan* should greatly change since it is the first reported place of the COVID-19 outbreak in early Jan. 2020.

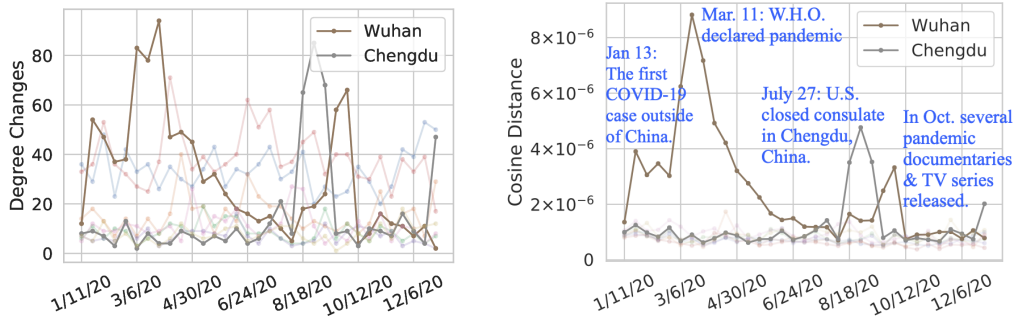


Figure 3.4: The changes of major Chinese cities in 2020. *Left:* Changes in Node Degree. *Right:* Changes in Cosine distance

Figure.3.4(a) shows the node degree changes of each city every 10 days. The curve is quite noisy, but we can still see several major peaks from *Wuhan* around 3/6/20 and *Chengdu* around 8/18/20. When using embedding changes¹⁶ as the measurement, Figure.3.4 (b) provides a more clear view of the changed cities. We

¹⁶Again, the embedding movement $\text{Dist}(\cdot, \cdot)$ is defined as $1 - \cos(\cdot, \cdot)$

Table 3.4: The top cities ranked by the z-score along time. The corresponding news titles are from the news in each time period. $d(v)$ is node degree, $\Delta d(v)$ is the degree changes from the previous timestamp.

Date	City	$d(v)$	$\Delta d(v)$	Z-score	Top News Title
1/22/20	Wuhan	2890	54	2.210	NBC: "New virus prompts U.S. to screen passengers from Wuhan, China"
2/2/20	Wuhan	2937	47	1.928	WSJ: "U.S. Sets Evacuation Plan From Coronavirus-Infected Wuhan"
2/13/20	Hohhot	631	20	1.370	Poeple.cn: "26 people in Hohhot were notified of dereliction of duty for prevention and control, and the director of the Health Commission was removed" (Translated from Chinese).
2/24/20	Wuhan	3012	38	2.063	USA Today: "Coronavirus 20 times more lethal than the flu? Death toll passes 2,000"
3/6/20	Wuhan	3095	83	1.723	Reuters: "Infections may drop to zero by end-March in Wuhan: Chinese government expert"
3/17/20	Wuhan	3173	78	1.690	NYT: "Politicians Use of 'Wuhan Virus' Starts a Debate Health Experts Wanted to Avoid"
3/28/20	Zhang Jia Kou	517	15	1.217	"Logo revealed for Freestyle Ski and Snowboard World Championships in Zhangjiakou"
4/8/20	Wuhan	3314	47	2.118	CNN: "China lifts 76-day lockdown on Wuhan as city reemerges from coronavirus crisis"
4/19/20	Luohe	106	15	2.640	Forbes: "The Chinese Billionaire Whose Company Owns Troubled Pork Processor Smithfield Foods"
4/30/20	Zunhua	52	17	2.449	XINHUA: "Export companies resume production in Zunhua, Hebei"
5/11/20	Shulan	88	46	2.449	CGTN: "NE China's Shulan City to reimpose community lockdown in 'wartime' battle against COVID-19"

observe strong signals from the curve of *Wuhan*, correlating to the initial COVID-19 outbreak and the declaration of pandemic¹⁷. In addition, we observed an peak

¹⁷COVID-19: <https://www.who.int/news/item/27-04-2020-who-timeline---covid-19>

from the curve of *Chengdu* around 8/18/20 when U.S. closed the consulate in Chengdu, China, reflecting the U.S.-China diplomatic tension¹⁸.

Top changed city along time We keep track of the embedding movement of 533 Chinese cities from year 2020 to 2021 in a 10-day time window, and filter out the inactive records by setting the threshold of degree changes (e.g. greater than 10). The final results are 51 Chinese cities from the major ones listed above and less famous cities like *Zhangjiakou*, *Hohhot*, *Shulan*,

Furthermore, we define the z-score of a target node u as $Z_t(u)$ based on the embedding changes within a specific period of time from $t-1$ to t .

$$Z_t(u|u \in S) = \frac{Dist(w_u^t, w_u^{t-1}) - \mu}{\sigma}$$

$$\mu = \frac{1}{|S|} \sum_{u' \in S} Dist(w_{u'}^t, w_{u'}^{t-1}), \quad \sigma = \sqrt{\frac{1}{|S|} \sum_{u' \in S} (Dist(w_{u'}^t, w_{u'}^{t-1}) - \mu)^2}$$

In Table 3.4, we list the highest ranked cities by the z-score from Jan.22 to May 11, 2020. In addition, we also attach the top news titles corresponding to the city within each specific time period. We found that Wuhan generally appears more frequently as the situation of the pandemic kept changing. Meanwhile, we found the appearance of *Hohhot* and *Shulan* reflects the time when COVID-19 outbreak happened in those cities. We also discovered cities unrelated to the pandemic. For example, *Luohe*, on 4/19/20, turns out to be the city where the headquarter of the organization which acquired Smithfield Foods (as mentioned in the news). In addition, *Zhangjiakou*, on 3/28/20, is the city, which will host World Snowboard competition, released the Logo of that competition.

3.6 Discussion and Conclusion

In this paper, we propose a new method to learn dynamic node embeddings over large-scale dynamic networks for a subset of interesting nodes. Our proposed method has time complexity that is linear-dependent on the number of edges m but independent on the number of nodes n . This makes our method applicable to applications of subset representations on very large-scale dynamic graphs. For the future work, as shown in Trivedi et al. [160], there are two dynamics on dynamic

¹⁸US Consulate: <https://china.usembassy-china.org.cn/embassy-consulates/chengdu/>

graph data, *structure evolution* and dynamics of *node interaction*. It would be interesting to study how one can incorporate dynamic of node interaction into our model. It is also worth to study how different version of local push operation affect the performance of our method.

Acknowledges This work was partially supported by NSF grants IIS-1926781, IIS-1927227, IIS-1546113 and OAC-1919752.

3.7 Appendix

3.7.1 Proof of lemmas

To prove Lemma 2, we first introduce the property of uniqueness of PPR π_s for any s .

Proposition 11 (Uniqueness of PPR [10]). *For any starting vector $\mathbf{1}_s$, and any constant $\alpha \in (0,1]$, there is a unique vector π_s satisfying (2.1).*

Proof. Recall the PPR equation

$$\pi_s = \alpha \mathbf{1}_s + (1 - \alpha) \mathbf{D}^{-1} \mathbf{A} \pi_s.$$

We can rewrite it as $(\mathbf{I} - (1 - \alpha) \mathbf{D}^{-1} \mathbf{A}) \pi_s = \alpha \mathbf{1}_s$. Notice the fact that matrix $\mathbf{I} - (1 - \alpha) \mathbf{D}^{-1} \mathbf{A}$ is strictly diagonally dominant matrix. To see this, for each $i \in \mathcal{V}$, we have $1 - (1 - \alpha) \sum_{j \neq i} |1/d(i)| = \alpha > 0$. By [106], strictly diagonally dominant matrix is always invertible. \square

Proposition 12 (Symmetry property [112]). *Given any undirected graph \mathcal{G} , for any $\alpha \in (0,1)$ and for any node pair (u,v) , we have*

$$d(u) \pi_u(v) = d(v) \pi_v(u). \quad (3.6)$$

Proof of Lemma 7. Assume there are T iterations. For each forward push operation $t = 1, 2, \dots, T$, we assume the frontier node is u_t , the run time of one push operation is then $d(u_t)$. For total T push operations, the total run time is $\sum_{i=1}^T d(u_i)$. Notice that during each push operation, the amount of $\|\mathbf{r}_s^{t-1}\|_1$ is reduced at least $\epsilon \alpha d(u_t)$, then we always have the following inequality

$$\epsilon \alpha d(u_t) < \|\mathbf{r}_s^{t-1}\|_1 - \|\mathbf{r}_s^t\|_1$$

Apply the above inequality from $t=1,2$, to T , we will have

$$\epsilon\alpha \sum_{t=1}^T d(u_t) \leq \|\mathbf{r}_s^0\| - \|\mathbf{r}_s^T\|_1 = 1 - \|\mathbf{r}_s\|_1, \quad (3.7)$$

where \mathbf{r}_s is the final residual vector. The total time is then $\mathcal{O}(1/\epsilon\alpha)$. To show the estimation error, we follow the idea of [111]. Notice that, the forward local push algorithm always has the invariant property by Lemma 2, that is

$$\pi_s(u) = p_s(u) + \sum_{v \in V} r_s(v) \pi_v(u), \forall u \in \mathcal{V}. \quad (3.8)$$

By proposition 12, we have

$$\begin{aligned} \pi_s(u) &= p_s(u) + \sum_{v \in V} r_s(v) \pi_v(u), \forall u \in \mathcal{V} \\ &= p_s(u) + \sum_{v \in V} r_s(v) \frac{d(u)}{d(v)} \pi_u(v), \forall u \in \mathcal{V} \\ &\leq p_s(u) + \sum_{v \in V} \epsilon d(u) \pi_u(v), \forall u \in \mathcal{V} = p_s(u) + \epsilon d(u), \end{aligned}$$

where the first inequality by the fact that $r_s(v) \leq \epsilon d(v)$ and the last equality is due to $\|\pi_u\|_1 = 1$. \square

Proposition 13 ([194]). *Let $\mathcal{G} = (V, E)$ be undirected and let t be a vertex of V , then $\sum_{x \in V} \frac{\pi_x(t)}{d(t)} \leq 1$.*

Proof. By using Proposition 12, we have

$$\sum_{x \in V} \frac{\pi_x(t)}{d(t)} = \sum_{x \in V} \frac{\pi_t(x)}{d(x)} \leq \sum_{x \in V} \pi_t(x) = 1.$$

\square

3.7.2 Heuristic method: Commute

We update the embeddings by their pairwise relationship (resistance distance). The commute distance (i.e. resistance distance) $C_{uv} = H_{uv} + H_{vu}$, where rescaled hitting time H_{uv} converges to $1/d(v)$. As proved in [168], when the number of nodes in the graph is large enough, we can show that the commute distance tends to $1/d_v + 1/d_u$.

Algorithm 5 COMMUTE

- 1: **Input:** An graph $\mathcal{G}^0(\mathcal{V}^0, \mathcal{E}^0)$ and embedding \mathbf{W}^0 , dimension d .
- 2: **Output:** \mathbf{W}^T
- 3: **for** $e^t(u, v, t) \in \{e^1(u^1, v^1, t_1), \dots, e^T(u^T, v^T, t_T)\}$ **do**
- 4: Add e^t to \mathcal{G}^t
- 5: **If** $u \notin V^{t-1}$ **then**
- 6: generate $\mathbf{w}_u^t = \mathcal{N}(\mathbf{0}, 0.1 \cdot \mathbf{I}_d)$ or $\mathcal{U}(-0.5, 0.5)/d$
- 7: **If** $v \notin V^{t-1}$ **then**
- 8: generate $\mathbf{w}_v^t = \mathcal{N}(\mathbf{0}, 0.1 \cdot \mathbf{I}_d)$ or $\mathcal{U}(-0.5, 0.5)/d$
- 9: $\mathbf{w}_u^t = \frac{d(u)}{d(u)+1} \mathbf{w}_u^{t-1} + \frac{1}{d(u)} \mathbf{w}_v^t$
- 10: $\mathbf{w}_v^t = \frac{d(v)}{d(v)+1} \mathbf{w}_v^{t-1} + \frac{1}{d(v)} \mathbf{w}_u^t$
- 11: **Return** \mathbf{W}_T

One can treat the Commute method, i.e. Algorithm 5, as the first-order approximation of RandNE [200]. The embedding generated by RandNE is given as the following

$$\mathbf{U} = (\alpha_0 \mathbf{I} + \alpha_1 \mathbf{A} + \alpha_2 \mathbf{A}^2 + \dots + \alpha_q \mathbf{A}^q) \mathbf{R}, \quad (3.9)$$

where \mathbf{A} is the normalized adjacency matrix and \mathbf{I} is the identity matrix. At any time t , the dynamic embedding of node i of Commute is given by

$$\begin{aligned} \mathbf{w}_i^t &= \frac{d(u)}{d(u)+1} \mathbf{w}_i^{t-1} + \frac{1}{d(u)} \mathbf{w}_v^t \\ &= \frac{1}{d(u)+1} \mathbf{w}_i^0 + \frac{1}{|\mathcal{N}(i)|} \sum_{j \in \mathcal{N}(i)} \frac{1}{d(u)} \mathbf{w}_j^t \end{aligned}$$

3.7.3 Details of data preprocessing

In this section, we describe the preprocessing steps of three datasets. **Enwiki20:** In Enwiki20 graph, the edge stream is divided into 6 snapshots, containing edges before 2005, 2005-2008, ..., 2017-2020. The sampled nodes in the first snapshot fall into 5 categories. **Patent:** In full patent graph, we divide edge stream into 4 snapshots, containing patents citation links before 1985, 1985-1990, ..., 1995-1999. In node classification tasks, we sampled 3,000 nodes in the first snapshot, which fall into 6 categories. In patent small graph, we divide into 13 snapshots with a 2-year window. All the nodes in each snapshot fall into 6 categories. **Coauthor graph:**

In full Coauthor graph, we divide edge stream into 7 snapshots (before 1990, 1990-1995, ..., 2015-2019). The sampled nodes in the first snapshot fall into 9 categories. In Coauthor small graph, the edge stream is divided into 9 snapshots (before 1978, 1978-1983,..., 2013-2017). All the nodes in each snapshot have 14 labels in common.

3.7.4 Details of parameter settings

Deepwalk: number-walks=40, walk-length=40, window-size=5

Node2Vec: Same as Deepwalk, $p = 0.5$, $q = 0.5$

DynamicTriad: iteration=10, beta-smooth=10, beta-triad=10. Each input snapshot contains the previous existing edges and newly arrived edges.

RandNE: $q=3$, default weight for node classification $[1, 1e2, 1e4, 1e5]$, input is the transition matrix, the output feature is normalized (l-2 norm) row-wise.

DynamicPPE: $\alpha = 0.15$, $\epsilon = 0.1$, projection method=hash. our method is relatively insensitive to the hyper-parameters.

Infrastructure: 64 CPUs with 16 cores on each (Intel(R) Xeon(R) Silver 4216 CPU @ 2.10GHz) with 376 GB memory.

3.7.5 Visualizations of Embeddings

We visualize the embeddings of small scale graphs using T-SNE[163] in Fig.3.5,3.6,3.7.

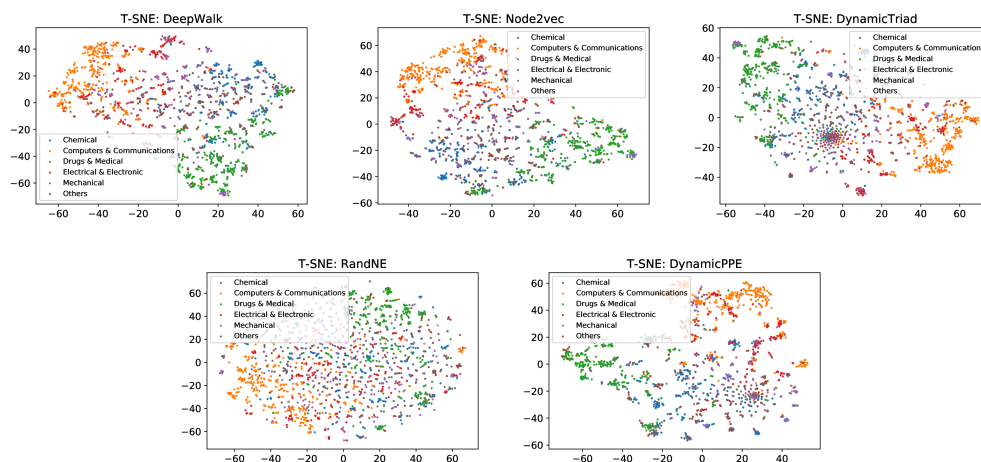


Figure 3.5: We randomly select 2,000 nodes from patent-small and visualize their embeddings using T-SNE[163]

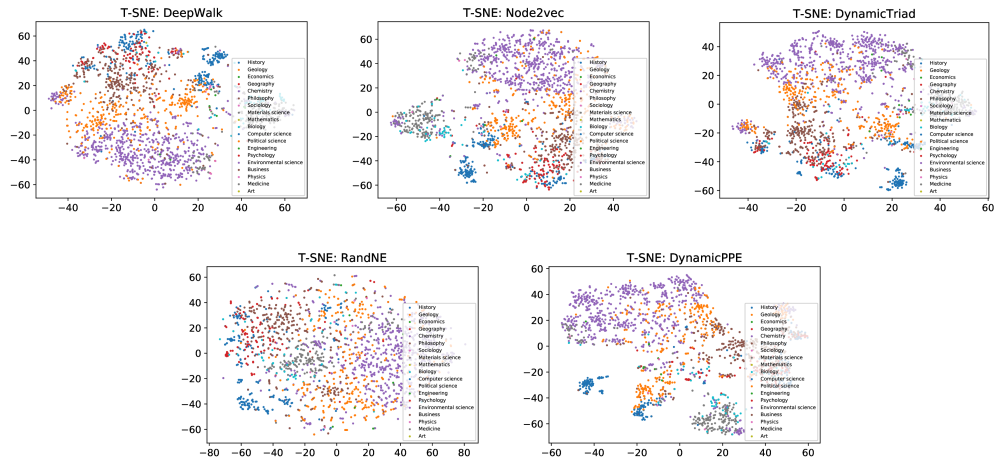


Figure 3.6: We randomly select 2,000 nodes from Coauthor-small graph and visualize their embeddings using T-SNE[163]

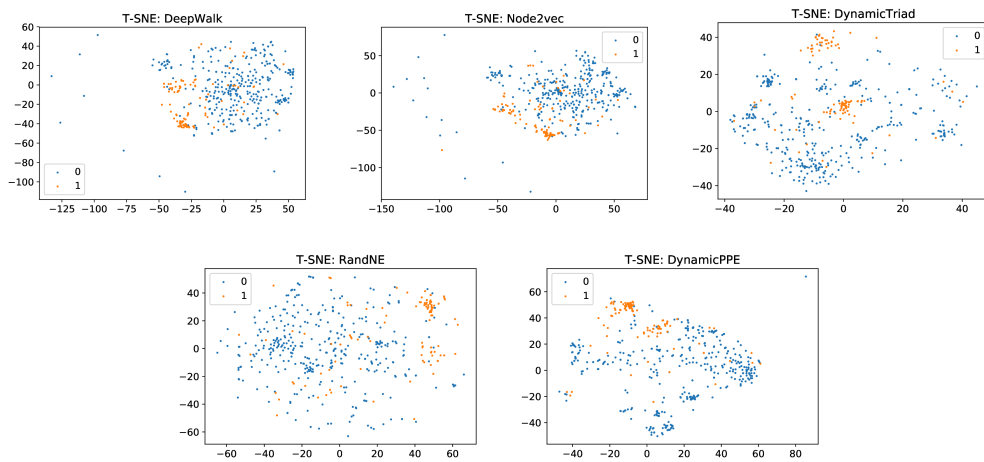


Figure 3.7: We select all labeled nodes from Academic graph and visualize their embeddings using T-SNE[163]

Chapter 4

Subset Node Anomaly Detection over Dynamic Graph¹

4.1 Introduction

Analyzing the evolution of events in a large-scale dynamic network is important in many real-world applications. We are motivated by the following specific scenario:

Given a person-event interaction graph containing millions of nodes with several different types (e.g., person, event, location) with a stream of weekly updates over many years, how can we identify when specific individuals significantly changed their context?

The example in Fig. 4.1 shows our analysis as Joe Biden shifted career from senator to vice president and finally to president. In each transition he relates with various intensity to other nodes across time. We seek to identify such transitions through analysis of these interaction frequencies and its inherent network structure. This task becomes challenging as the graph size and time horizon scale up. For example, the raw graph data used in Fig. 4.1 contains roughly 3.2 million nodes and 1196 weekly snapshots (where each snapshot averages 4 million edges) of Person Graph from 2000 to 2022.

Despite the extensive literature [8, 18, 191, 193] on graph anomaly detection, previous work focuses on different problem definitions of *anomaly*. On the other

¹Xingzhi Guo, Baojian Zhou, and Steven Skiena. Subset Node Anomaly Tracking over Large Dynamic Graphs. In *Proceedings of the 28th ACM SIGKDD Conference on Knowledge Discovery & Data Mining (KDD '22)*. Association for Computing Machinery, New York, NY, USA, 475–485. <https://doi.org/10.1145/3534678.3539389> [72]

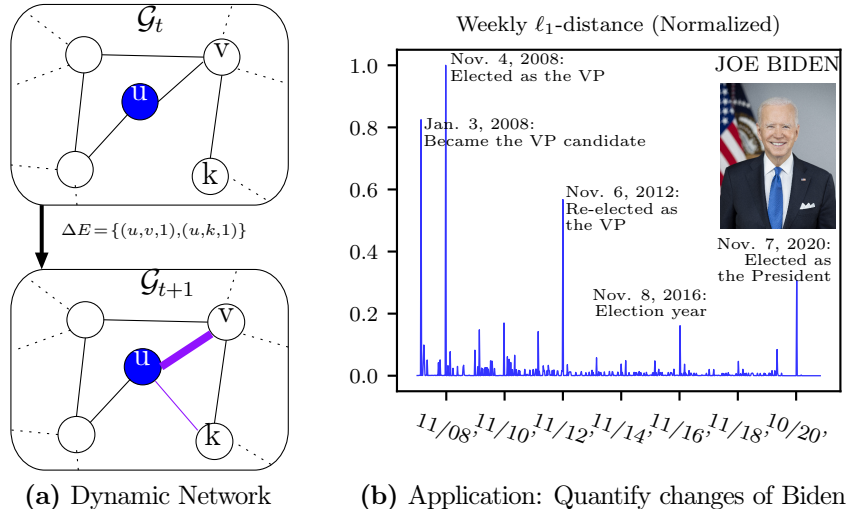


Figure 4.1: (a) Two consecutive snapshots \mathcal{G}_t and \mathcal{G}_{t+1} from a dynamic weighted-graph. The inserted edge $(u,v,1)$ further strengthens an existing relation, while edge $(u,k,1)$ builds a new link. (b) Anomaly tracking of Joe Biden over the *Person Knowledge-Graph* using our proposed DYNANOM. We track Joe Biden on a weekly basis from 2007 to 2020, and calculate the ℓ_1 -distance between the representations on consecutive weeks. The detected peaks correlate well with significant changes in Biden’s life.

hand, works [190] on graph-level anomaly detection cannot identify individual node changes but only uncover the global changes in the overall graph structure. Most representative methods leverage tensor factorization [27] and graph sketching [19], detecting the sudden dis/appearance of dense subgraphs. However, we argue that since most anomalies are locally incurred by a few anomalous nodes/edges, the global graph-level anomaly signal may overlook subtle local changes. Similarly, edge-level anomaly detection [48] cannot identify node evolution when there is no direct edge event associated with that node. When Donald Trump became the president, his wife (*Melania Trump*) changed status to become First Lady, but no explicit edge changes connected her to other politicians except Trump. According to the edge-level anomaly detection, there is no evidence for Melania’s status change.

Node representation learning-based methods such as [162, 191] could be helpful to identify anomaly change locally. However, it is impractical to directly apply these methods on large-scale dynamic settings due to 1) the low efficiency: re/training all node embeddings for snapshots is prohibitively expensive; 2) the missing alignment: node representations of each snapshot in the embedding space

may not be inherently aligned, making the anomaly calculation difficult.

Inspired from the recent advances on local node representation methods [70, 128] for both static and dynamic graphs, we could efficiently calculate the node representations based on approximated Personalized PageRank vectors. These dynamic node representations are keys for capturing the evolution of dynamic graph. One important observation is that time complexity of calculating approximate PPV is $\mathcal{O}(\frac{1}{\alpha\epsilon})$ for per queried node, where α is PageRank [123] teleport probability and ϵ is the approximation error tolerance. As the graph evolves, the per-node update complexity is $\mathcal{O}(\frac{|\Delta E|}{\epsilon})$, where $|\Delta E|$ is the total edge events. The other key observation is that the representation space is inherently consistent and aligned with each other, thus there is a meaningful metric space defined directly over the Euclidean space of every node representation across different times. Current local node representation method [70] only captures the node-level structural changes over unweighted graphs, which ignores the important interaction frequency information over the course of graph evolution. For example, in a communication graph, the inter-node interaction frequency is a strong signal, but the unweighted setting ignores such crucial feature. This undesirable characteristic makes the node representation becomes less expressive in weighted-graph.

Based on the above observations, in this paper, we generalize the local node representation method so that it is more expressive and supports dynamic weighted-graph, and resolve the practical subset node anomaly tracking problem. We summarize our contributions as follows:

- We generalize dynamic forward push algorithm [194] for calculating Personalized PageRank, making it suitable for weighted-graph anomaly tracking. The algorithm updates node representations per-edge event (i.e., weighted edge addition/deletion), and the per-node time complexity linear to edge events ($|\Delta E|$) and error parameter(ϵ) which is independent on the node size.
- We propose an efficient anomaly framework, namely DYNANOM that can support both node and graph-level anomaly tracking, effectively localizing the period when a specified node significantly changed its context. Experiments demonstrate its superior performance over other baselines with the accuracy of 0.5425 compared with 0.2790, the baseline method meanwhile 2.3 times faster.
- A new large-scale real-world graph, as new resources for anomaly tracking: PERSON graph is constructed as a more interpretable resource, bringing

more research opportunities for both algorithm benchmarking and real-world knowledge discovery. Furthermore, we conduct a case study over it, successfully capturing the career shifts of three public figures in the U.S., showing the usability of DYNANOM.

The rest paper is organized as follows: Section 5.2 reviews previous graph anomaly tracking methods. Section 4.3 describes the notation and preliminaries. Section 4.4 gives the problem formulation. We present our proposed framework – DYNANOM in Section 4.5. Section 4.6 gives the experiment results over standard benchmark graphs and a case study on the real-world graph. Finally, we conclude and discuss future directions in Section 6.5. Source code and datasets will be released upon publication, and included in supplementary file (compiled datasets are in <https://bit.ly/3rAshBn>).

4.2 Related Work

We review the three most common graph anomaly tasks over dynamic graphs, namely graph, edge and node-level anomaly.

Graph-level and edge-level anomaly. Graph anomaly refers to sudden changes in the graph structure during its evolution, measuring the difference between consecutive graph snapshots [7, 16, 48, 49]. Aggarwal et al. [7] use a structural connectivity model to identify anomalous graph snapshots. Shin et al. [149] apply incremental tensor factorization to spot dense connection formed in a short time. Yoon et al. [190] use the first and second derivatives of the global PageRank Vectors as the anomaly signal, assuming that a normal graph stream will evolve smoothly. On the other hand, edge anomaly identifies unexpected edges as the graph evolves where anomalous edges adversarially link nodes in two sparsely connected components or abnormal edge weight changes [17, 48, 133]. Specifically, Eswaran and Faloutsos [48] propose to use the approximated node-pair Personalized PageRank (PPR) score before and after the new edges are inserted. Most recently, Chang et al. [27] estimate the interaction frequency between nodes, and incorporate the network structure into the parameterization of the frequency function. However, these methods cannot be able to reveal the node local anomalous changes, and cannot identify the individual node changes for those without direct edge modification as we illustrated in introduction.

Node-level local anomaly. Node anomaly measures the sudden changes in individual node’s connectivity, activity frequency or community shifts [173, 191]. Wang et al. [173] uses hand-crafted features (e.g., node degree, centrality) which

involve manual feature engineering processes. Recently, the dynamic node representation learning methods [63, 105, 113, 142, 191, 205] were proposed. For example, a general strategy of them [105, 191] for adopting such dynamic embedding methods for anomaly detection is to incrementally update node representations and apply anomaly detection algorithms over the latent space. To measure the node changes over time, a comparable or aligned node representation is critical. Yu et al. [191] uses auto-encoder and incremental random walk to update the node representations, then apply clustering algorithm to detect the node outliers in each snapshot. However, its disadvantage is that the embedding space is not aligned, making the algorithm only detects anomalies in each static snapshot. Even worse, it is inapplicable to large-scale graph because the fixed neural models is hard to expand without retraining. Similar approaches [105] with more complicated deep learning structure were also studied. These existing methods are not suitable for the subset node anomaly tracking. Instead, our framework is inspired from recent advances in efficient local node representation algorithms [66, 70, 128, 194], which is successful in handling subset node representations over large-scale graph.

4.3 Forward Local Push Algorithm over Weighted Graphs

As we introduced in Section 2, *forward push algorithm* [9], a.k.a. the bookmark-coloring algorithm [15], approximates $\pi_s(v)$ locally via an approximate $p_s(v)$. The key idea is to maintain solution vector \mathbf{p}_s and a residual vector \mathbf{r}_s (at the initial $\mathbf{r}_s = \mathbf{1}_s, \mathbf{p}_s = \mathbf{0}$). When the graph updates from \mathcal{G}_t to \mathcal{G}_{t+1} , a variant forward push algorithm [194] dynamically maintains \mathbf{r}_s and \mathbf{p}_s . We generalize it to a weighted version of *dynamic forward push* to support dynamic updates on dynamic weighted-graph as presented in Algo. 6. At each local push iteration, it pushes large residuals to neighbors whenever these residuals are significant ($|r_s(u)| > \epsilon d(u)$). Compare with power-iteration, this operation avoids the access of whole graph hence speedup the calculations. Based on [194], we consider a more general setting where the graph could be weighted-graph. Fortunately, this weighted version of FORWARD-LOCALPUSH still has *invariant property* as presented in the following lemma.

Lemma 14 (PPR Invariant Property in weighted graphs [194]). *Suppose π_s is the PPV of node s on graph \mathcal{G}_t . Let \mathbf{p}_s and π_s be returned by the weighted version of DYNAMICFORWARDPUSH presented in Algo. 6. Then, we have the following*

Algorithm 6 FORWARDLOCALPUSH (WEIGHTED VERSION) [194]

```

1: Input:  $p_s, r_s, \mathcal{G}_t, \epsilon, \alpha$ 
2: while exists  $u$  such that  $|r_s(u)| > \epsilon d(u)$  do
3:   PUSH( $u$ )
4: return  $(p_s, r_s)$ 
5: procedure PUSH( $u$ )
6:    $p_s(u) += \alpha r_s(u)$ 
7:   for  $v \in \text{Nei}(u)$  do
8:      $r_s(v) += \frac{(1-\alpha)r_s(u)w(u,v)}{\sum_{v \in \text{Nei}(u)} w(u,v)}$ 
9:    $r_s(u) = 0$ 

```

invariant property.

$$\pi_s(u) = p_s(u) + \sum_{x \in \mathcal{V}} r_s(x) \pi_s(x), \text{ for all } u \in \mathcal{V}, \quad (4.1)$$

$$p_s(u) + \alpha r_s(u) = (1-\alpha) \sum_{x \in \text{Nei}(u)} \frac{w(u,x) p_s(x)}{d(x)} + \alpha 1_{u=s}, \quad (4.2)$$

where $1_{u=s} = 1$ if $u = s$, 0 otherwise.

From PPVs to node representations. Obtained PPVs are not directly applicable to our anomaly tracking problem as operations on these n -dimensional vectors is time-consuming. To avoid this, we treat PPVs as the intriguing similarity matrix and project them into low-dimensional spaces using transformations such as SVD [132], random projection [28, 200], matrix sketch [162], or hashing [128] so that the original node similarity is well preserved by the low dimension node representations. We detail this in our main section.

4.4 Problem formulation

Before we present the subset node anomaly tracking problem. We first define the edge events in the dynamic graph model as the following: A set of edge events ΔE_t from t to $t+1$ is a set of operations on edges, i.e., edge insertion, deletion or weight adjustment while the graph is updating from \mathcal{G}_t to \mathcal{G}_{t+1} . Mathematically, $\Delta E_t \triangleq \{(u_0, v_0, \Delta w_{(u_0, v_0)}), (u_1, v_1, \Delta w_{(u_1, v_1)}), \dots, (u_i, v_i, \Delta w_{(u_i, v_i)})\}$ where each $\Delta w_{(u_i, v_i)}$ represents insertion (or weight increment) if it is positive, or deletion (decrement)

if it is negative. Therefore, our dynamic graph model can be defined as a sequence of edge events. We state our formal problem definition as the following.

Definition 15 (Subset node Anomaly Tracking Problem). *Given a dynamic weighted-graph $\mathcal{G}_t = \langle \mathcal{V}_t, \mathcal{E}_t, \mathcal{W}_t \rangle, \forall t \in [0, T]$, consisting of initial snapshot \mathcal{G}_0 and the following T snapshots that have edge events $\Delta E_t, |\Delta E_t| \geq 0$ (e.g., edge addition, deletion, weight adjustment from $t-1$ to t). We want to quantify the status change of a node v in the targeted node subset $v \in \mathcal{S} \triangleq \{v_0, v_1, \dots, v_k\}$ from \mathcal{G}_{t-1} to \mathcal{G}_t with the anomaly measure function $f(\cdot, \cdot)$ so that the measurement is consistent to human judgement, or reflects the ground-truth of node status change if available. To illustrate this edge event process, Table 4.1 presents the process for better understanding.*

Table 4.1: Illustration of subset node anomaly tracking problem. At each time t , node representations \mathbf{x}_i^t are provided, and anomaly of node changes is quantified by $f(\mathbf{x}_i^{t-1}, \mathbf{x}_i^t)$, which is expected to correlated with the anomaly label if available.

Timestamp	0	1	2	3	...
Edge events	-	ΔE_1	ΔE_2	ΔE_3	...
Snapshots	G_0	G_1	G_2	G_3	...
Score for $v_i \in \mathcal{S}$	-	$f(x_i^0, x_i^1)$	$f(x_i^1, x_i^2)$	$f(x_i^2, x_i^3)$...
Label for $v_i \in \mathcal{S}$	-	Normal	Normal	Abnormal	...

4.5 The Proposed Framework

In order to localize the node anomaly across time, the basic idea is to incrementally obtain the PPVs as the node representation at each time, then design anomaly score function $f(\cdot, \cdot)$ to quantify the PPVs changes from time to time. This section presents our proposed framework DYNANOM which has three components: 1) A provable dynamic PPV update strategy extending [194] to weighted edge insertion/deletion; 2) Node level anomaly localization based on incremental PPVs; and 3) Graph level anomaly detection based on approximation of global PageRank changes. We first present how local computation of PPVs can be generalized to dynamic weighted graphs, then present the unified framework for node/graph-level anomaly tracking, finally we analyze the complexity of an instantiation algorithm.

4.5.1 Maintenance of Dynamic PPVs

Multi-edges record the interaction frequency among nodes, and reflect the evolution of the network not only in topological structure, but also in the strength of communities. Previous works [70, 194] focus only on the structural changes over unweighted graph, ignoring the multi-edge cases. In a communication graph (e.g., Email graph), the disadvantage of such method is obvious: as more interactions/edges are observed, the graph becomes denser, or even turn out to be fully-connected in an extreme case. Afterwards, all the upcoming interactions will not change the node status since the ignorance of interaction frequency. This aforementioned scenario motivates us to generalize dynamic PPV maintenance to weighted graph, expanding its usability for more generic graphs and diverse applications. In order to incorporate edge weights into the dynamic forward push algorithm to obtain PPVs, we modify the original algorithm [9, 194] by adding a weighted push mechanism as presented in Algo. 6. Specifically, for a specific node v , at each iteration of the push operation, we update its neighbor residual $r_s(v)$ as the following

$$r_s(v) += \frac{(1-\alpha)r_s(u)w_{(u,v)}}{\sum_{v \in \text{Nei}(u)} w_{(u,v)}}. \quad (4.3)$$

The modified update of $r_s(v)$ in Equ. (4.3) efficiently approximate the PPR over static weighted graph with same time complexity as the original one. At time snapshot \mathcal{G}_t , the weight of each edge event $\Delta w_{(u,v)}$ could be either positive or negative, representing edge insertion or deletion) at time t so that the target graph \mathcal{G}_t updates to \mathcal{G}_{t+1} . However, this set of edge events will break up the invariant property shown in Lemma 14. To maintenance the invariant property on weighted graphs, we present the following Thm. 16, a generalized version from [194]. The key idea is to update $\mathbf{p}_s, \mathbf{r}_s$ so that updated weights satisfy the invariant property. We present the theorem as following.

Generalized PPR update rules. Figure 4.2 illustrates the dynamic maintenance of PPV over a weighted graph where two new edges are added, incurring edge weight increment between node 0 and 2, and new connection between node 2 and 3. Note that one only needs to have $\mathcal{O}(1)$ time to update $p_s(u), r_s(u)$, and $r_s(v)$ for each edge event. As proved, the total cost of m edge events will be linearly dependent on, i.e., $\mathcal{O}(m)$. This efficient update procedure is much better than naive updates where one needs to calculate all quantities from scratch.

Theorem 16 (Generalized PPR update rules). *Given an edge event $(u,v,\Delta w_{(u,v)})$.*

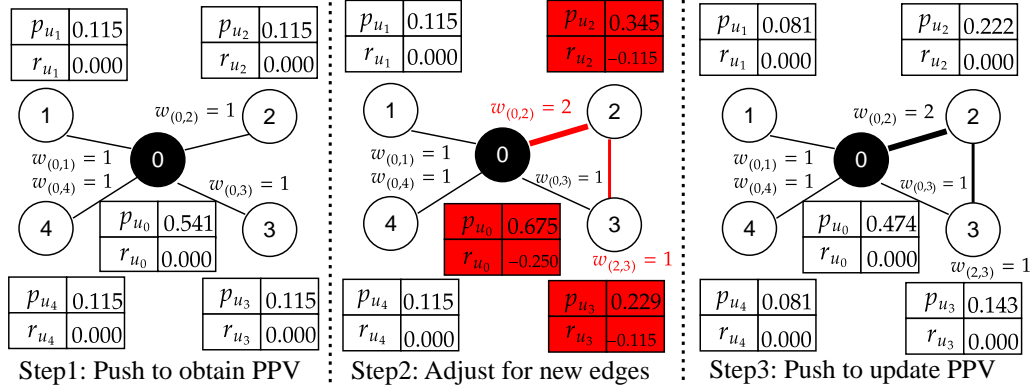


Figure 4.2: Illustration of the PPR adjustment over a weighted graph of five nodes. *Step1:* Apply Algo.6 to calculate the initial p_s, r_s where $s = v_0, \alpha = 0.15$ over the initial graph. *Step2:* After inserting new edges $(v_0, v_2, 1), (v_2, v_3, 1)$, the strength between v_0 and v_2 increases, and v_2 builds a new connection to v_3 , which both break the invariant in Lemma 14. We adjust to recover the invariant by applying Theorem 16 in the red-colored blocks. *Step3:* We re-apply Algo.6 and update p_s for better approximation error.

We use the the following update rules

$$p'_s(u) = p_s(u) \frac{\sum_{v \in \text{Nei}(u)} w(u,v) + \Delta w(u,v)}{\sum_{v \in \text{Nei}(u)} w(u,v)}, \quad (4.4)$$

$$r'_s(u) = r_s(u) - \frac{\Delta w(u,v) p_s(u)}{\alpha \sum_{v \in \text{Nei}(u)} w(u,v)}, \quad (4.5)$$

$$r'_s(v) = r_s(v) + \frac{(1-\alpha) \Delta w(u,v) p_s(u)}{\alpha \sum_{v \in \text{Nei}(u)} w(u,v)}. \quad (4.6)$$

After applying a sequence of updating rules above and using DYNAMICFORWARD-PUSH algorithm, then \mathbf{p}_s and \mathbf{r}_s satisfy invariant property in Lemma 14 and accurately approximate PPV. We detail the proof in Appendix 4.8.1.

From dynamic PPVs to node representations. The above theorem provides efficient rules to incrementally update PPVs for dynamic weighted graphs. To obtain dynamic node representation, two universal hash functions h_d and h_{sgn} are used (see details in [128]). In the following section, we describe how to leverage PPVs as node representation for tracking node/graph-level anomaly.

4.5.2 Anomaly Tracking Framework: DYNANOM

The key idea of our proposed framework is to measure the individual node anomaly by the embedding space based on Personalized PageRank [70, 128], and aggregate the individual anomaly scores to represent graph-level anomaly. By the fact that the PPV-based embedding space is aligned, we could directly measure the node anomaly by existing distance functions.² We describe our design in following subsections.

Node-level Anomaly Tracking

Since the inherently local characteristic of our proposed framework, we can efficiently measure the status of arbitrary nodes in two consecutive snapshots in an incrementally manner. Therefore, we could efficiently solve the problem defined in Def. 15 and localize where the anomaly actually happens by ranking the anomalous scores. To do this, the key ingredient is to measure node difference from $t-1$ to t as $\delta_s^t = f(\mathbf{x}_s^{t-1}, \mathbf{x}_s^t)$ where \mathbf{x}_s^t is the node representation of node s at time t . Based on the above motivation, we first present the node-level anomaly detection algorithm DYNANOM in Algo. 7 where the score function $f(\cdot, \cdot)$ is realized by ℓ_1 norm in our experiments. There are three key steps: *Step 1.* calculating dynamic PPVs for all nodes in S over T snapshots (Line 3); *Step 2.* obtaining node representations of S by local hash functions. Two universal hash functions³ are used in DYNNODEREP (Line 5); *Step 3.* calculating node anomaly scores based on node representation \mathbf{x}_s for all $s \in S$.

Noted that our design directly use the first-order difference (∇x_s) between two consecutive time. Although there are more complex design of $f(\cdot, \cdot)$ under this framework, such as, second-order measurement $\nabla^2 x_s$ similar as in Yoon et al. [190], clustering based anomaly detection [191], or supervised anomaly learning. We restrict our attention on the simplest form by setting $p = 1$ or 2 with the first-order measure. In our framework, the definition of anomaly score can be highly flexible for various applications.

²In this paper, we explored ℓ_1 -distance function where given \mathbf{x}, \mathbf{y} , $f(\mathbf{x}, \mathbf{y}) = \|\mathbf{x} - \mathbf{y}\|_1$.

³We use `sklearn.utils.murmurhash3_32` in our implementation.

Algorithm 7 DYNANOM($\mathcal{G}_0, \Delta E_{1, \dots, T}, \mathcal{S}, \epsilon, \alpha, p$)

```

1: Input: Initial graph  $\mathcal{G}_0$ , Edge events  $\Delta E_{1, \dots, T}$ ,
   Subset target nodes  $\mathcal{S}$ , PPV quality  $\epsilon$ , teleport
   factor  $\alpha$ .
2: //Step 1: Incrementally calculate PPVs
3:  $\mathbf{p}_{s \in \mathcal{S}} = \text{INCREMENTPUSH}(\mathcal{G}_0, \Delta E_{1, \dots, T}, \mathcal{S}, \epsilon, \alpha)$ 
4: //Step 2: Obtain node representations in target
   set  $\mathcal{S}$ 
5:  $\mathbf{x}_{s \in \mathcal{S}} = \text{DYNODEREP}(p_s^0, \dots, p_s^T)$ 
6: //Step 3: Calculate node anomaly for all nodes in  $\mathcal{S}$ 
7: for  $s \in \mathcal{S}, t \in [1, T]$  do
8:    $\delta_s^t = f(x_s^{t-1}, x_s^t) = \left( \sum_i |x_s^t(i) - x_s^{t-1}(i)|^p \right)^{1/p}$ 
9: return  $\delta_s = [\delta_s^1, \delta_s^2, \dots, \delta_s^T], \forall s \in \mathcal{S}$ 
10: procedure INCREMENTPUSH( $\mathcal{G}_0, \Delta E_{1, \dots, T}, \mathcal{S}, \epsilon, \alpha$ )
11:    $t = 0$ 
12:   for  $s \in \mathcal{S} := \{v_1, v_2, \dots, v_k\}$  do
13:      $p_s^t = \mathbf{0}, r_s^t = \mathbf{1}_s$ 
14:      $p_s^t, r_s^t = \text{DYNAMICFORWARDPUSH}(\mathcal{G}^0, s, p_s^t, r_s^t, \epsilon, \alpha)$ 
15:   for  $t \in [1, T]$  do
16:     for  $s \in \mathcal{S}$  do
17:       for  $(u, v, \Delta w_{(u, v)}) \in \Delta E_t$  do
18:         update  $p_s^t(u), r_s^t(u), r_s^t(v)$  uses rules
           in Thm. 16.
19:        $p_s^t, r_s^t = \text{DYNAMICFORWARDPUSH}(\mathcal{G}^0, s, p_s^t, r_s^t, \epsilon, \alpha)$ 
20:        $\mathcal{G}_t += (u, v, \Delta w_{(u, v)})$ 
21:       return  $\mathbf{p}_s = [p_s^0, \dots, p_s^T], \forall s \in \mathcal{S}$ 
22: procedure DYNODEREP( $p_s^0, \dots, p_s^T$ )
23:    $\epsilon_c = \min(\frac{1}{|\mathcal{V}|}, 1e-5), dim = 1024$ 
24:   for  $t \in [1, T]$  do
25:     for  $i \in \cup_{t' \in \{t, t-1\}} \text{SUPP}(p_s^{t'})$  do
26:        $p_s^{t-1}(i) = 0$  if  $p_s^{t-1}(i) \leq \epsilon_c$ 
27:        $p_s^t(i) = 0$  if  $p_s^t(i) \leq \epsilon_c$ 
28:        $x_s^t = \text{REDUCEDIM}(\frac{p_s^t}{\|p_s^t\|_1}, dim)$ 
29:        $x_s^{t-1} = \text{REDUCEDIM}(\frac{p_s^{t-1}}{\|p_s^{t-1}\|_1}, dim)$ 
30:   return  $\mathbf{x}_s = [x_s^0, \dots, x_s^T], \forall s \in \mathcal{S}$ 
31: procedure REDUCEDIM( $x, dim$ )
32:   // Hash function  $h_{dim}(i) : \mathbb{N} \rightarrow [dim]$ , ash
   function  $h_{sgn}(i) : \mathbb{N} \rightarrow \{\pm 1\}$ 
33:   if  $\text{DIM}(x) \leq dim$  then
34:     return  $x$ 
35:   else
36:      $\bar{x} = \mathbf{0} \in \mathcal{R}^{dim}$ 
37:     for  $i \in \text{SUPP}(x)$  do
38:        $\bar{x}(h_{dim}(i)) += h_{sgn}(i) \log(x(i))$ 
39:     return  $\frac{\bar{x}}{\|\bar{x}\|}$ 

```

Graph-level Anomaly Tracking

Based on the node-level anomaly score proposed in Algo. 7, we propose the graph-level anomaly. The key property we used for graph-level anomaly tracking is the linear relation property of PPV. More specifically, let $\boldsymbol{\pi}$ be the PageRank vector. We note that the PPR vector is linear to personalized vector $\boldsymbol{\pi}_s$. Therefore, global PageRank could be calculated by the weighted average of single source PPVs.

$$\boldsymbol{\pi} = \alpha \frac{\mathbf{1}}{|\mathcal{V}|} \sum_{i=0}^{\infty} (1-\alpha)^i \mathbf{P}^i = \sum_{s \in \mathcal{V}} \frac{1_s}{|\mathcal{V}|} \boldsymbol{\pi}_s = \frac{1}{|\mathcal{V}|} \sum_{s \in \mathcal{V}} \boldsymbol{\pi}_s, \quad (4.7)$$

From the above linear equality, we formulate the global PPV, denoted as $\boldsymbol{\pi}_g$, as the linear combination of single-source PPVs as following:

$$\boldsymbol{\pi}_g = \sum_{s \in \mathcal{V}} \gamma_s \boldsymbol{\pi}_s, \gamma_s = \frac{d(s)}{m}, m = \sum_{i \in \mathcal{V}} d(i) \quad (4.8)$$

In order to capture the graph-level anomaly, we use the similar heuristic weights [190] $\gamma_s = \frac{d(s)}{m}$, which implies that π_α is dominated by high degree nodes, thus the anomaly score is also dominated by the greatest status changes from high degree nodes as shown below:

$$\begin{aligned}
\|\pi_g^t - \pi_g^{t-1}\|_1 &= \left\| \sum_{s \in \mathcal{V}} \gamma_s^{t-1} \pi_s^{t-1} - \sum_{s \in \mathcal{V}} \gamma_s^t \pi_s^t \right\|_1 \\
&= \left\| \sum_{s \in \mathcal{V}} \frac{d_s^{t-1}}{m^{t-1}} \pi_s^{t-1} - \sum_{s \in \mathcal{V}} \frac{d_s^t}{m^t} \pi_s^t \right\|_1 \\
&\approx \sum_{s \in \mathcal{V}_{high}^t} \frac{d_s^t}{m^t} \|\pi_s^{t-1} - \pi_s^t\|_1 \\
&\leq \sum_{s \in \mathcal{V}_{high}^t} \|\pi_s^{t-1} - \pi_s^t\|_1, \tag{4.9}
\end{aligned}$$

where \mathcal{V}_{high}^t denotes the set of high-degree nodes. Note that the above approximated upper bound of $\|\pi_g^t - \pi_g^{t-1}\|_1$ can lower bounded by the following

$$\sum_{s \in \mathcal{V}_{high}^t} \|\pi_s^{t-1} - \pi_s^t\|_1 \geq \text{MAX}(\{\|\pi_s^{t-1} - \pi_s^t\|_1, \forall s \in \mathcal{V}_{high}^t\}). \tag{4.10}$$

By the approximation of global PPV difference in Equ. (4.10), we discover that the changes of high degree nodes will greatly affect ℓ_1 -distance, and similarly for ℓ_2 -distance. The above analysis assumes $d_s^{t-1}/m^{t-1} \approx d_s^t/m^t$. We could also hypothesize that the changes in high-degree node will flag the graph-level anomaly signal. Therefore, we propose to use high node tracking strategy for graph-level anomaly detection:

$$\text{DYNANOM}_{graph}^t := \text{MAX}(\{\|\pi_s^{t-1} - \pi_s^t\|_1, \forall s \in \mathcal{V}_{high}\}). \tag{4.11}$$

In practice, we incrementally add high degree nodes (e.g., top-50) into the tracking list from each snapshots and extract the maximum PPV changes among them as the graph-level anomaly score. This proposed score could capture the anomalous scenario where one of the top nodes (e.g., popular hubs) encounter great structural changes, similar to the DDoS attacks on the internet.

Comparison between DYNANOM and other methods.

The significance of our proposed framework compared with other anomaly tracking methods is illustrated in Table 4.2. DYNANOM is capable of detecting both node

and graph-level anomaly, supporting all types of edge modifications, efficiently updating node representations (independent of $|\mathcal{V}|$), and working with flexible anomaly score functions customized for various downstream applications.

Table 4.2: The comparison of supported features between DynAnom and other methods.

Method \ Feature	Anomaly		Edge Event Types			Algorithm		
	Node level	Graph level	Edge Stream	Add/ Delete	Weight Adjust	$ \mathcal{V} $ Ind.	Align Repr.	Flex. Score
SedanSpot	✗	✗	✓	✗	✗	✓	✗	✗
AnomRank	✗	✓	✗	✓	✓	✗	✗	✗
NetWalk	✓	✗	✗	✓	✗	✗	✗	✗
DynPPE	✓	✗	✓	✓	✗	✓	✓	✗
DynAnom	✓	✓	✓	✓	✓	✓	✓	✓

Time Complexity Analysis. The overall complexity of tracking subset of k nodes across T snapshots depends on run time of three main steps as shown in Algo. 7: 1. the run time of INCREMENTPUSH for nodes \mathcal{S} ; 2. the calculation of dynamic node representations, which be finished in $\mathcal{O}(kT|\text{supp}(\mathbf{p}_{s'})|)$ where $|\text{supp}(\mathbf{p}_{s'})|$ is the maximal support of all k sparse vectors, i.e. $|\text{supp}(\mathbf{p}_{s'})| = \max_{s \in \mathcal{S}} |\text{supp}(\mathbf{p}_s)|$. The overall time complexity of our proposed framework is stated as in the following theorem.

Theorem 17 (Time Complexity of DYNANOM). *Given the set of edge events where $\mathbb{E} = \{e_1, e_2, \dots, e_m\}$ and T snapshots and subset of target nodes \mathcal{S} with $|\mathcal{S}| = k$, the instantiation of our proposed DYNANOM detects whether there exist events in these T snapshots in $\mathcal{O}(km/\alpha^2 + k\bar{d}^t/(\epsilon\alpha^2) + k/(\epsilon\alpha) + kTs)$ where \bar{d}^t is the average node degree of current graph \mathcal{G}_t and $s \triangleq \max_{s \in \mathcal{S}} |\text{supp}(\mathbf{p}_s)|$.*

Note that the above time complexity is dominated by the time complexity of INCREMENTPUSH following from [70]. Hence, the overall time complexity is linear to the size of edge events. Notice that in practice, we usually have $s \ll n$ due to the sparsity we controlled in DYNNODEREP.

4.6 Experiments

In this section, we demonstrate the effectiveness and efficiency of DYNANOM for both node-level and graph-level anomaly tasks over three state-of-the-art baselines,

followed by one anomaly visualization of ENRON benchmark, and another case study of a large-scale real-world graph about changes in person’s life.

4.6.1 Datasets

DARPA: The network traffic graph [109]. Each node is an IP address, each edge represents network traffic. Anomalous edges are manually annotated as network attack (e.g., DDoS attack). **ENRON**[37, 139]: The email communication graph. Each node is an employee in Enron Inc. Each edge represents the email sent from one to others. There is no human-annotated anomaly edge or node. Following the common practice used in [27, 190], we use the real-world events to align the discovered highly anomalous time period. **EU-CORE:** A small email communication graph for benchmarking. Since it has no annotated anomaly, we use two strategies (Type-s and Type-W), similar to [48], to inject anomalous edge into the graph. **EU-CORE-S** includes anomalous edges, creating star-like structure changes in 20 random snapshots. Likewise, **EU-CORE-L:** is injected with multiple edges among randomly selected pair of nodes, simulating node-level local changes. We describe details in appendix. 4.8.5. **Person Knowledge Graph (PERSON):** We construct PERSON graph from EventKG [60, 61]. Each node represents a person or an event. The edges represent a person’s participation history in events with timestamps. The graph has no explicit anomaly annotation. Similarly, we align the detected highly anomalous periods of a person with the real-world events, which reflects the person’s significant change as his/her life events update. We summarize the statistics of dataset in the following table:

Table 4.3: Dataset Statistics. Graphs are converted into undirected by repeating edges with reversed source and destination node. We detect anomalies after the initial snapshot (Init. t).

Dataset	DARPA	EU-CORE	ENRON	PERSON
$ V $	25,525	986	151	609,930
$ E $	4,554,344	333,734	50,572	8,782,630
$ \mathcal{G}_{0,\dots,T} $	1463	115	1138	43
Init. t	256	25	256	20

4.6.2 Baseline Methods

We compare our proposed method to four representative state-of-the-art methods over dynamic graphs: **Graph-level method: AnomRank**[190]⁴ uses the global Personalized PageRank and use 1-st and 2-nd derivative to quantify the anomaly score of graph-level. We use the node-wise AnomRank score for the node-level anomaly, **Edge-level method: SadenSpot** [48] approximates node-wise PageRank changes before and after inserting edges as the edge-level anomaly score. **Node-level method: NetWalk** [191] incrementally updates the node embeddings by extending random walks. However, since the *anomaly* defined in the original paper is the outlier in each static snapshot, we re-alignment [62, 169] NetWalk embeddings and apply ℓ_2 -distance for node-level anomaly.⁵

Node-level DynPPE [70] used the local node embeddings based on PPVs for unweighted graph. We extend its core PPV calculation algorithm for weighted graphs. The detailed hyper-parameter settings are listed in Table 4.9 in appendix. In the following experiment, we demonstrate that our proposed algorithm significantly outperform over the strong baselines.

4.6.3 Exp1: Node-level Anomaly Localization

Experiment Settings: As detailed in Def.15, given a sequence of graph snapshots $\mathcal{G} = \{\mathcal{G}_0, \mathcal{G}_1, \dots, \mathcal{G}_T\}$ and a tracked node subset $\mathcal{S} = \{u_0, u_1, \dots, u_i\}$. We denote the set of anomalous snapshots of node u as ground-truth, such that \mathbf{Y}_u , containing k_u timestamps where there is at least one new anomalous edge connected to node u in that time. We calculate the node anomaly score for each node. For example for node u : $\delta_u = \{\hat{\delta}_u^1, \hat{\delta}_u^2, \dots, \hat{\delta}_u^T\}$, and rank its anomaly scores across time. Finally, we use the set of the top- k_u highest anomalous snapshots $\hat{\mathbf{Y}}_u$ as the predicted anomalous snapshot⁶ and calculate the averaged prediction precision over all nodes as the final performance measure as shown below:

$$Precision_{avg} = \frac{1}{|\mathcal{S}|} \sum_{u \in \mathcal{S}} \frac{|\hat{\mathbf{Y}}_u \cap \mathbf{Y}_u|}{|\hat{\mathbf{Y}}_u|}$$

⁴We discovered potential bugs in the official code, which make the results different from the original paper. We have contacted authors for further clarification.

⁵We use Procrustes analysis to find optimal scale, translation and rotation to align

⁶In experiment, we assume that the number of anomalies is known for each node to calculate the prediction precision.

For DARPA dataset, we track 151 nodes⁷ which have anomalous edges after initial snapshot. Similarly we track 190,170 anomalous nodes over EU-CORE-S and EU-Core-L. We exclude edge-level method SedanSpot for node-level task because it can not calculate node-level anomaly score. We present the precision and running time in Table 4.4 and Table 4.5.

Table 4.4: The average precision of node-level anomaly localization. Our proposed DYNANOM outperforms other baselines.

	DARPA	EU-CORE-S	EU-CORE-L
Random	0.0075	0.0142	0.0088
AnomRank	0.2790	0.2173	0.4019
AnomRankW	0.2652	0.2213	0.4078
NetWalk	OOM	0.0421	0.0416
DynPPE	0.1701	0.2478	0.2372
DynAnom	0.5425	0.4242	0.5215

Effectiveness. In Table 4.4, the low scores of *Random*⁸ demonstrate the task itself is very challenging. We note that our proposed DYNANOM outperforms all other baselines, demonstrating its effectiveness for node-level anomaly tracking.

Scalability. NetWalk hits Out-Of-Memory (OOM) on DARPA dataset due to the Auto-encoder (AE) structure where the parameter size is related to $|\mathcal{V}|$. Specifically, the length of input/output one-hot vector is $|\mathcal{V}|$, making it computationally prohibitive when dealing with graphs of even moderately large node set. Moreover, since the AE structure is fixed once being trained, there is no easy way to incrementally expand neural network to handle the new nodes in dynamic graphs. While DYNANOM can easily track with any new nodes by adding extra dimensions in $\mathbf{p}_s, \mathbf{r}_s$ and \mathbf{d} and apply the same procedure in an online fashion.

Power of Node-level Representation. The core advantage of DYNANOM over AnomRank(W) is the power of node-level representation. AnomRank(W) essentially represents individual node’s status by one element in the PageRank vector. While DYNANOM uses node representation derived from PPVs, thus having far more expressivity and better capturing node changes over time.

Advantage of Aligned Space. Despite that NetWalk hits OOM on DARPA

⁷We track totally 200 nodes, but 49 nodes have all anomalous edges before the initial snapshot, so we exclude them in precision calculation.

⁸For Random baseline, we randomly assign anomaly score for each node across snapshots

dataset, we hypothesize that the reason of its poor performance on EU-CORE{S,L} is the embedding misalignment. The incremental training makes the embedding space not directly comparable from time to time even after extra alignment. Although it’s useful for classification or clustering within one snapshot, the misaligned embeddings may cause troublesome overhead for downstream tasks, such as training separate classifiers for every snapshot.

Importance of Edge Weights. Over all datasets, our proposed DYNANOM consistently outperforms DynPPE, which is considered as the unweighted counterpart of DYNANOM. It demonstrates the validity and versatility of our proposed framework.

Table 4.5: For comparing running time (in seconds), excluding the time for data loading and graph update.

	DARPA	EU-CORE-S	EU-CORE-L
AnomRank(W)	905.983	26.084	26.865
NetWalk	OOM	3649.14	3644.58
DynPPE	84.247	33.835	30.933
DynAnom	379.334	30.054	26.359

Efficiency. Table 4.5 presents the wall-clock time ⁹. Deep learning based NetWalk is the slowest. Although it can incrementally update random walk for the new edges, it has to re-train or fine-tune for every snapshot. At the first glance, DynPPE achieves the shortest running time on DAPRA dataset, but it is an illusive victory caused by dropping numerous multi-edge updates at the expense of precision. Furthermore, the Power Iteration-based AnomRank(W) is slow on DARPA as we discussed in Section 4.3, but the speed difference may not be evident when the graph is small (e.g., DARPA has 25k nodes, and EU-CORE has less than 1k nodes). Moreover, our algorithm can independently track individual nodes as a result of its local characteristic, it could be further speed up by embarrassingly parallelization on a computing cluster with massive cores.

⁹We track function-level running time by CProfile, and remove those time caused by data loading and dynamic graph structure updating

4.6.4 Exp2: Graph-level Anomaly Detection

Experiment Setting: Given a sequence of graph snapshots $\mathcal{G} = \{\mathcal{G}_0, \mathcal{G}_1, \dots, \mathcal{G}_T\}$, we calculate the snapshot anomaly score and consider the top ones as anomalous snapshots, adopting the same experiment settings in [190]. We use both ℓ_1 and ℓ_2 as distance function to test the practicality of DYNANOM. We modify edge-level SedanSpot for Graph-level anomaly detection by aggregating edge anomaly score with $\text{MEAN}()$ ¹⁰ in each snapshot. We describe detailed hyper-parameter settings in Appendix. 4.8.4. For DAPRA dataset, as suggested by Yoon et al. [190], we take the precision at top-250¹¹ as the performance measure in Table 4.6, and present Figure 4.3 of recall-precision curves as we vary the parameter $k \in \{50, 100, \dots, 800\}$ for top- k snapshots considered to be anomalous.

Practicality for Graph-level Anomaly: The precision-recall curves show that DYNANOM have a good trade-off, achieving the competitive second/third highest precision by predicting the highest top-150 as anomalous snapshots, and the precision decreases roughly at a linear rate when we includes more top- k snapshots as anomalies. Table 4.6 presents the precision at top-250, and we observe that DYNANOM could outperform all other strong baselines, including its unweighted counterpart – DYNPPE. It further demonstrates the high practicality of the proposed flexible framework even with the simplest ℓ_1 and ℓ_2 distance function.

ENRON graph records the emails involved in the notorious Enron company scandal, and it has been intensively studied in [27, 48, 190]. Although ENRON graph has no explicit anomaly annotation, a common practice [27, 189] is to visualize the detected anomaly score against time and discover the associated real-world events. Likewise, Figure 4.4 plots the detected peaks side-by-side with other strong baselines¹². We find that DYNANOM shares great overlaps with meaningful peaks and detects more prominent peak at Marker.1 when Enron got investigated for the first time, demonstrating its effectiveness for sensible change discovery. For better interpretation, we annotate the peaks associated to the events collected from the Enron Timeline¹³, and present some milestones as followings:

¹⁰For a fair comparison, we tried $\{\text{Mean}(), \text{Median}(), \text{Min}(), \text{Max}()\}$ operators for SedanSpot, and found that $\text{Mean}()$ yields the best results.

¹¹ $k = 250$ reflects its practicality since it is the closest k without exceeding total 288 graph-level anomalies

¹²All values are post-processed by dividing the maximum value. For SedanSpot, we use $\text{Mean}()$ to aggregate edge anomaly score for the best visualization. Other aggregator (e.g., $\text{Max}()$) may produce flat curve, causing an unfair presentation.

¹³Full events are included in Table 4.7 in Appendix. Enron timeline: <https://www.agsm.edu.au/bobm/teaching/BE/Enron/timeline.html>

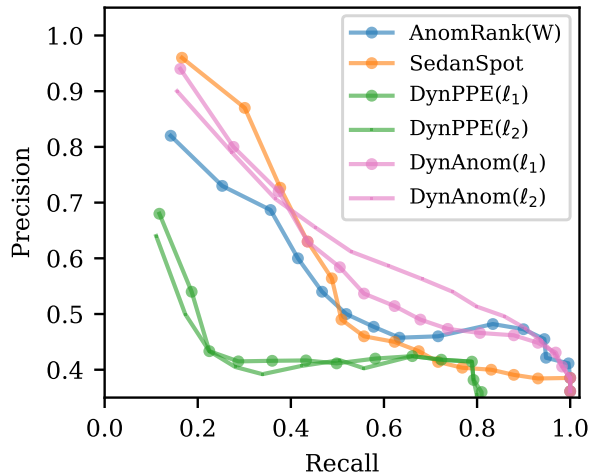


Figure 4.3: Precision-Recall Curve

Table 4.6: The precision of top-250 anomalies

Algorithms	Precision
NetWalk	OOM
AnomRankW	0.5400
SedanSpot	0.5640
DynPPE(ℓ_1)	0.4160
DynPPE(ℓ_2)	0.3920
DynAnom(ℓ_1)	0.5840
DynAnom(ℓ_2)	0.6120

- 1 :(2000/08/23) Investigated Enron when stock was high.
- 6 :(2001/08/22) CEO was warned of accounting irregularities.
- 10 :(2002/01/30) CEO was replaced after bankruptcy.

4.6.5 Case Study: Localize Changes in Person’s Life over Real World Graph

To demonstrate the scalability and usability of DYNANOM, we present an interesting case study over our constructed large-scale PERSON graph, which records the structure and intensity of person-event interaction history. We apply DYNANOM to track public figures (Joe Biden, Arnold Schwarzenegger, Al Franken) of the U.S. from 2000 to 2022 on a yearly basis, and visualize their changes by ℓ_1 -distance, together with annotated peaks in Figure 4.5.

As we can see, *Biden* has his greatest peak in year 2008 when he became the 47-th U.S. Vice President for the very first time, which is considered to be his first major advancement. The second peak occurs in 2012 when he won the re-election. This time the peak has smaller magnitude because he was already the VP, thus the re-election caused less difference in him, compared to his transition in 2008. The third peak is in 2020 when he became the president, the magnitude is even smaller as he had been the VP for 8 years without huge context changed. Similarly, the middle sub-figure captures *Arnold Schwarzenegger*’s transition to be California

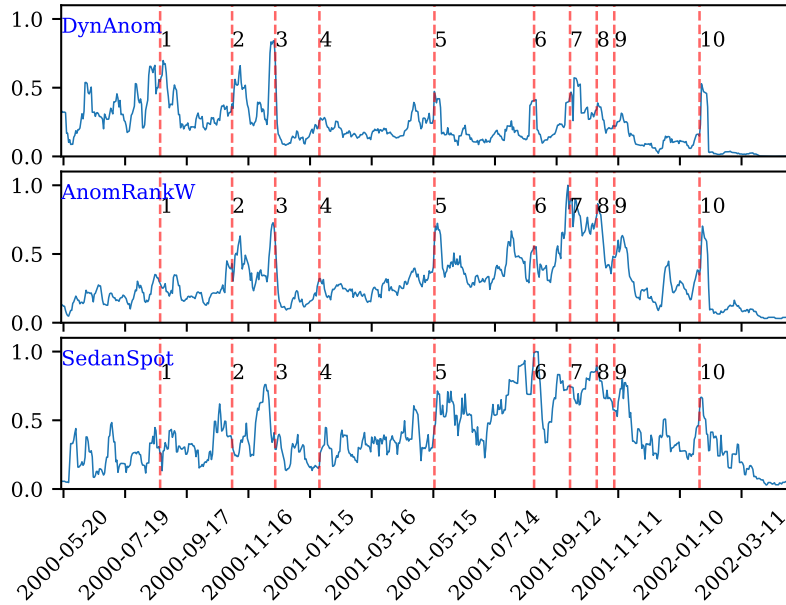


Figure 4.4: The anomaly scores of ENRON graph. DYNANOM well correlates with other baselines, and detect novel peaks at beginning.

Governor in 2003, and high activeness in election years. *Al Franken* is also a famous comedian who shifted career to be a politician in 2008, the peaks well capture the time when he entered political area and the election years. Table 4.8 lists full events in Appendix 4.8.3. This resources could bring more opportunities for knowledge discovery and anomaly mining studies in the graph mining community.

Moreover, based on our current Python implementation, it took roughly 37.8 minutes on a 4-core CPU machine to track the subset of three nodes over the PERSON graph, which has more than 600k nodes and 8.7 million edges. Both presented results demonstrate that our proposed method has great efficiency and usability for practical subset node tracking.

4.7 Discussion and Conclusion

In this paper, we propose an unified framework DYNANOM for subset node anomaly tracking over large dynamic graphs. This framework can be easily applied to different graph anomaly detection tasks from local to global with a flexible score function customized for various application. Experiments show that

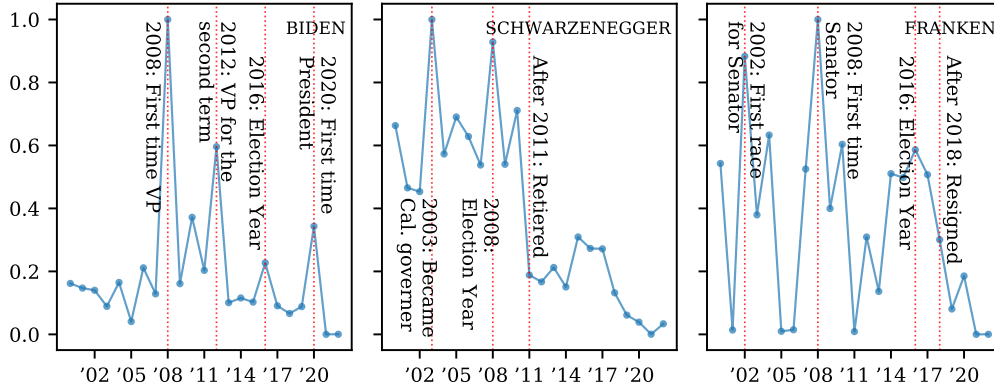


Figure 4.5: The yearly changes of public figures in PERSON graph from 2000-2022: The detected peaks are well correlated to the major events of the individuals as we annotated.

our proposed framework outperforms current state-of-the-art methods by a large margin, and has a significant speed advantage (2.3 times faster) over large graphs. We also present a real-world PERSON graph with an interesting case study about personal life changes, providing a rich resource for both knowledge discovery and algorithm benchmarking. For the future work, it remains interesting to explore different type of score functions, automatically identify the interesting subset of nodes as better strategies for tracking global-level anomaly, and further investigate temporal-aware PageRank as better node representations.

4.8 Appendix

4.8.1 Proof of Weighted Dynamic Push

Proof. By the invariant property in Lemma 14, we have

$$p_s(i) + \alpha r_s(i) = (1 - \alpha) \sum_{x \in N^{in}(i)} \frac{w_{(x,i)} p_s(x)}{d(x)} + \alpha \times 1_{i=s}, \forall i \in \mathcal{V}, \quad (4.12)$$

Initially, this invariant holds and keeps $\frac{r_s(i)}{d(i)} \leq \epsilon$ after applying Algo.6. When the new edge $(u,v, \Delta w_{(u,v)})$ arrives, it changes the out-degree of u , breaking up the balance for all invariant involving $d(u)$. Our goal is to recover such invariant by adjusting small amount of p_s, r_s . While such adjustments may compromise

the quality of PPVs, we could incrementally invoke Algo.6 to update p_s and r_s for better accuracy afterwards. We denote the initial vectors as p_s, r_s, d and post-change vectors as p'_s, r'_s, d' .

As $d'(u)$ is involved in $p_s(u)/d'(u)$, one need to have $p'_s(u)$ such that $p_s(u)/d(u) = p'_s(u)/d'(u)$, i.e. the invariant maintenance of Equ. (4.12). The updated amount of weight is $\delta w_{(u,v)}$, which indicates $p'_s(u) = (d(u) + \Delta w_{(u,v)})p_s(u)/d(u)$. So, we have

$$p'_s(u) = p_s(u) \frac{\sum_{v \in \text{Nei}(u)} w_{(u,v)} + \Delta w_{(u,v)}}{\sum_{v \in \text{Nei}(u)} w_{(u,v)}}. \quad (4.13)$$

Hence, we reach Equ. 4.13 implies that we should scale up $p_s(u)$ to recover balance. This strategy is the general case of Zhang et al. [194] for unweighted graphs where $\Delta w_{(u,v)} = 1$.

However, once we assign $p'_s(u)$, it breaks the invariant for u since $p_s(u) + \alpha r_s(u) \neq p'_s(u) + \alpha r_s(u)$. Likewise, we maintain this equality by introducing $r'_s(u)$:

$$\begin{aligned} p_s(u) + \alpha r_s(u) &= p'_s(u) + \alpha r'_s(u) \\ &\text{Substitute } p'_s(u) \text{ from eq.4.4} \\ &= p_s(u) + \frac{\Delta w_{(u,v)} p_s(u)}{d(u)} + \alpha r'_s(u), \\ \implies \alpha r'_s(u) - \alpha r_s(u) &= -\frac{\Delta w_{(u,v)} p_s(u)}{d(u)}, \\ r'_s(u) &= r_s(u) - \frac{\Delta w_{(u,v)} p_s(u)}{\alpha d(u)} \end{aligned} \quad (4.14)$$

Equ. (4.14) implies that we should decrease $r_s(u)$. From a heuristic perspective, it's consistent to the behavior of BCA-algorithm which keeps taking mass from r_s to p_s . In this updating case, we artificially create mass for p'_s at the expense of r_s 's decrements. When $\Delta w_{(u,v)} = 1$ in case of unweighted graphs, this update rule is also equivalent to Zhang et al. [194].

So far, we have the updated $p'_s(u)$ and $r'_s(u)$ so that all nodes (without direct edge update, except for v) keep the invariant hold. However, due to the introduction of $\Delta w_{(u,v)}$, the shares of mass pushed to v is changes, breaking the invariant for v as shown below:

$$\begin{aligned} p_s(v) + \alpha r_s(v) &\neq (1 - \alpha) \left(\frac{(w_{(u,v)} + \Delta w_{(u,v)}) p'_s(u)}{d'(u)} \right. \\ &\quad \left. + \sum_{x \in N^{in}(v) \setminus \{u\}} \frac{w_{(u,x)} p_s(x)}{d(x)} \right) + \alpha \times 1_{t=s} \end{aligned}$$

In order to recover the balance with minimal effort, we should update $r_s(v)$ instead of $p_s(v)$. The main reason is that any change in $p_s(v)$ will break the balance for v 's neighbors, similar to the breaks incurred by the change of $p_s(u)$. We present the updated $r'_s(v) = r_s(v) + \Delta$ as following:

$$p_s(v) + \alpha(r_s(v) + \Delta) = (1 - \alpha) \left(\frac{\Delta w_{(u,v)} p'_s(u)}{d'(u)} + \sum_{x \in N^{in}(v)} \frac{w_{(u,x)} p_s(x)}{d(x)} \right) + \alpha 1_{t=s}. \quad (4.15)$$

Note that $p'_s(u)/d'(u) = p_s(u)/d(u)$, and

$$p_s(v) + \alpha r_s(v) = (1 - \alpha) \sum_{x \in N^{in}(v)} \frac{w_{(x,v)} p_s(x)}{d(x)}.$$

Reorganize Equ. (4.15) and cancel out $p_s(v), r_s(v)$, we have

$$\Delta = \frac{(1 - \alpha) \Delta w_{(u,v)} p_s(u)}{\alpha d(u)} \\ r'_s(v) = r_s(v) + \frac{(1 - \alpha) \Delta w_{(u,v)} p_s(u)}{\alpha d(u)} \quad (4.16)$$

Combining Equ. (4.13), (4.14), and (4.16), we prove the theorem. \square

Remark 18. *The above proof mainly follows from [194] where unweighted graph is considered while we consider weighted graph in our problem setting.*

4.8.2 Proof of Time Complexity

Before we proof the theorem, we present the known time complexity of INCREMENTPUSH as in the following lemma.

Lemma 19 (Time complexity of INCREMENTPUSH [70]). *Suppose the teleport parameter of obtaining PPR is α and the precision parameter is ϵ . Given current weighted graph snapshot \mathcal{G}_t and a set of edge events ΔE_t with $|\Delta E_t| = m$, the time complexity of INCREMENTPUSH is $\mathcal{O}(m/\alpha^2 + \bar{d}^t/(\epsilon\alpha^2) + 1/(\epsilon\alpha))$ where \bar{d}^t is the average node degree of current graph \mathcal{G}_t .*

Proof. The total time complexity of our instantiation DYNANOM has components, which correspond to three steps in Algo. 7. The run time of step 1, INCREMENT-PUSH is $\mathcal{O}(m/\alpha^2 + \bar{d}^t/(\epsilon\alpha^2) + 1/(\epsilon\alpha))$ by Lemma 19. The run time of step 2, DYNNODEREP is bounded by $\mathcal{O}(n)$ as the component of DYNNODEREP is the procedure of the dimension reduction by using two hash functions. The calculation of two has functions given \mathbf{p}_s is linear on $|\text{supp}(\mathbf{p}_s)|$, which is $|\text{supp}(\mathbf{p}_s)| \leq n$. Finally, the instantiation of our score function is also linear on n . Therefore, the whole time complexity is dominated by $\mathcal{O}(km/\alpha^2 + k\bar{d}^t/(\epsilon\alpha^2) + k/(\epsilon\alpha) + kTs)$ where s is the maximal allowed sparsity defined in the theorem. We proof the theorem. \square

4.8.3 Timelines of real world graphs

We list the real-world events for the ENRON and PERSON graph in table 4.7 and 4.8.

4.8.4 Hyper-parameter Settings

we (re)implement the algorithms in Python to measure comparable running time. We list the hyper-parameter in Table 4.9.

4.8.5 Experiment Details

Infrastructure: We conduct our experiment on machine with 4-core Intel i5-6500 3.20GHz CPU, 32 GB memory, and GeForce GTX 1070 GPU (8 GB memory) on Ubuntu 18.04.6 LTS.

Datasets: For DARPA dataset: we totally track 200 anomalous nodes, and 151 of them have at least one anomalous edge after initial snapshot, the ground-truth of node-level anomaly is derived from the annotated edge as aforementioned. For EU-CORE dataset: Since EU-CORE dataset does not have annotated anomalous edges, we randomly select 20 snapshots to inject artificial anomalous edges using two popular injection methods, which are similar to the approach used in [190]. For each selected snapshot in *EU-CORE-S*, we uniformly select one node, u_{high} , from the top 1% high degree nodes, and injected 70 multi-edges connecting the selected node to other 10 random nodes which were not connected to u_{high} before, which simulates the structural changes. In each selected snapshot in *EU-CORE-L*, we uniformly select 5 pairs of nodes, and injected edge connect each pair with totally 70 multi-edges as anomaly, which simulates the sudden peer-to-peer communication. We include all datasets in our supplementary materials.

Table 4.7: The events in Enron scandal timeline

Index	Date	Event Description
1	2000/08/23	Stock hits all-time high of \$90.56. the Federal Energy Regulatory Commission orders an investigation.
2	2000/11/01	FERC investigation exonerates Enron for any wrongdoing in California.
3	2000/12/13	Enron announces that president and chief operating officer Jeffrey Skilling will take over as chief executive in February. Kenneth Lay will remain as chairman.
4	2001/01/25	Analyst Conference in Houston, Texas. Skilling bullish on the company. Analysts are all convinced.
5	2001/05/17	"Secret" meeting at Peninsula Hotel in LA – Schwarzenegger, Lay, Milken.
6	2001/08/22	Ms Watkins meets with Lay and gives him a letter in which she says that Enron might be an "elaborate hoax."
7	2001/09/26	Employee Meeting. Lay tells employees: Enron stock is an "incredible bargain." "Third quarter is looking great."
8	2001/10/22	Enron acknowledges Securities and Exchange Commission inquiry into a possible conflict of interest related to the company's dealings with the partnerships.
9	2001/11/08	Enron files documents with SEC revising its financial statements to account for \$586 million in losses. The company starts negotiations to sell itself to head off bankruptcy.
10	2002/01/30	Stephen Cooper takes over as Enron CEO.

Table 4.8: The person events of *Schwarzenegger* and *Franken*

Year	Major Event
Arnold Schwarzenegger	
2003	Arnold Schwarzenegger won the California gubernatorial election as his first politician role
2008	Arnold began campaigning with McCain as the key endorsement for McCain’s presidential campaign
2010	mid-term election
2011	Arnold reached his term limit as Governor and returned to acting
Al Franken	
2002	Al Franken consider his first race for office due to the tragedy of Minnesota Sen. Paul Wellstone.
2004	The Al Franken Show aired
2007	Al Franken announced for candidacy for Senate.
2008	Al Franken won election.
2012	Al Franken won re-election.
2018	Al Franken resigned

Table 4.9: The hyper-parameter configurations of algorithms in experiments.

Algorithm	Hyper-parameter Settings
AnomRank	alpha = 0.5 (default) , epsilon = 1e-2 (default) or 1e-6 (for better accuracy)
SedanSpot	sample-size = 500 (default settings)
NetWalk	epoch_per_update=10, dim=128, default settings for the rest parameters
DynAnom and DynPPE	For exp1 and exp2: alpha = 0.15, minimum epsilon = 1e-12 , dim=1024; For exp2: we keep track of the top-100 high degree nodes for graph-level anomaly. For case studies: alpha = 0.7, the rest are the same.

Chapter 5

Efficient Contextual Node Representation Learning over Dynamic Graphs ¹

5.1 Introduction

Many real-world graphs evolve with structural changes[76, 178] and node attributes refinement over time. Considering Wikipedia as an evolving graph where Wiki pages (nodes) are interconnected by hyperlinks, each node is associated with the article’s descriptions as attributes. For example, the node "*ChatGPT*" initially ² contained only had a few links redirecting to the nodes *OpenAI* and *Chatbot*, before being gradually enriched ³ with more hyperlinks and detailed descriptions. Such examples motivate the following problem:

How can we design an **efficient** and **robust** node representation learning model that can be updated quickly to reflect graph changes, even when node attributes are limited or noisy?

The proposed problem consists of two parts– **1)**: how to design a high-quality and robust node representation algorithm and **2)**: how to efficiently update the

¹Xingzhi Guo, Baojian Zhou, and Steven Skiena. Efficient Contextual Node Representation Learning over Dynamic Graphs. In Submission.

²The initial ChatGPT Wikipedia page: <https://en.wikipedia.org/w/index.php?title=ChatGPT&oldid=1125621134>

³The refined ChatGPT Wikipedia page shortly after the creation: <https://en.wikipedia.org/w/index.php?title=ChatGPT&oldid=1125717452>

node representation along with the graph changes.

One possible approach is through Graph Neural Networks (GNNs). Pioneered by SGC[181], APPNP [54], PPRGo[23], and AGP [170], they replace recursive local message passing with an approximate feature propagation matrix. For example, SGC formulates the node classification problem into $\bar{\mathbf{y}} = \text{Softmax}(\mathbf{S}^k \mathbf{X} \Theta)$ where \mathbf{S}^k is the k^{th} power of the normalized adjacency matrix, \mathbf{X} is the node attribute matrix and Θ is the learnable classifier parameter. This formulation decouples propagation from the learning process because \mathbf{S}^k can be explicitly calculated independent of the neural model.

More importantly, this formulation provides a novel interpretation of GNN as a feature propagation process, opening doors to new propagation mechanism designs. In particular, Personalized PageRank (PPR) is a popular choice, and PPR-based models significantly improve GNN’s efficiency and scalability. However, our interested problem is in dynamic settings. Although one can naively train multiple GNNs on every graph snapshot, the efficiency is compromised because they are designed for static graphs and have to re-calculate the propagation from scratch as the graph changes over time.

Recently, several works [53, 69, 73, 202] have adopted PPR in dynamic graph learning, and use incremental PPR maintenance algorithm [194] to update PPR as the graph evolves. Despite the fact that PPR is a very successful vertex proximity measure and provides great empirical performance, there is no clear formal framework to justify the choice of using PPR, and little theoretical guidance on the propagation mechanism design. In addition, the PPR-based GNN’s efficiency largely depends on the PPR solver’s speed. To our best knowledge, all the previous works favored *ForwardPush* as the underlying PPR method, which still has a large room for improvement, especially under dynamic settings.

On the other hand, recent research [51, 52] proposed a variational formulation of PPR as an explicit ℓ_1 -regularized quadratic optimization problem. Different from the traditional PPR interpretation as the random surfer model that can be solved algorithmically by power iteration[123] and *ForwardPush* [9], the PPR-equivalent ℓ_1 -regularized optimization problem bridges two seemingly disjoint subjects (graph learning and optimization). One benefit is that this well-defined PPR-equivalent optimization problem can be solved efficiently by standard proximal gradient methods such ISTA and FISTA[13, 41], which have great potential for more efficient GNNs. Most importantly, the ℓ_1 -regularization reveals PPR’s inherent sparse property, which is similar to the well-known *LASSO* regression [157] and online learning [196–198, 203?] for robustness and interpretability. While *LASSO* keeps the most important subset of feature dimensions, the ℓ_1 -regularizer

in PPR enforces to only keep a subset of active or important nodes, especially in large graphs. Therefore, the resulting models are robust by only aggregating the most important *local* features.

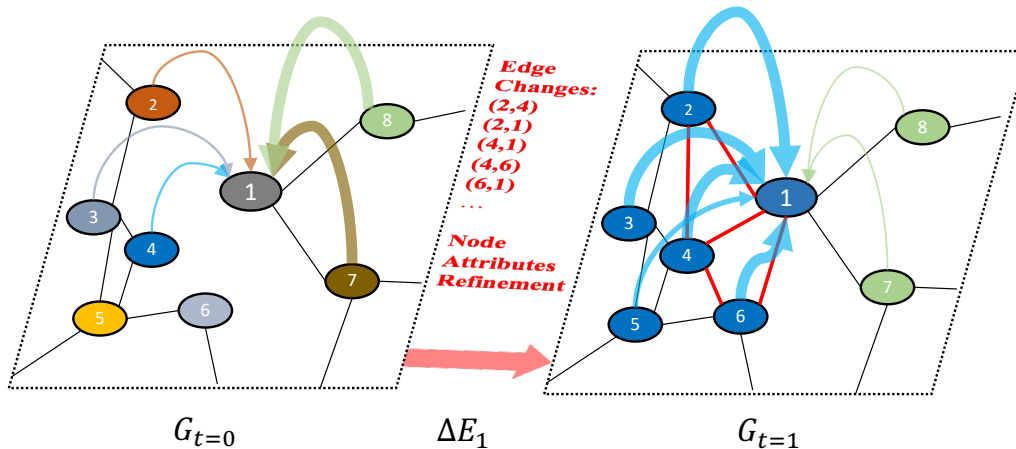


Figure 5.1: A cartoon illustrating contextualized node representation over a dynamic graph. In the beginning, the graph has few edges (black line) and relatively noisy node attributes (various colors). For example, the node u_1 only has two edges and receives features (arrows over nodes) mainly from the right-hand side. As the graph evolves, the edges and node attributes become more complete, represented by red new edges and more consistent colored attributes. Accordingly, the node-wise attention for u_1 changes, favoring the nodes on its left side. We adopt u_1 's Personalized PageRank or π_1 as the attention design which is sparse, informative, and can be justified by our proposed desired properties in our framework.

These findings inspire us to formulate PPR-based GNNs as a unified contextual node representation learning framework (shown in Figure 5.1) together with a new design of node positional encodings. Within this framework, we propose an elegant and fast solution to maintain PPR as the graph evolves and discuss several desired properties to justify the PPR choice with the theoretical ground. Finally, we instantiate a simple-yet-effective model (GOPPE) which has PPR-based node positional encodings, making the representation robust and distinguishable even when the node attributes are very noisy. The experiments demonstrate the potential of this framework for tackling the dynamic graph problem we are interested in.

We summarize our main contributions as follows:

- *A novel contextual node representation framework for dynamic graphs* – We propose a unified framework based on global node attention, which can

explain the designs in the STOA propagation-based GNNs. We identify the desired properties (e.g., attention sparsity, bounded ℓ_p -norm, update efficiency) for the attention design, providing a guideline to justify the use of PPR and for designing the future attention-based GNN.

- *Improved efficiency of PPR-based dynamic GNNs through an optimization lens* – Inspired by the new PPR optimization formulation, we improve the efficiency of PPR-based GNNs using the proximal gradient methods, specifically *Iterative Shrinkage-Thresholding Algorithm* or *ISTA*, demonstrating roughly three times speedup in dynamic settings.
- *Instantiating GOPPE: a simple, effective and robust method* – Within the proposed framework, we instantiate GOPPE, a simple-yet-effective method which is comparable in quality to and faster than the STOA baselines. Specifically, our novel PPR-based node positional encodings and the attention-based framework significantly outperform on noisy graphs, demonstrating its robustness against noise attributes during graph evolution.

The rest of this paper is organized as follows: Section 5.2 clarifies different settings for dynamic graphs. Section 5.3-5.4 discuss the preliminaries and problem formulation. We present our proposed node contextual learning framework in Section 5.5, and discuss experimental results in Section 5.6. Finally, we conclude and discuss future directions in Section 6.5. *We have made our code accessible at <http://bit.ly/3JQCUCX> for review and will make it publicly available upon publication.*

5.2 Related Work

Learning over dynamic graphs is an emerging topic, and has been studied from three perspectives with different problem settings:

Co-evolution Models over Dynamic Graphs: The problem of dynamic co-evolution focuses on the relations between node attributes and the growing network topology. For example, DynRep [160] is the pioneering model. A typical task is to predict whether two vertices will be connected or interact in the future given the current graph topology and the node attributes. The key is to learn a node-wise relation model to represent the interaction probability among vertices, rather than updating the node embedding w.r.t. the graph changes. Due to the nature of $\mathcal{O}(|\mathcal{V}|^2)$ complexity, these models are not scalable when the node size is large.

Node Time Series Models over Dynamic Graphs: Several temporal GNNs [138, 142, 183] have been proposed for modeling the node embeddings w.r.t. the graph changes in *discrete or continuous time*, then predict the anomaly using time series analysis [196–198]. A typical example is JODIE[105], which models the *trajectory* of node embeddings across time and predicts its *position* at a future timestamp. Similar to the co-evolution models, the essence is to obtain a compact embedding from the node history, and use it to extrapolate for future prediction. However, these models cannot update node embeddings quickly and usually involve data re-sampling and model fine-tuning while the graph changes.

Maintainable Node Embeddings Models over Dynamic Graphs: Maintainable or incremental node embedding models focus on efficient embedding updates as the graph changes. Starting from the dynamic network embeddings which do not consider the node’s raw attributes, previous works focus on online matrix factorization methods (e.g., incremental SVD [25]), and incremental fine-tuning algorithms to adapt the static node embedding algorithms into dynamic (e.g., NetWalk[191]). However, they are not scalable because of the embedding dependency issue. For example, using the re-sample and fine-tune strategy, one must update all node embeddings *globally* to have one node embedding updated.

Fortunately, *localized* node embedding algorithms [69, 73, 128] adopt PPR which can be calculated for a subset of nodes individually with the complexity independent of node size. Meanwhile, one node’s PPR is incrementally updatable and avoids calculating from scratch when the graph updates. Due to PPR’s nature of local computation and maintainability, there have been follow-up works on the applications of efficient node anomaly tracking and efficient feature propagation GNNs over dynamic graphs. Specifically, DynPPE [69] employs incremental FORWARDPUSH algorithm to maintain PPR and apply local hashing method to obtain high-quality PPR-based embeddings, showing promising results in both node classification and anomaly tracking tasks. Another recent development is INSTANTGNN [202], which applies the same incremental PPR solver, but uses PPR as the feature aggregation weights for GNNs design. Like its counterparts for static graphs (PPRGO [23] and AGP [170]), the model obtains high-quality node representation while achieving high efficiency with the increment PPR algorithm.

Our approach: Following this research line, we are curious about how to justify PPR as a good design choice for dynamic GNNs. Despite the fact that it can be interpreted as a specific GNN design with infinite layers, what are the desired properties (e.g., sparsity, locality) for one propagation mechanism to be suitable and efficient? We seek to propose such properties within a contextual graph learning framework, justify PPR as a good choice and provide guidelines for future GNN designs.

In addition, as PPR has been widely adopted with FORWARDPUSH as its solver, we are curious about its efficiency under various dynamic settings (e.g., with large/small graph changes), and how to further improve GNN’s efficiency. Finally, as the motivating scenario suggests, since the node attributes may be noisy during graph evolution, we aim to build a robust node representation against noisy attributes. Specifically, we can re-use PPR (previously as the node attention) and convert it as node positional encodings with constant computation cost.

Table 5.1: Different STOA models can be realized within the proposed framework of various design choices. a : PPRGO only selects the top- k PPR as attention weights. b: INSTANTGNN uses the generalized transitional matrix $D^\alpha \mathbf{A} D^{1-\alpha}$. c: "S" stands for Static PPR calculated from scratch in each snapshot. d: "D" means maintain PPR dynamically or incrementally.

Method	Dynamic	Attribute	Attention	PE	Solver
INSTANTEMB.	✗	✗	✗	PPR	Push-S ^c
PPRGO	✗	✓	PPR ^a	✗	Push-S
DYNAMICPPE	✓	✗	✗	PPR	Push-D ^d
INSTANTGNN	✓	✓	PPR ^b	✗	Push-D
GoPPE-{S,D}	✓	✓	PPR	PPR	ISTA-{S,D}

5.3 Preliminaries

5.3.1 Message Passing as Approx. Propagation

In many successful and popular GNNs designs [78, 101], the node attributes \mathbf{x}_i serve as the message or graph signal, propagating to its local neighbors $\text{Nei}(v_i)$ defined explicitly by the network structure \mathcal{G} . Meanwhile, v_i locally *convolutes* the incoming neighbors’ messages as its hidden representation, denoted as \mathbf{h}_i . Typically, a set of trainable convolutional kernels $\mathbf{W}^{(l)} \in \mathbb{R}^{h \times d}$ is used in a permutation-invariant function recursively (l is the recursion level). For example, $\mathbf{h}_i^{(l+1)} = \frac{1}{d_i} \sum_{j \in \text{Nei}(v_i)} \mathbf{W}^{(l)} \mathbf{h}_j^{(l)}$, where $\mathbf{h}_i^{l=0} := \mathbf{x}_i$. The GNN models are usually trained in a supervised setting, learning local message aggregation and label prediction end-to-end.

Interestingly, SGC [181] has simplified GNN design and decoupled the feature propagation from label prediction learning:

$$\begin{aligned}
\mathbf{H}^{(L)} &= \mathbf{W}^{(L-1)} \mathbf{H}^{(L-1)} \mathbf{P}^\top, \mathbf{P} = \mathbf{D}^{-1} \mathbf{A} \\
\mathbf{H}^{(L-1)} &= \mathbf{W}^{(L-2)} \mathbf{H}^{(L-2)} \mathbf{P}^\top \\
&\dots \\
\mathbf{H}^{(1)} &= \mathbf{W}^{(0)} \mathbf{H}^{(0)} \mathbf{P}^\top \\
\mathbf{H}^{(0)} &:= \mathbf{X} \in \mathbb{R}^{d \times |\mathcal{V}|}, \text{ by definition.} \\
\mathbf{H}^{(L)} &= \mathbf{W}^{(L-1)} \mathbf{W}^{(L-2)} \dots \mathbf{W}^{(0)} \mathbf{X} \mathbf{P}^\top \dots \mathbf{P}^\top \mathbf{P}^\top \\
&= \hat{\mathbf{W}} \mathbf{X} \hat{\mathbf{P}}^\top, \text{ note that } \hat{\mathbf{W}} := \prod_{l=0}^{L-1} \mathbf{W}^{(l)}, \hat{\mathbf{P}} := \mathbf{P}^L, \tag{5.1}
\end{aligned}$$

where Equ.(5.1) reveals strong connections between the GNN message-passing mechanism and well-studied vertex proximity measures in network science. Specifically, $\hat{\mathbf{P}} := (\mathbf{D}^{-1} \mathbf{A})^L$ is the core component in power-method [59] for problems like PageRank [123]. Let \mathbf{p}_i is i^{th} row of $\hat{\mathbf{P}}$, where $\|\mathbf{p}_i\|_1 = 1$ and each element $\mathbf{p}_i[j]$ represents the probability of a random surfer stops at v_j from v_i by taking L times random walk, representing a sense of proximity between v_i and v_j . As $L \rightarrow \infty$, Equ.5.1 essentially represents each node feature $\hat{\mathbf{x}}_i$ by *Global Feature Aggregation*: $\hat{\mathbf{x}}_i = \mathbf{X} \hat{\mathbf{P}}^\top[:,i] = \sum_{j=0}^{|\mathcal{V}|} \mathbf{p}_i[j] \mathbf{x}_j$ where the probability vector \mathbf{p}_i serves as aggregation weights.

Alternatively, by taking into account $\hat{\mathbf{W}} \mathbf{X}$ as a whole, Equ. 5.1 can be interpreted as *global label smoothing* and each node is *pre-classified* without accessing the graph structure: $\mathbf{Y}' = \hat{\mathbf{W}} \mathbf{X}$ where

$$\mathbf{Y}' \in \mathbb{R}^{|\mathcal{C}| \times |\mathcal{V}|},$$

\mathcal{C} is the label set, then smooth the labels according to the vertex proximity: $\mathbf{Y}[:,i] = \mathbf{Y}' \hat{\mathbf{P}}^\top[:,i] = \sum_{j=0}^{|\mathcal{V}|} \mathbf{p}_i[j] \mathbf{Y}[:,j]$. Both interpretations give a *contextualized* node representation for v_i over \mathcal{V} . However, as $L \rightarrow \infty$, $(\mathbf{D}^{-1} \mathbf{A})^L$ will converge w.r.t. its first eigenvector (stationary property), making the output less distinctive and causing the over-smoothing issue [122].

PPR as a node proximity design for GNNs: The celebrated algorithm Personalized Pagerank (PPR) provides a successful *localized* design of node proximity. One intriguing property of PPR is the *locality* governed by the teleport component, making PPR vector with quantities concentrated *around* the source node. Starting from APPNP [54], PPR became a popular GNN design choice and empirically achieves outstanding performance. However, there is little theoretical framework or justification for using PPR. In section 5.5.2, we will propose a novel GNN framework and discuss the desired properties of proximity design, then justify the choice of PPR.

5.3.2 Calculate PPR as ℓ_1 Regularized Optimization

The key ingredient in PPR-based GNNs is PPR calculation. Many algorithms have been designed to approximate PPR while having better run-time complexity. In this section, we discuss the recent research on efficient PPR approximation, including traditional algorithmic approaches and newly emerging optimization perspectives.

Algorithmic approaches: Power iteration and Forward push [9] are designed to compute PPR algorithmically. The key idea of the push-based methods [171, 182] is to exploit PPR invariant[9] and gradually reduce the residual vector to approximate the high-precision PPR.

Approximate PPR via optimization: Interestingly, recent research [51, 52] discovered that Algorithm 1 is equivalent to the Coordinate Descent algorithm, and can be solved as an explicit optimization problem (Lemma 4). To this end, we can apply the Proximal Gradient Descent algorithm, specifically ISTA (Algorithm 2) to solve this well-defined PPR-equivalent ℓ_1 -regularized optimization problem.

5.4 Problem Definition

Definition 20 (Node Classification Problem over Dynamic Graph). *Given an initial graph at timestamp $t = 0$ $\mathcal{G}_0 = (\mathcal{V}, \mathcal{E}_0, \mathbf{X}_0)$ ⁴, where $\mathbf{X}_0 \in \mathbb{R}^{n \times d}$ denotes the node attribute matrix, we want to predict the labels of a subset of nodes in $\mathcal{S} = \{u_0, u_1, \dots, u_k\}$ as the graph evolves over time. At time $t \in \{1, \dots, T\}$, the graph \mathcal{G}_{t-1} is updated with a batch of edge events $\Delta\mathcal{E}_t$ and a new node attribute \mathbf{X}_t . For each snapshot \mathcal{G}_t , we train a new classifier with updated node representation $\mathbf{H}_t^{\mathcal{S}} \in \mathbb{R}^{|\mathcal{S}| \times \bar{d}}$ to predict the node labels \mathbf{y}_t and evaluate with the ground truth \mathbf{y}_t^* .*

Key Challenges: Since⁵ $|\mathcal{S}| \ll |\mathcal{V}|$ the efficiency bottleneck for PPR-based models is at calculating $\mathbf{H}_t^{\mathcal{S}}$, rather than training prediction models given $\mathbf{H}_t^{\mathcal{S}}$. The key challenges under the framework of the PPR-based GNNs boil down to two questions – **1)**: *How to efficiently calculate PPR as the graph evolves?* and **2)**: *How to effectively fold in PPR as part of the node representation?* In the following section, we answer these key questions using a justifiable PPR design and a faster ISTA-based PPR solver.

⁴For simplicity, we assume $|\mathcal{V}|=n$ does not change over time.

⁵In practice, given a large graph we may use a small subset of nodes for training and evaluation.

5.5 Proposed Framework

To efficiently and effectively learn node representations over time, we formulate PPR-based GNNs as a contextual node representation learning framework which has two key components: **1)**: Efficient PPR maintenance through an optimization lens; **2)**: Effective PPR-based node contextualization and positional encodings. Meanwhile, we discuss the desired properties of GNN design and justify the usage of PPR. Then we instantiate a simple-yet-effective model called *GoPPE*, analyze the overall complexity, and discuss its relations to other successful PPR-based GNN designs.

5.5.1 Maintain PPR in the lens of Optimization

Over an evolving graph, the new interactions between vertices are captured by adding edges, causing graph structure changes and making the previously calculated PPRs stale. To make the PPR-based GNNs reflect the latest graph structure, we propose to use ISTA as the PPR solver through an optimization lens and further explore its efficiency for dynamic graphs in various change patterns.

Naive Approach: Always from Scratch: One can simply re-calculate PPRs from scratch in each snapshot, however, this is sub-optimal because it does not leverage any previous PPR results, turning the dynamic graph into independent static graph snapshots. However, if the PPR solver is fast enough, it may still achieve reasonable efficiency.

Improved Approach: Warm starting with local update rules: By exploiting the PPR invariant, PPR adjustment rules [194] have been proposed to maintain PPR w.r.t. a sequence of edge changes (add/delete edges), which can be proved equivalently to adjust the solution and gradient in the PPR’s optimization formulation. By adjusting the previous PPR and using it as the warm-starting point, we can maintain PPR incrementally. It provides an elegant solution to dynamically maintain PPR while enjoying a favorable convergence rate inherent in ISTA.

Theorem 21 (PPR Adjustment Rules for Dynamic Graphs). *Given a new edge inserted denoted as $(u,v,1)$, The internal state of the PPR solver can be adjusted by the following rules to reflect the latest PPR but in compromised quality. Instead of starting from $\mathbf{x}=\mathbf{0}$, we use the adjusted solution as a warm-start for ISTA-solver*

(Algorithm. 2).

$$\mathbf{x}'(u) = \mathbf{x}(u) * \frac{\mathbf{d}(u)+1}{\mathbf{d}(u)} \quad (5.2)$$

$$\nabla f'(\mathbf{x}')(u) = \nabla f(\mathbf{x})(u) - \frac{\mathbf{x}(u)}{\alpha \mathbf{d}^{1/2}(u)}$$

$$\nabla f'(\mathbf{x}')(v) = \nabla f(\mathbf{x})(v) + \frac{(1-\alpha) \mathbf{d}^{-1/2}(v) * \mathbf{x}(u)}{\alpha \mathbf{d}^{1/2}(u)},$$

where $\mathbf{x}'(u), \nabla f'(\mathbf{x}')$ denotes the value after adjustment.

We attach the proof in Section 5.8.2 in Appendix.

Remark 22. As defined in Appendix 5.8.1, $\nabla f'(x')$ can be evaluated analytically, so the above rules can be reduced to a single update using Equ.5.2. Each update is a local operation having complexity $\mathcal{O}(1)$ per edge event for each node in \mathcal{S} .

5.5.2 PPR-based Contextual Node Representation and Positional Encodings

Local message passing is the key ingredient in many GNN designs. Inspired by SGC, we provide another interpretation of GNN as a global node contextualization process. It aggregates node features in a global manner, in contrast to the viewpoint of recursive local neighbor message passing. We start the analysis from the simplified local message passing design. Recall the serialized GNNs in Equ. 5.1:

$$\mathbf{H}^{(L)} = \hat{\mathbf{W}} \mathbf{X} \hat{\mathbf{P}}^\top, \quad \hat{\mathbf{W}} := \prod_{l=0}^{L-1} \mathbf{W}^{(l)}, \quad \hat{\mathbf{P}} := (\mathbf{D}^{-1} \mathbf{A})^L,$$

where L is the hyperparameter controlling how many hops should the GNN recursively aggregates the local neighbors' features. We can further organize Equ.5.1 into $\mathbf{H}^{(L)} = \hat{\mathbf{W}} \hat{\mathbf{H}}$, where $\hat{\mathbf{H}} = \mathbf{X} \hat{\mathbf{P}}^\top$. Let $\hat{\mathbf{h}}_i, \hat{\mathbf{p}}_i$ denote the i^{th} column of $\hat{\mathbf{H}}$ and $\hat{\mathbf{P}}^\top$. $\hat{\mathbf{p}}_i(j)$ refers to its j^{th} element. We re-organize Equ.5.1 into vector form:

$$\begin{aligned} \hat{\mathbf{h}}_i &= \mathbf{X} \hat{\mathbf{p}}_i = \sum_{j \in \mathcal{V}} \hat{\mathbf{p}}_i(j) \mathbf{x}_j \\ &= \sum_{j \in \mathcal{V}} \frac{\hat{\mathbf{p}}_i(j)}{z_i} \mathbf{x}_j, \quad \text{where} \end{aligned} \quad (5.3)$$

$$z_i = \sum_{k \in \mathcal{V}} \hat{\mathbf{p}}_i(k) = \|\hat{\mathbf{p}}_i\|_1 = 1 \quad \text{and} \quad \mathbf{p}_i(k) \geq 0 \quad (5.4)$$

Regardless of the exact form of $\hat{\mathbf{p}}_i$, Equ.5.3 shows that $\hat{\mathbf{h}}_i$ can be decomposed into a weighted-sum formula with a proper normalizer z_i , perhaps thought of as "global attention over other nodes" in deep learning terms. In this specific case, the attention weight $\hat{\mathbf{p}}_i$ is in its simplest form without any learnable parameter but it guarantees⁶ that $\|\hat{\mathbf{p}}_i\|_1=1$ for any $L>0$ so that we do not need explicitly evaluate z_i in a potentially expensive $|\mathcal{V}|$ -length loop when $|\mathcal{V}|$ is large. This observation provides an insightful viewpoint to interpret and design GNNs w.r.t. the node-wise attention weight $\hat{\mathbf{p}}_i(j)$. In the following, we summarize the desired properties of $\hat{\mathbf{p}}_i$ and justify our choice of using PPR (letting $\hat{\mathbf{p}}_i = \boldsymbol{\pi}_i$), then enhance the feature expressivity with PPR-based positional encodings.

Definition 23. (The desired properties of node-wise attention design) Given the formulation in Equ.5.3, a well-designed node-wise attention vector $\hat{\mathbf{p}}_i$ should have the following properties:

- *Locality:* Under the assumption of homophily graphs, $\hat{\mathbf{p}}_i(j)$ should capture the locality/proximity between node u_i and u_j , making the feature aggregation informative. For example, the self-weight $\hat{\mathbf{p}}_i(i)$ should be emphasized.
- *Efficiency:* $\hat{\mathbf{p}}_i$ should be computed and maintained quickly, in particular, independently of node size $|\mathcal{V}|$.
- *Sparsity:* $\hat{\mathbf{p}}_i$ should be sparse $|\text{supp}(\hat{\mathbf{p}}_i)| \ll |\mathcal{V}|$ so that feature aggregation is memory bounded by $|\text{supp}(\hat{\mathbf{p}}_i)|$.
- *Well-bounded normalizer $\|\hat{\mathbf{p}}_i\|_p$:* The ℓ_p -norm of $\hat{\mathbf{p}}_i$ should be bounded to avoid exhaustively calculating the normalizer z_i over \mathcal{V} when $|\mathcal{V}|$ is large.

A bad naive design: One widely-adopted attention design is $\hat{\mathbf{p}}_i(j) := \text{CosSim}(\mathbf{W}\mathbf{x}_i, \mathbf{W}\mathbf{x}_j)$ where \mathbf{W} is the learnt feature transformation. However, the resulting $\hat{\mathbf{p}}_i$ is neither sparse nor bounded and involves the node-wise calculation of complexity $\mathcal{O}(|\mathcal{V}|)$ per node, not to mention the ignorance of the graph structure.

PPR-based Attention Design and Justifications: To fulfill the desired properties, we use PPR vector as the attention design ($\hat{\mathbf{p}}_i := \boldsymbol{\pi}_i$) with the following justifications: 1). PPR vector is a well-designed proximity measure over the graph with locality controlled by the teleport parameter α , specifically, emphasizing the significance of node u_i with the personalized vector \mathbf{e}_i . 2). PPR vector can be

⁶ $(\mathbf{D}^{-1}\mathbf{A})^k$ guarantees to have row-wise ℓ_1 -norm equals to 1, and same for the column of its transpose.

maintained efficiently with complexity $\mathcal{O}(\frac{1}{\epsilon\alpha})$ and independent of $|\mathcal{V}|$. 3). PPR vector is inherently sparse, explicitly revealed by the ℓ_1 -regularization in Equ.2.3 through optimization lens. 4). The ℓ_1 -norm of the PPR vector is guaranteed to be 1, making the normalizer z_i a constant and free of computation. Finally, we have a very simple-yet-effective global contextual node formulation :

$$\hat{\mathbf{h}}_i = \mathbf{X} \hat{\boldsymbol{\pi}}_i \quad (5.5)$$

Although there are other designs for node-wise attention, To the best knowledge, we are the first to propose this framework with the desired properties and justify the choice of using PPR. This novel framework provides insights for future GNN design and motivates us to propose the following PPR-based positional encodings.

Robust Node Positional Encodings for Enhanced Locality Feature: The concept of "*locality*" is crucial in many GNN designs as well as PPR formulation. In the original GCN design, the neighbor features are aggregated by $\mathbf{D}^{-1}(\mathbf{I} + \mathbf{A})$ with the added self-loop to enhance its own features. On the other hand, PPR has the restart probability $\alpha \mathbf{e}_s$ to govern the locality. Given the importance of the node locality information and the global contextualization framework, we seek to design a node Positional Encodings (PE) $\mathbf{p}_i \in \mathbb{R}^{d_{pe}}$ for node u_i . It is analogous to the token PE [166] in NLP community to distinguish the tokens in different positions whereas node PE tells vertex's *position* or *address* in the graph.

We present the two simplest formulations of PE ⁷ in Equ.5.6 and then discuss its desired properties. Note that the node positional encodings are fused into the node u_i to enhance its own locality feature, providing an attribute-agnostic representation.

$$\mathbf{h}_i = \begin{cases} \mathbf{X} \boldsymbol{\pi}_i \oplus \mathbf{W}_{pe} \mathbf{p}_i, \text{Additive PE} \\ \mathbf{X} \boldsymbol{\pi}_i \parallel \mathbf{W}_{pe} \mathbf{p}_i, \text{Concatenative PE} \end{cases} \quad (5.6)$$

where $\mathbf{W}_{pe} \in \mathbb{R}^{d \times d_{pe}}$ is the learnable mapping parameter to align dimensions with attributes for fusion.

Definition 24 (The Desired Properties of Node Positional Encodings). *Given the graph \mathcal{G} , the positional encodings \mathbf{p}_i for node u_i is well-designed if it has the following properties:*

⁷We elide $\hat{\mathbf{h}}_i$ for simplicity; \oplus is the element-wise addition operator. \parallel is the vector concatenation operator.

Algorithm 8 GOPPE($\mathcal{G}_0, \Delta E_{1,\dots,T}, \mathbf{X}_{1,\dots,T}, \mathcal{S}, \epsilon, \alpha$)

```

1: Input: Initial graph  $\mathcal{G}_0 = (\mathcal{V}, \mathcal{E}_0, \mathbf{X}_0)$ , Edge events
    $\Delta E_{1,\dots,T}$ , Node attributes  $\mathbf{X}_{1,\dots,T}$ , The
   train/test node sets, denoted as  $\bar{\mathcal{S}}$  and  $\hat{\mathcal{S}}$ , respectively.
   And  $\mathcal{S} = \bar{\mathcal{S}} \cup \hat{\mathcal{S}}$ . PPR teleport factor  $\alpha$ ,
   PPR Vector  $\ell_1$ -error control parameter  $\epsilon$ .
2:  $\boldsymbol{\pi}_{u,init} = \mathbf{0}, \forall u \in \mathcal{S}$ 
3: // Calculate Initial PPR for each node  $u$  in  $\mathcal{S}$  using
   Algorithm 2.
4:  $\mathbf{x}_{u,t=0}, \nabla_{u,t=0} = \text{PPRISTA}(\mathcal{G}_0, \boldsymbol{\pi}_{u,init}), \forall u \in \mathcal{S}$ 
5:  $\boldsymbol{\pi}_{u,t=0} = \sqrt{d(u)} \times \mathbf{x}_{u,t=0}, \forall u \in \mathcal{S}$ 
6: // Get Contextualized Node Features and Positional
   Encodings
7:  $\mathbf{h}_{u,t=0} = \text{FEATUREFORMER}(\boldsymbol{\pi}_{u,t=0}, \mathbf{X}_0), \forall u \in \mathcal{S}$ 
8: // Train classifier with the training samples
    $\bar{u} \in \bar{\mathcal{S}} \subset \mathcal{S}$ 
9:  $f_{\boldsymbol{\Theta},t=0}(\cdot) = \text{TRAIN}(\mathbf{h}_{\bar{u},t=0}, \mathbf{y}(\bar{u})), \forall \bar{u} \in \bar{\mathcal{S}}$ 
10: // Infer for the testing samples  $\mathbf{h}_{\hat{u},t=0}, \forall \hat{u} \in \hat{\mathcal{S}}$ 
11:  $\bar{y}_{\hat{u},t=0} = f_{\boldsymbol{\Theta},t=0}(\mathbf{h}_{\hat{u}}), \forall \hat{u} \in \hat{\mathcal{S}}$ 
12: // Update graphs, maintain PPR, then train/evaluate
   repeatedly.
13: for  $t \in [1, T]$  do
14:    $\bar{\mathbf{x}}_{u,t-1} = \text{PPRADJUST}(\mathbf{x}_{u,t-1}, \Delta E_t)$ 
15:    $\mathcal{G}_t = \text{GRAPHUPDATE}(\mathcal{G}_{t-1}, \Delta E_t, \mathbf{X}_t)$ 
16:    $\mathbf{x}_{u,t}, \nabla_{u,t} = \text{PPRISTA}(\mathcal{G}_t, \bar{\mathbf{x}}_{u,t-1}), \forall u \in \mathcal{S}$ 
17:    $\boldsymbol{\pi}_{u,t} = \sqrt{d(u)} \times \mathbf{x}_{u,t}, \forall u \in \mathcal{S}$ 
18:    $\mathbf{h}_{u,t} = \text{FEATUREFORMER}(\boldsymbol{\pi}_{u,t}, \mathbf{X}_t), \forall u \in \mathcal{S}$ 
19:    $f_{\boldsymbol{\Theta},t}(\cdot) = \text{TRAIN}(\mathbf{h}_{\bar{u},t}, \mathbf{y}(\bar{u})), \forall \bar{u} \in \bar{\mathcal{S}}$ 
20:    $\bar{y}_{\hat{u},t} = f_{\boldsymbol{\Theta},t}(\mathbf{h}_{\hat{u}}), \forall \hat{u} \in \hat{\mathcal{S}}$ 
21: return  $\bar{y}_{\hat{u},t \in \{0,1,\dots,T\}}, \forall \hat{u} \in \hat{\mathcal{S}}$ 


---


22: procedure FEATUREFORMER( $\boldsymbol{\pi}_u, \mathbf{X}$ )
23:   // PPR-guided Node Contextualization
24:    $\mathbf{h}_u^c = \mathbf{X} \boldsymbol{\pi}_u$ 
25:   // PPR-based Node Positional Encodings
26:    $\mathbf{p}_i = \text{HASHREDUCEDIM}(\boldsymbol{\pi}_u, \bar{d} = 512)$ 
27:    $\mathbf{h}_u^p = \mathbf{W}_{pe} \mathbf{p}_i$ 
28:   return Apply Concatenative PE in Equ.5.6


---


29: procedure PPRADJUST( $\mathbf{x}, \Delta E$ )
30:   for  $(u, v) \in \Delta E$  do
31:      $\bar{\mathbf{x}}_u :=$  update  $\mathbf{x}_u$  Using Theorem 21.
32:   return  $\bar{\mathbf{x}}$ 


---


33: procedure HASHREDUCEDIM( $x, d$ )
34:   // Hash function  $h_d(i): \mathbb{N} \rightarrow [d]$ 
35:   // Hash function  $h_{\text{sgn}}(i): \mathbb{N} \rightarrow \{\pm 1\}$ 
36:    $\bar{x} = \mathbf{0} \in \mathbb{R}^d$ 
37:   for  $i \in \text{SUPP}|x|$  do
38:      $j = h_{\text{dim}}(i)$ 
39:      $\bar{x}(j) += h_{\text{sgn}}(i) \log(x(i))$ 
40:   return  $\frac{\bar{x}}{\|\bar{x}\|_1}$ 

```

- *Effectiveness:* \mathbf{p}_i should represent the node's "position" or "locality" over the graph and be distinguishable among vertices even if the node attributes are indistinguishable. For example, $\mathbf{p}_i \neq \mathbf{p}_j$ while $\mathbf{x}_i = \mathbf{x}_j, \forall i, j \in \mathcal{V}$.
- *Efficiency:* \mathbf{p}_i should be computationally cheap $\ll \mathcal{O}(|\mathcal{V}|)$ and low-dimensional with $d_{pe} \ll |\mathcal{V}|$ if $|\mathcal{V}|$ is large.

PPR-based node positional encodings and justifications: Interestingly, as the by-product of the PPR-based node contextualization, we re-use the unique and sparse PPR vector $\boldsymbol{\pi}_i \in \mathbb{R}^{|\mathcal{V}|}, \forall i \in \mathcal{S}$ as the source to derive the node positional encoding $\mathbf{p}_i \in \mathbb{R}^{d_{pe}}$ using simple dimension reduction operations. Specifically, we can use sparse random projection (Equ.5.15 in Appendix) or hashing-based dimension reduction (Line 33 in Algorithm 8). The reduction operation has time complexity $\mathcal{O}(|\text{supp}(\boldsymbol{\pi}_i)|) \ll \mathcal{O}(|\mathcal{V}|)$ per node, and maximizes the usage of PPR vector. Meanwhile, the resulting \mathbf{p}_i encodes a strong vertex positional signal per se. In an extreme case, where the node attributes are weak (noisy), \mathbf{p}_i alone

can provide good-quality embeddings from pure network structure, consistently providing a robust node representation.

GoPPE as an instantiated model: Putting all together, we instantiate a very simple-yet-effective GNN called *GoPPE* for dynamic graphs. Although there are more sophisticated neural network designs under the proposed framework, we aim to demonstrate its usefulness with the simplest choices. We present the detailed model components in Algorithm 8.

Relations to other PPR-based GNNs: Interestingly, many successful PPR-based GNNs⁸ fit the proposed framework with various design choices. For example, DYNAMICPPE and INSTANTEMB can be considered as the feature-less GOPPE with only positional encodings, which is robust when the node attribute is noisy. Meanwhile, INSTANTGNN is equivalent to GOPPE without positional encodings and chooses FORWARDPUSH as the PPR solver. We summarize their design choices in Table 5.1 within our proposed framework.

Complexity Analysis: Given total T graph snapshots with m edge events and $|\mathcal{S}|=K$, the complexity of GOPPE (Algorithm 8) involves four parts:

- 1: $\mathcal{O}(\frac{KT}{\epsilon\alpha})$ for the ISTA solver for PPR calculation .
- 2: $\mathcal{O}(KT \max(|\text{supp}(\pi_i)|), \forall i \in \mathcal{S})$ for the positional encoding calculation hashing method.
- 3: $\mathcal{O}(KTm)$ for the PPR adjustment of m edge events.
- 4: $\mathcal{O}(KT)$ for neural network training/inference. Since we use the simple stacked MLPs, we consider roughly $\mathcal{O}(1)$ per sample.

To sum up, the total complexity is $\mathcal{O}(KTm + \frac{KT}{\epsilon\alpha})$. Note that the complexity is independent of $|\mathcal{V}|$, indicating the algorithm only involves efficient local computation and is scalable to large graphs.

5.6 Experiments

In this section, we describe the experiment configurations and present and discuss the results of running time and prediction accuracy. Finally, we demonstrate the effectiveness of the introduced positional encodings when the node attributes are noisy.

⁸we assume that all use the standard PPR formulation with transitional matrix $D^{-1}A$

5.6.1 Experiment Configurations

Datasets: To evaluate GNNs in a dynamic setting, we divide the edges of static undirected graphs into snapshots ⁹. For node classification tasks, the first graph snapshot \mathcal{G}_0 contains the 50% of the total edges, and the other half is evenly divided into edge events in each snapshot $\Delta\mathcal{E}_i, i \in \{1, \dots, T-1\}$ for the following $\mathcal{G}_{\{1, \dots, T-1\}}$. We fix the node labels in each snapshot, while the node attributes may change according to the experiment settings. In the efficiency test, we report the running time in two dynamic setting detailed in Section 5.6.2. The statistics of datasets are presented in Table 5.2.

Table 5.2: Datasets used in our experiments. $|\mathcal{V}|$: number of nodes. $|\mathcal{E}|$ number of edges, T : number of snapshots for node classification, $|\mathcal{S}|$: total nodes in train/test sets, d : dimension of node raw feature, $|\mathcal{L}|$: number of node labels.

Dataset	Size	$ \mathcal{V} $	$ \mathcal{E} $	T	$ \mathcal{S} $	d	$ \mathcal{L} $
cora	small	2,708	5,277	5	1,000	1,433	7
citeseer	small	3,279	4,551	5	1,000	3,703	6
pubmed	small	19,717	44,323	5	1,000	500	3
flickr	medium	89,250	449,877	5	1,000	500	7
arvix	medium	169,343	1,157,798	5	1,000	128	40

Data splits: To evaluate the performance over snapshots, all train/dev/test nodes (70%/10%/20%) are sampled from the first snapshots without any dangling node. We apply the stratified sampling and add at least one sample of each class into the train/dev/test set. The total sampled nodes are presented $|\mathcal{S}|$ in Table 5.2.

Baselines: Besides the Random ¹⁰ and MLPs as the naive baselines, we compare with the State-of-the-Art PPR-based methods as listed in Table 5.1. Within our framework, we implement the baselines which are equivalent to DYNAMICPPE, PPRGO and INSTANTGNN, together with our proposed GOPPE. We use the same hyperparameters ¹¹ for a fair comparison.

Metrics: We evaluate the model’s efficiency and prediction accuracy. Since the PPR weights calculating are the most time-consuming bottleneck, we measure

⁹Although such conversion breaks the temporal correlation, we focus on a more fundamental problem of node embedding updates instead of temporal relations, which is similar to [202].

¹⁰We use random Gaussian as feature

¹¹We use $\alpha = 0.15$ and $\epsilon = 1e - 8$ by default. We denote DYNAMICPPE as DYNPPE, INSTANTGNN as INSGNN

the total CPU time for PPR calculation along with the graph updates. We use the multi-class classification setting, train the classifier separately for each snapshot ¹², then report the testing accuracy. We repeat all experiments three times with various random seeds and report the average value.

Training protocol: We use 2-layer MLPs together with RELU activations with dropout rate $p=0.15$. The inputs are the node representations produced by the aforementioned methods. We apply the same neural classifier and hyper-parameter settings to test the embedding quality across all methods for a fair comparison. More details are presented in the Appendix 5.8.4.

5.6.2 Efficiency Experiments

In PPR-based GNNs for dynamic graphs, the main computational bottleneck is the PPR maintenance over time. In this section, we present the running time under two cases regarding the intensity of graph changes between snapshots – **1: Major change case** where we start from 50% of the total edges, then add 10% edges between snapshots until all edges are used. ¹³ **2: Minor change case** where we start from a almost full graph but held out a few edges, then we add a fixed number of edges (e.g., 100) between snapshots until all edges are added. We design these two cases to evaluate the efficiency of PPR maintenance under different dynamic patterns. In the following, we discuss the insights from our empirical observations.

GoPPE is efficient and scalable in major change case: Table 5.3 presents the total running time of PPR calculation. Our proposed GoPPE is consistently faster than others while maintaining a similar PPR precision. Table 5.7 in Appendix shows the consistent approximate ℓ_1 -error as specified for each dataset. In general, GoPPE can achieve 2~3 times faster than forward push-based methods. The gain is more significant over large graphs. The advantage mainly comes from the ISTA-based PPR solver, which enjoys both the ISTA’s favorable convergence rate and the warm-starting strategy as the incremental PPR maintenance method. Note that even the static GoPPE-S is faster than the incremental Push-based method.

Remark 25. *FORWARDPUSH and ISTA has the same theoretical worst-case complexity $\mathcal{O}(\frac{1}{\alpha\epsilon})$, the observed running time difference is caused by their formulations where algorithmic FORWARDPUSH is implemented by queue, while ISTA adopts*

¹²For benchmarking purposes, we train the classifier individually for each snapshot to minimize the variability caused by continual learning.

¹³Same as we described in Section 5.6.1, we also evaluate accuracy in this case.

Table 5.3: The total CPU time (in seconds) for PPR maintenance in major change case. GoPPE uses the least time to obtain the approximate PPR weights with similar ℓ_1 -error. We elide DYNPPE since it use the same PPR solve as used in INSGNN.

Method	cora	citeseer	pubmed	arxiv	flickr
PPRGo	288.07	149.89	3,254.14	79,133.65	19,035.70
INSGNN	430.57	223.41	4,786.90	108,048.49	31,889.43
GoPPE-S	150.53	148.38	1,376.25	45,320.18	7,452.47
GoPPE-D	137.21	121.29	1,212.33	38,830.99	7,249.87

numerical computing on cache-friendly continuous memory. Similar observations are also in [182].

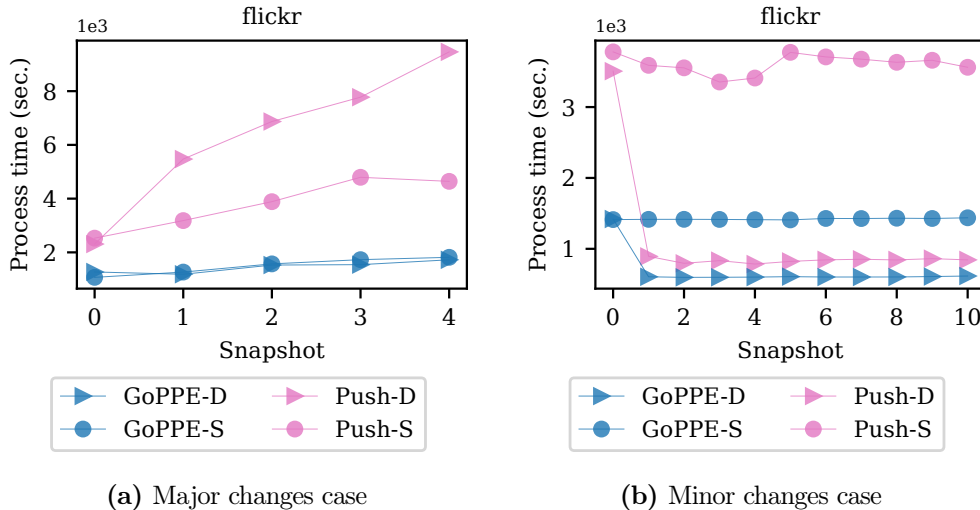


Figure 5.2: Subfigures (a) and (b) show the CPU time in *Major/Minor* graph change experiment settings, respectively. The intensity of graph changes between snapshots (major vs minor) may greatly affect the PPR updating time. In both cases, GoPPE is consistently efficient in terms of total CPU time. PPRGo uses PUSH-S while DYNPPE and INSGNN use PUSH-D. Note that the absolute time is not directly comparable between subfigures due to different settings.

The efficiency of Push-based method is limited in major change case while boosts up in minor change case: One interesting observation is that the incremental push-based method (*Push-D* used by DYNPPE and INSGNN) is not

faster than their static counterparts (*Push-S* used by PPRGo), as presented in Table 5.3 and Figure 5.2a. The root reason relates to how "*different*" the graph will be after the edge events. In major change case, we cause the graph changes drastically between snapshots by adding a large number of edges. Consequently, the quality of the approximate PPR is too compromised after applying the PPR update rules. Unfortunately, the update rules create negative residuals and incur more push operations than their static version¹⁴. When the graph changes drastically, it eventually exceeds the total operations required from scratch to maintain the PPR precision.

Table 5.4: The total CPU time (in seconds) used in the minor change case. The incremental PPR maintenance methods (GOPPE-D and INSGNN) achieve significantly better efficiency than their static counterparts. In addition, GOPPE-D is steadily faster, and even the static GOPPE-S is comparable to the incremental push-based methods. Note that the reported CPU time is not directly comparable to Table 5.3 due to different experimental settings.

Method	cora	citeseer	pubmed	arxiv	flickr
PPRGo	548.24	135.96	5,852.38	138,513.10	39,692.24
INSGNN	358.51	87.17	2,896.12	24,742.79	11,883.08
GOPPE-S	319.60	142.20	2,847.84	75,117.79	15,632.07
GOPPE-D	190.16	64.77	1,495.70	22,512.81	7,462.86

GoPPE is consistently faster regardless of the graph change intensity: Table 5.4 and Figure 5.2b present PPR efficiency results in the minor change case where only a small number of edges are added between snapshots. It shows that the update rules greatly boost PPR efficiency for both increment PPR maintenance methods (PUSH-D and GOPPE-D). Besides, GOPPE is a steadily fast method, achieving impressive speed consistently in both cases.

5.6.3 Accuracy and Robustness Experiments

We have two node classification settings described as follows to evaluate the performance and robustness of GOPPE. In both cases, we adopt *major change* as the dynamic pattern. **1: Intact case** where we use the intact raw node attributes for global feature aggregation; **2: Noisy case** where we add Gaussian noise to the node attributes (similar to [110]) at the beginning, then gradually reduce the

¹⁴Static push method only has a positive and monotonic decreasing residual.

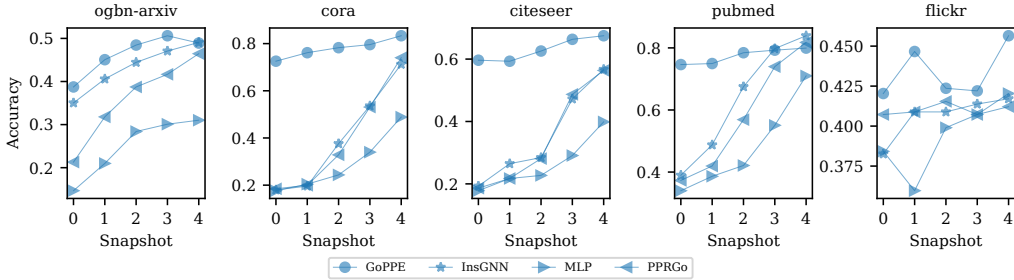


Figure 5.3: Performance Robustness against noise: We gradually add Gaussian noise into the node feature as the graph keeps evolving. GOPPE are robust against noise and greatly outperform others at the first snapshots. Note that we exclude DYNPPE because it is an attributes-free algorithm and has the same performance reported in Table. 5.5 and Figure 5.4 in Appendix.

noise level to simulate the node attributes getting better over time. The added noise is monotonically reducing defined as:

$$\hat{\mathbf{x}}_t = \lambda_t \mathbf{x}_t + (1 - \lambda_t) \mathcal{N}(\mu, \sigma^2), \quad (5.7)$$

where $\lambda_t = \frac{t}{T} + \lambda_{base} \in [0, 1]$ controls noise level, t is the snapshot stamp, T is the total number of snapshots, $\lambda_{base} \in [0, 1]$ controls the initial noise level, μ, σ^2 are the mean and variance of the elements in node attributes matrix \mathbf{X} , respectively. As t increases from 0 to T , the noisy component decays linearly. We use this noise model to simulate the feature refinement process, similar to the volunteers helping enrich Wikipedia articles and make the articles more clear and relevant.

GOPPE achieves comparable performance with intact features : Table 5.5 present the averaged prediction accuracy across all snapshots. Specifically, we found the positional encoding (DYNPPE) alone can yield strong performance, further demonstrating the importance of locality information. Meanwhile, we will analyze the performance difference in *pubmed* and *flickr* later in Section 5.6.4.

GOPPE is robust against noisy node attributes and consistently outperforms the baselines: Figure 5.3 presents the accuracy over snapshots where the node features are gradually refined as defined in Equ.5.7. As expected, the models without positional encodings (MLP, PPRGo, and InsGNN) perform poorly at the beginning as they heavily depend on the node attributes. Meanwhile, GOPPE demonstrates its robustness by having positional encodings and consistently outperforms others.

Table 5.5: We present the average accuracy across snapshots in the intact case. GOPPE is comparable to or better than the baselines while it’s the fastest as discussed in Section 5.6.2. We present full results in Figure 5.4 in Appendix. Although GOPPE generally performs well, we will discuss its performance on *pubmed* graph later.

models	cora	citeseer	pubmed	arxiv	flickr
Random	0.1977	0.1667	0.3731	0.1343	0.3530
MLP	0.4886	0.3987	0.7098	0.3102	0.4204
PPRGo	0.7101	0.5458	0.8139	0.4244	0.4128
InsGNN	0.6925	0.5588	0.8362	0.4772	0.4138
DynPPE	0.7984	0.6314	0.7821	0.4648	0.4220
GoPPE	0.7935	0.6310	0.7861	0.4843	0.4427

Table 5.6: GoPPE is robust to noisy node attributes. We exclude DYNPPE as it is an attribute-free algorithm and has the same results as reported in Table 5.5.

methods	cora	citeseer	pubmed	arxiv	flickr
MLP	0.2905	0.2624	0.4816	0.2503	0.3941
PPRGo	0.3967	0.3471	0.5837	0.3599	0.4102
InsGNN	0.4000	0.3562	0.6378	0.4324	0.4062
GoPPE	0.7797	0.6307	0.7745	0.4636	0.4338

5.6.4 Discussions and Future Works

Robust positional encodings achieves better accuracy over graphs of weak node attributes : Table 5.5 shows that MLPs provides poor performance on *cora* and *citeseer*, implying that these graphs have weak node attributes for prediction. It makes PPRGo and INSGNN harder to extract signals from attributes. Meanwhile, the positional encodings successfully capture the node context and achieve better performance. On the other hand, on the attribute-rich graphs, even MLP performs relatively well, for example, on *pubmed* graph. It is because *pubmed* has dense and informative node attributes, which makes the PPR-based feature aggregation (PPRGo, INSGNN) produce a succinct and predictive signal.

How to adapt PPR propagation over dynamic heterotrophic graph remains an open problem: Besides the attribute-rich property in *pubmed*, it is also known for its homophily property [115] which makes the nodes of the same labels well-connected. As we discussed in the Definition 23, one of the assumptions

is graph homophily, which makes PPR-based aggregation predictive with local *peer* nodes. However, *flickr* is a heterotrophic graph [100]. Table 5.5 shows that the accuracy of all models is worse or just slightly better than MLP. Inspired by Chien et al. [32], we are interested in adapting PPR for dynamic heterotrophic graphs.

Faster PPR-GNN with efficient PPR solver: Given the impressive efficiency of ISTA-based PPR solver, it motivates us to explore more toward faster optimization methods for dynamic PPR settings. For example, FISTA or Blockwise Coordinate Descent methods with faster rule and active set [121]. Such research directions have the potential for even faster GNN designs for dynamic graphs and tackle larger-scale problems.

5.7 Conclusion

In this paper, we proposed an efficient framework for node representation learning over dynamic graphs. Within the framework, we propose the desired properties in node attention design for global feature aggregation, and we justify the use of PPR under its ℓ_1 -regularized formulation. Besides, we proposed to use ISTA as the PPR solver and use warm-start as an elegant solution to maintain PPR over dynamic graphs. Finally, we introduce the PPR-based node positional encodings, maximizing the usage of PPR for robust representation against noisy node attributes. The experiments show that our instantiated model GOPPE is 2-3 times faster than the current state-of-the-art models while achieving comparable or better prediction accuracy over graphs with intact node attributes. In the noisy environment, GOPPE significantly outperforms the others, demonstrating the effectiveness of the proposed positional encodings.

5.8 Appendix

5.8.1 Formulate Quadratic Objective from Forward Push

From Push to the objective function : The proofs follows [52]. One can rewrite Forward Push algorithm into CD:

Given Equ.2.1, we define Residual Vector $\mathbf{r} \in \mathbb{R}^n$ as followings:

$$\mathbf{r} := (\mathbf{I}_n - (1 - \alpha)\mathbf{A}\mathbf{D}^{-1})\boldsymbol{\pi} - \alpha\mathbf{e}_s \quad (5.8)$$

By multiplying $\mathbf{D}^{-1/2}$ on both sides of Equ.5.8 and $\boldsymbol{\pi} := \mathbf{D}^{1/2}\mathbf{x}$:

$$\begin{aligned} \mathbf{D}^{-1/2}\mathbf{r} &= \mathbf{W}\mathbf{x} + \mathbf{b}, \\ \text{where } \mathbf{W} &= \mathbf{D}^{-1/2}(\mathbf{D} - (1-\alpha)\mathbf{A})\mathbf{D}^{-1/2}, \\ \mathbf{b} &= -\alpha\mathbf{D}^{-1/2}\mathbf{e}_s \end{aligned} \tag{5.9}$$

Equ.5.9 has a linear form w.r.t. \mathbf{x} which can be interpreted as the gradient $\nabla f(\mathbf{x}) := \mathbf{D}^{-1/2}\mathbf{r} = \mathbf{W}\mathbf{x} + \mathbf{b}$ of a quadratic function $f(\cdot)$ such that:

$$f(\mathbf{x}) := \frac{1}{2}\mathbf{x}^\top \mathbf{W}\mathbf{x} + \mathbf{b}^\top \mathbf{x}, \tag{5.10}$$

The most intriguing finding is that by applying coordinate descent to Equ.2.3 and minimizing the objective function, the solution $\mathbf{x}^* = \operatorname{argmin}_{\mathbf{x}} f(\mathbf{x})$ is the approximate PPR given the fact that $\boldsymbol{\pi} = \mathbf{D}^{1/2}\mathbf{x}^*$. Such formulation bridges two seemingly disjoint fields and provides more opportunities to solve PPR through the lens of optimization.

Rewrite Coordinate Descent for PPR

Note that $\mathbf{r} = \mathbf{D}^{1/2}\nabla f(\mathbf{x})$, $\boldsymbol{\pi} = \mathbf{D}^{1/2}\mathbf{x}$,

Algorithm 9 CD SOLVER FOR PPR

- 1: **Input:** $k=0, \mathbf{x}^{(0)} = \mathbf{0}, \mathcal{G}, \epsilon, \alpha$
 - 2: $\nabla f(\mathbf{x}^{(0)}) = -\alpha\mathbf{D}^{-1/2}\mathbf{e}_s$
 - 3: **while** exists i such that $\|\nabla f(\mathbf{x})(i)\|_1 > \epsilon' d(i)^{1/2}$ **do**
 - 4: CD(i)
 - 5: **return** ($\boldsymbol{\pi} = \mathbf{D}^{1/2}\mathbf{x}^{(k)}, \mathbf{r} = \mathbf{D}^{1/2}\nabla f(\mathbf{x}^{(k)})$)
 - 6: **procedure** CD(i)
 - 7: /*apply coordinate descent*/
 - 8: $\mathbf{x}^{(k+1)}(i) = \mathbf{x}^{(k)}(i) - \nabla_i f(\mathbf{x}^{(k)})$
 - 9: /*update gradient*/
 - 10: $\nabla f(\mathbf{x}^{(k+1)})(i) = 0$
 - 11: **for** $j \in \operatorname{Nei}_{out}(i)$ **do**
 - 12: $\nabla_j f(\mathbf{x}^{(k+1)}) = \nabla_j f(\mathbf{x}^{(k)}) + \frac{(1-\alpha)\mathbf{A}_{(i,j)}}{d(i)^{1/2}d(j)^{1/2}} \nabla_i f(\mathbf{x}^{(k)})$
 - 13: $k = k + 1$
-

By looking closely to the termination condition: $\|\nabla f(\mathbf{x})(i)\|_1 \leq \epsilon' d(i)^{1/2} \Rightarrow \nabla f(\mathbf{x})(i) \geq -\epsilon' d(i)^{1/2}$ given $\nabla f_i(\mathbf{x}) \leq 0, \forall i$, Note that the optimality conditions imply the termination condition, and $\nabla_i f(\mathbf{x}^*) \in [-\epsilon' d(i)^{1/2}, 0]$ if $\mathbf{x}^*(i) = 0$ implies its sparsity. $\operatorname{prox}(\mathbf{x}) = \operatorname{argmin}_{\bar{\mathbf{x}}} \frac{1}{2}\|\mathbf{x} - \bar{\mathbf{x}}\|_2^2 + \epsilon' \|\mathbf{D}^{1/2}\mathbf{x}\|_1$

5.8.2 PPV maintenance on dynamic graphs

From [194]: Given a new edge $e_{u,v}$, the adjustments are :

$$\boldsymbol{\pi}'(u) = \boldsymbol{\pi}(u) * \frac{\mathbf{d}(u)+1}{\mathbf{d}(u)} \quad (5.11)$$

$$\mathbf{r}'(u) = \mathbf{r}(u) - \frac{\boldsymbol{\pi}(u)}{\alpha \mathbf{d}(u)} \quad (5.12)$$

$$\mathbf{r}'(v) = \mathbf{r}(v) + \frac{1-\alpha}{\alpha} \frac{\boldsymbol{\pi}(u)}{\mathbf{d}(u)} \quad (5.13)$$

Note that, in PPR-equivalent quadratic formulation, we define:

$$\mathbf{r} = \mathbf{D}^{1/2} \nabla f(\mathbf{x}) \text{ and } \boldsymbol{\pi} = \mathbf{D}^{-1/2} \mathbf{x} \quad (5.14)$$

In addition, the PPR invariant property still holds for the results from the solution. When a new edge event arrives, the update rules adjust \mathbf{x} and $\nabla f(\mathbf{x})$ for further updating. We substitute them back to the update rules and have:

$$\mathbf{d}^{-1/2}(u) * \mathbf{x}'(u) = \mathbf{d}^{-1/2}(u) * \mathbf{x}(u) * \frac{\mathbf{d}(u)+1}{\mathbf{d}(u)}$$

$$\Rightarrow \mathbf{x}'(u) = \mathbf{x}(u) * \frac{\mathbf{d}(u)+1}{\mathbf{d}(u)}$$

$$\mathbf{d}^{1/2}(u) * \nabla f'(\mathbf{x}')(u) = \mathbf{d}^{1/2}(u) * \nabla f(\mathbf{x})(u) - \frac{\mathbf{d}^{-1/2}(u) * \mathbf{x}(u)}{\alpha \mathbf{d}(u)}$$

$$\Rightarrow \nabla f'(\mathbf{x}')(u) = \nabla f(\mathbf{x})(u) - \frac{\mathbf{x}(u)}{\alpha \mathbf{d}^{1/2}(u)}$$

$$\mathbf{d}^{1/2}(v) * \nabla f'(\mathbf{x}')(v) = \mathbf{d}^{1/2}(v) * \nabla f(\mathbf{x})(v) + \frac{1-\alpha}{\alpha} \frac{\mathbf{d}^{1/2}(u) * \mathbf{x}(u)}{\mathbf{d}(u)}$$

$$\Rightarrow \nabla f'(\mathbf{x}')(v) = \nabla f(\mathbf{x})(v) + \frac{(1-\alpha)}{\alpha} \frac{\mathbf{d}^{-1/2}(v) * \mathbf{x}(u)}{\mathbf{d}^{1/2}(u)}$$

5.8.3 Dimension Reduction using Random Projection

The sparse Gaussian random projection can be constructed:

$$\mathbf{p}_i = \mathbf{R}\pi_i, \text{ and } \mathbf{R} \in \mathbb{R}^{d_i \times |\mathcal{V}|} := \begin{cases} +\sqrt{3} \text{ with probability } \frac{1}{6} \\ \sqrt{0} \text{ with probability } \frac{2}{3} \\ -\sqrt{3} \text{ with probability } \frac{1}{6} \end{cases} \quad (5.15)$$

5.8.4 Experiment Details and Reproducibility

Table 5.7: We maintain a similar precision level ($\epsilon \approx 1e-6$ or $1e-8$) across all graphs. The error was calculated against the power iteration results with a smaller ϵ setting for higher precision.

ppr-algo	increment	cora	citeseer	pubmed	ogbn-arxiv	flickr
push	False	3.99e-08	2.25e-08	4.57e-08	4.76e-06	4.32e-08
ista	False	5.22e-08	2.78e-08	6.03e-08	6.08e-06	2.84e-08
push	True	4.06e-08	2.30e-08	4.65e-08	4.85e-06	4.34e-08
ista	True	5.14e-08	2.73e-08	5.94e-08	6.00e-06	2.80e-08

5.8.5 Infrastructure

All the experiments are done on a machine equipped with 4 processors of Intel(R) Xeon(R) CPU E5-2630 v4 @ 2.20GHz, where each processor has 10 cores, resulting in 40 cores in total and 125GB main memory. Besides, we have 4 Nvidia-Titan-XP GPUs where each has 12GB GPU memory.

5.8.6 PPR Implementation

We implemented all PPR routines (Power iteration, Forward Push (w/o dynamic adjustment), ISTA) in Python and ensured that all are Numba-accelerated (@njit). Numba acceleration compiles python routines to LLVM native code, which has a comparable speed to C/C++. We particularly chose Python+Numba as the main programming tool because it's easier to maintain and is gradually being accepted by the scientific computing community.

5.8.7 Neural Model Configurations

We implemented the neural networks using PyTorch. Table 5.8. We use LINEAR \rightarrow RELU \rightarrow DROPOUT as the basic neural component for classification. Besides, we set dropout ratio $p=0.15$ during training. During training, we use ADAM optimizer and force all models to train for 50/100 epochs before early exit. More details can be found in the training scripts in our codebase included in this submission.

Table 5.8: To have a fair comparison, we use the same model configurations except for the proposed feature aggregation function. Note that we denote the dimension of the node’s raw feature as $|Feat|$ and the total node label as $|L|$. We use the presented hidden state sizes (128, 32, 16) in MLP- $\{0,1,2\}$ for small graphs, while use larger size (128, 512, 256) for larger graph. Likewise, all methods share the same architecture configs.

	MLP-Feat	MLP-PPE	MLP-0	MLP-1	MLP-2
Gaussian	$ Feat * 128$	-	128*32	32*16	16* $ L $
PPE	-	$ PPE * 128$	128*32	32*16	16* $ L $
MLP	$ Feat * 128$	-	128*32	32*16	16* $ L $
PPRGo	$ Feat * 128$	-	128*32	32*16	16* $ L $
InstantGNN	$ Feat * 128$	-	128*32	32*16	16* $ L $
GoPPE	$ Feat * 128$	$ PPE * 128$	128*32	32*16	16* $ L $

5.8.8 Reproducibility

We repeated the experiments with three different random seeds for all stochastic parts (e.g., python, numpy and PyTorch) during training and testing. We included the source code and the scripts needed to reproduce the results and will release them to the public upon publication.

5.8.9 Edge event sampling

We create dynamic graphs from static graphs. First, we associate each edge event with a distinctive timestamp from 1 to $|\mathcal{E}|$. Then, we use the first edges $\Delta\mathcal{E}_0$ (e.g., with timestamp < 100) to construct \mathcal{G}_0 as the base graph. Finally, we inject a fixed number of edges $\Delta\mathcal{E}_1$ (e.g. with the timestamp from 100 to 120) to simulate graph evolution to create the next graph snapshot $\mathcal{G}_1 = \mathcal{G}_0 + \Delta\mathcal{E}_1$. Iteratively, we create all snapshots. Note that the created dynamic graph may not have temporal characteristics and temporal modeling is not in the scope of this paper.

5.8.10 Extra results

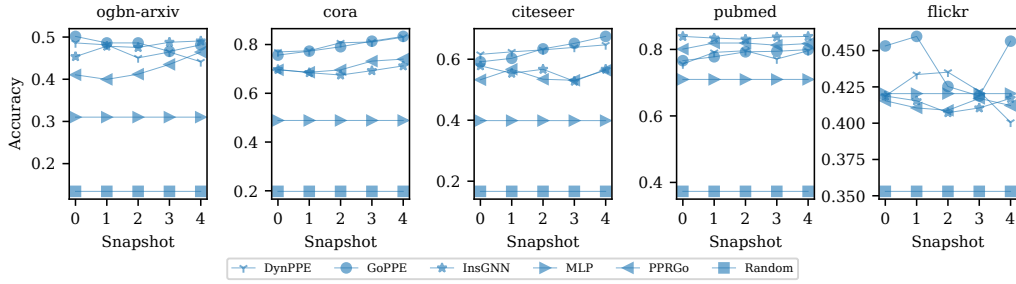


Figure 5.4: Prediction accuracy on intact features across snapshots. GoPPE has comparable or better accuracy than other baselines.

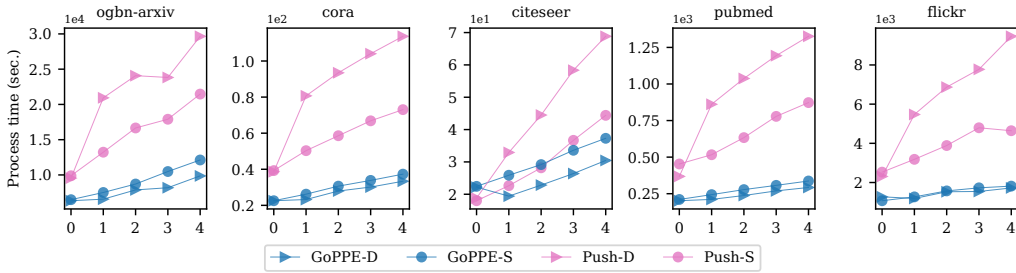


Figure 5.5: PPR calculation time in major change case.

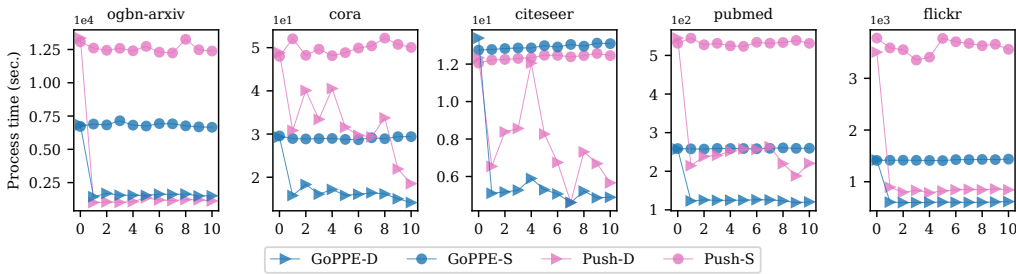


Figure 5.6: PPR calculation time in minor change case.

Chapter 6

Post-publication Modification in News Outlets¹

6.1 Introduction

The growth of the Internet has shifted the distribution of news articles from traditional channels such as print and radio to online websites and social media platforms. Today, 86% of people consume news on digital devices via the Internet [147]. This new medium has greatly reduced the time between the occurrence of newsworthy events and the publishing of articles reporting on them. One of the strategies that news agencies appear to be regularly using is to publish articles with incomplete information, taking advantage of their ability to modify online articles *after* their publication [71]. Consequently, readers who view an article or headline immediately after publication may be exposed to radically different information and therefore arrive at different conclusions, compared to readers consuming the same article at a later time. For example, *The Atlantic* published the following article on February 11th, 2021 with the title:

Original title[118]: "*I Miss the Thrill of Trump*"

However, five hours later the title of the article changed to:

Altered title[119] : "*I Was an Enemy of the People*"

¹Xingzhi Guo, Brian Kondracki, Nick Nikiforakis, and Steven Skiena. 2022. Verba Volant, Scripta Volant: Understanding Post-publication Title Changes in News Outlets. In *Proceedings of the ACM Web Conference 2022 (WWW '22)*. Association for Computing Machinery, New York, NY, USA, 588-598. <https://doi.org/10.1145/3485447.3512219>

Given the documented tendency of users to skim through titles rather than read the content of every news article that they encounter [6], a radical modification of a headline translates to two or more groups of people who have consumed the same news from the same sources, yet arrive at potentially different worldviews.

In this paper, we explore the phenomenon of post-publication modifications of news article headlines. We monitor the titles of articles from several top news publishers, and capture all post-publication changes for later analysis. We analyze our compiled dataset to create a taxonomy of title changes using an automated NLP pipeline allowing us to determine the reasons for article title changes, the entities responsible, and the tangible benefits the publisher may receive for doing so. Further, we examine the spread of news over social networks by collecting time-series impression statistics (e.g., number of retweets/likes) of tweets containing links to news articles for the Twitter accounts of news publishers.

The primary contributions of our work are as follows:

- *Temporal News Headline Data Set*: We have developed a temporal news headline corpus consisting of 30,930 distinct news articles where the headline changed at least once. Our dataset of 41,906 total altered headlines pairs (some articles change headlines more than once) provides a unique resource for future studies of news trustworthiness as well as user trust, which we will make available upon publication.
- *Characterizing Changes in News Headlines*: We create an NLP categorization pipeline for assessing headline changes by the proposed nine-class taxonomy, based on journalism domain knowledge and a state-of-the-art language model (BERTScore [199]), from which we successfully discover that 23.13% headline edits are perceived as harmful. This analysis enables us to quantify why headline changes occur in practice, and how policies differ with particular news agencies.
- *Estimating Effective Timing over Twitter*: We present a temporal analysis showing how rapidly news is fully propagated over social networks. We observe that most news tweets are shared/retweeted within the first 10 hours following their initial posting, before gradually fading out due to losing the public’s attention, or achieving their maximum audience. This suggests that an effective headline correction must occur quickly to avoid propagating misinformation.

6.2 Related Work

A genuine news headline summarizes the content and enables readers to draw quick conclusions [44, 87, 135]. However, in the digital media era, false information or fake news [50, 104, 150, 206] threatens the public’s information consumption by inducing readers with clickbait headlines and fabricated content. Vargas et al. [165] developed techniques to distinguish legitimate activity on Twitter from disinformation campaigns using coordination network analysis. Additionally, a large research line [58, 95, 134, 206] focus on fake news detection, satire detection [43, 141], and clickbait detection [129]. Hounsel et al. [84] proposed methods to discover disinformation websites using characteristics of their hosting infrastructure. In this work, we investigate news outlets that, in the process of publishing legitimate articles, modify their headlines.

The headline modifications may be harmless (e.g., updating competition score) or malicious (e.g., making the headline clickbaity [21], or starting with an inaccurate headline that maximizes user views and eventually changing it to an accurate one). Hagar and Diakopoulos [75] discussed A/B testing on news headlines and gather audiences’ feedback on several headline writing practices (e.g., starting headlines with "why" or "how" and subjective ideals) and reported that headlines are optimized for specific metric (e.g., click-through rate) from A/B testing. Kuiken et al. [103] investigated the effectiveness of headlines by comparing click-through rate of the original title and its of the rewritten one, suggesting that clickbait features led to statistically significant increase in number of clicks. However, the size of their dataset was limited, with 1,836 pairs of headlines that were rewritten from a single groups of editors.

Another related research line is text edit classification. Previous work [42] analyzed linguistic features for the task of edit category classification, organizing English Wikipedia’s edits into 21 categories, from spelling corrections to vandalism. Yang et al. [184] investigated the intentions behind text edits and created a 13-category taxonomy of edit intentions, then developed supervised learning models for automatic identification. Similarly, Marrese-Taylor et al. [114], Yin et al. [187] employed encoder-decoder deep learning framework to learn the edit representation and predict its categories. Due to data availability, previous research mainly focus on Wikipedia post-edit instead of news headlines. Given our unique, large-scale dataset of 41K pairs of title changes, we aim to understand real-world headline modifications and derive a taxonomy for automated edit categorizations. In addition, we analyze the speed of news propagation over social networks, how they relate to post-publication headline changes, and offer guidance

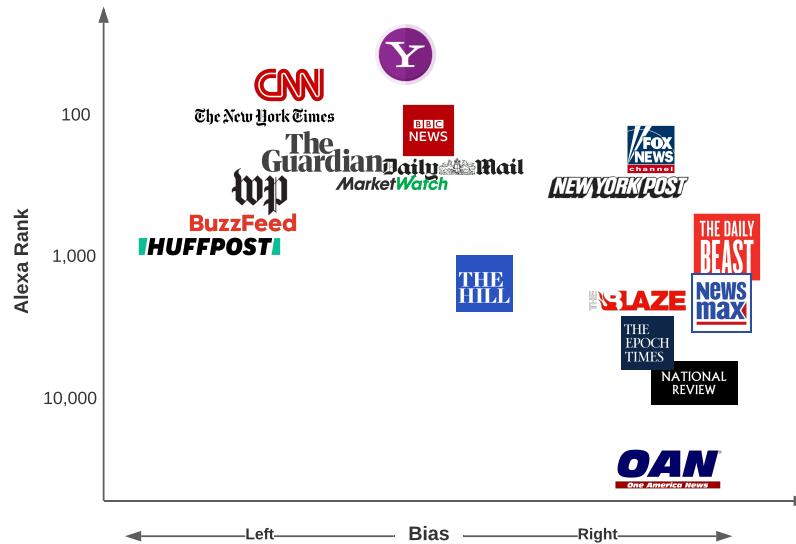


Figure 6.1: News publishers chosen based on their political bias and Alexa ranking on the timings of responsible post-publication modification.

6.3 Dataset Preparation

In this section, we discuss our process for selecting news publishers to include in our study. We then describe the infrastructure we designed and implemented to capture news articles, as well as detect post-publication headline changes and measure the spread of news on social media.

6.3.1 News Publisher Identification

Prior to capturing and studying post-publication article headline changes, we must first identify a set of news publishers to collect article data from that are representative of a broad range of audiences, biases, and platform sizes. To this end, we constructed a set of news publishers by first consulting the Media Bias Chart created by Ad Fontes Media [2]. This chart maps news publishers onto a two-dimensional plane representing political bias, and reputability. We focus only on the political bias of each news publisher, selecting an equal number of publishers from each region of this axis.

Rather than utilize the reputability ranking of each publisher on this chart, we

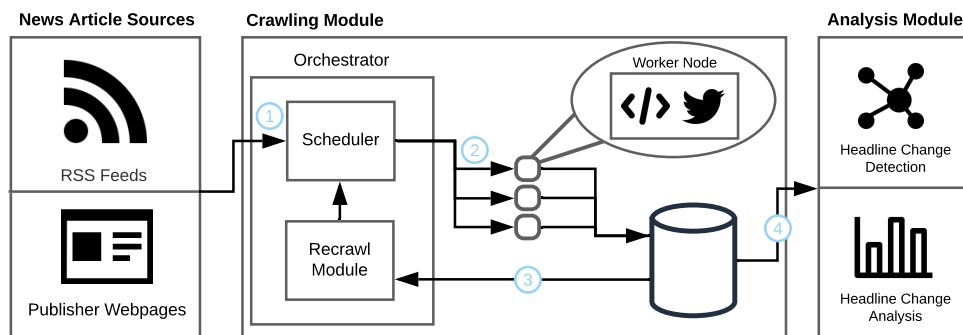


Figure 6.2: The overview of news crawling infrastructure

opt instead to measure reputability with the Alexa ranking [1] of each publisher’s website. We reason that the Alexa ranking of each publisher is an effective and unbiased proxy for a publisher; with more reputable publishers drawing a larger audience and higher rank. We group publishers into buckets representing different Alexa rank ranges aiming for an equal number of publishers from each bucket. Figure 6.1 shows the news publishers we chose, and their positions in the two-dimensional plane we described.

6.3.2 Data Collection Infrastructure

To measure the extent in which news publishers modify the titles of their articles post-publication, we created a data collection infrastructure that visits the web pages of news articles as they are posted and continually monitors them to detect changes to their titles and content. Additionally this infrastructure monitors the spread of news on Twitter.

Post-publication Article Headline Changes Figure 6.2 provides an overview of our infrastructure. (i) News article URLs are collected using a set of input modules corresponding to the source in which the URLs are gathered from. For all news publishers we study, URLs are collected using the RSS feeds provided by each publisher. However, our infrastructure can be easily extended to support additional URL sources, such as scraping the home page of a news publisher, by creating a new module for that source. Our RSS module queries the RSS servers of each news publisher periodically to gather the URLs of new articles shortly after they are posted.

The URLs for each new article are placed onto a queue in the article crawling module (ii) where workers consume new URLs by visiting each URL and parsing

metadata from the article web page. We collect and save each HTML web page for future processing, but specifically parse out the article title using the Python Newspaper library [4].

In order to detect title changes in news articles, (iii) we recrawl each article web page periodically for the two days following its original publication and parse out the same information as previously described. We arrived at this two-day threshold via a pilot crawling experiment where we established that any headline modifications were typically occurring in the first few hours after an article was published. **Measuring the Spread of News on Twitter** In many cases, modifications to news articles occur *after* these articles have already been consumed and shared. Social media platforms only exacerbate this problem due to the speed in which information propagates among users. We chose to study the propagation of news on Twitter because, unlike other social media platforms, Twitter prevents users from editing tweets after they are posted, leading to discrepancies in the information shared in the tweets of news agencies, and their related articles. When crawling an article found to have a modified title, our infrastructure also searches the Twitter feed of the relevant news publisher for a tweet containing a link to the article in question. If such a tweet is discovered, it is recrawled at the same interval as the article itself. For each crawl of a tweet, our infrastructure records the tweet text, as well as the current number of favorites and retweets. To measure the base level of interaction tweets from each news publisher receive, our data collection infrastructure also crawls a random sample of tweets from each publisher.

6.4 Post-Publication Headline Changes

Using our data collection infrastructure, we monitored 411,070 articles published by the news agencies listed in Figure 6.1 from March 1st, 2021 to August 31st, 2021. In total, we observed 30,930 (7.5%) articles modify their headlines at least once, resulting in 41,906 changed pairs². Figure 6.3 shows that over 90% of changes occur within the first 10 hours after publication. Readers who encounter an article shortly after publication will likely come away with a different opinion on the subject-matter than a reader who encounters the same article after the headline has changed. Furthermore, if the headline change is to correct invalid information, this can lead to rapid spread of misinformation through channels such as social media. In this section, we explore the magnitude of headline changes in our dataset,

²We consider one pair as two consecutive headline versions. Additionally, we list news categories of changed pairs per agency in Table 6.8 in Appendix

assign labels to these changes corresponding to the nature of the modification, and compare the consistency of headlines published by popular news outlets.

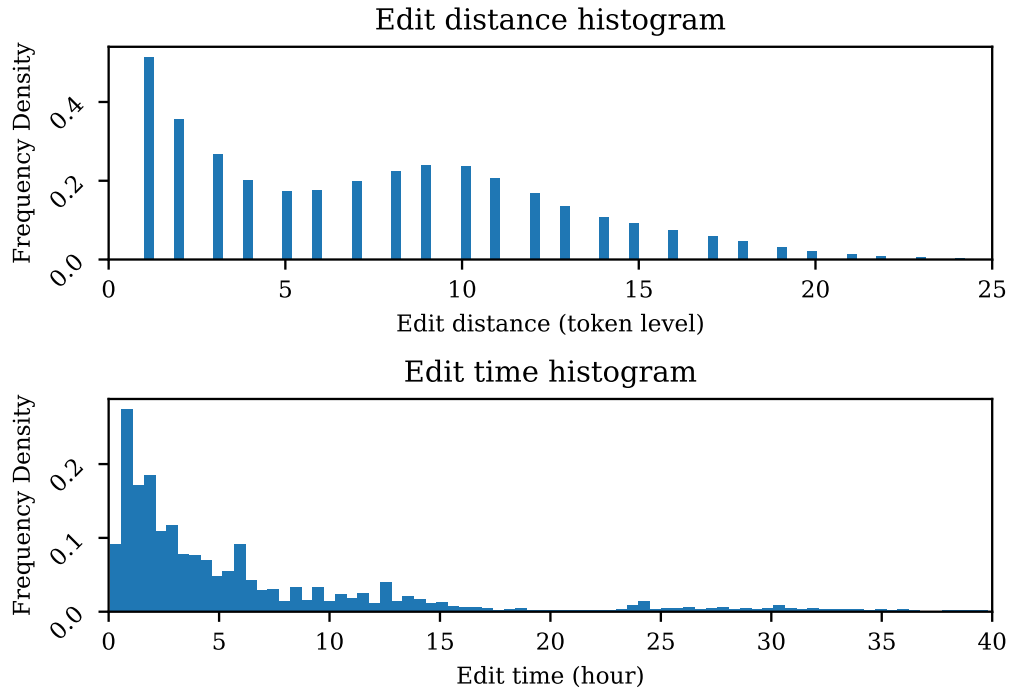


Figure 6.3: Edit distance histogram (*top*): a large fraction of edits are local edits with distance 1 to 3. Timing of title changes (*bottom*): Most title changes occur within 10 hours after initial publishing. We present plots per publisher in Figure 6.8 in the appendix.

6.4.1 Headline Change Magnitude

The inclusion, exclusion, or modification of a single word or phrase in a headline can lead to large differences in reader perception. Figure 6.3 shows the edit distance of headline modifications we detected during our data collection period. In the context of headline modifications, we define a token as a single word. We observe a bi-modal distribution in our dataset, with a majority of headline changes resulting in an edit distance of a single token, and a second local peak at approximately 10 tokens. Since we expect headline modifications in these two groups to be the result of distinct contributing factors, we discuss them separately.

Single-token Edit Distance. During our data-collection period, we observed 6,036 single-token edit changes. Among them, 3,767 are word substitution. Table 7.7 shows the top five most common part-of-speech (POS) changes in headlines. We find that headlines with single-token substituted typically correspond to either updates of ongoing events, or error corrections.

Table 6.1: The top-5 changes in part of speech

POS Changes	#
(NOUN, NOUN)	861
(VERB, VERB)	573
(NUM, NUM)	396
(PUNCT, PUNCT)	242
(ADJ, ADJ)	216
Others	1,479

Specifically for word substitution, 44.1% of noun changes and 54.6% of verb changes are synonyms, hyponymns, hypernymns, or otherwise share the same lemma. Tables 7.8 and 6.7 in the appendix list these breakdowns for nouns and verbs, respectively. These modifications typically occur at the end of a newsworthy event; with modified verbs transitioning from present to past tense, indicating the end of the event. Similarly, changes in headlines correspond to updates in ongoing events (e.g. score changes in sporting events). We observe that 68.39% of numerical headline changes result in the number increasing by some value (e.g. reflecting more discovered injuries/casualties from an ongoing natural disaster). Table 6.5 in the appendix shows the full breakdown of all numerical changes we observed.

Arbitrary Edit Distance. To model headline modifications of arbitrary edit distance, we compute the difference of lexicon in changed pairs to distinguish whether it is a minor update or a complete rewrite. BERT-based word alignment score $-BERTScore$ [199] as defined in Eq.6.1 – is a lexical alignment statistic using contextual word embeddings with attention mechanism. BERTScore can capture the semantic similarity in two sentences of dissimilar structures and lexicons, whereas an edit distance only measures superficial lexical differences. We extend our analysis to all changed pairs with $BERTScore_{F1} \in [-1,1]$ as the semantic similarity measure. The relationship between edit distance and $BERTScore_{F1}$ is shown in Figure 7.6 (*left*).

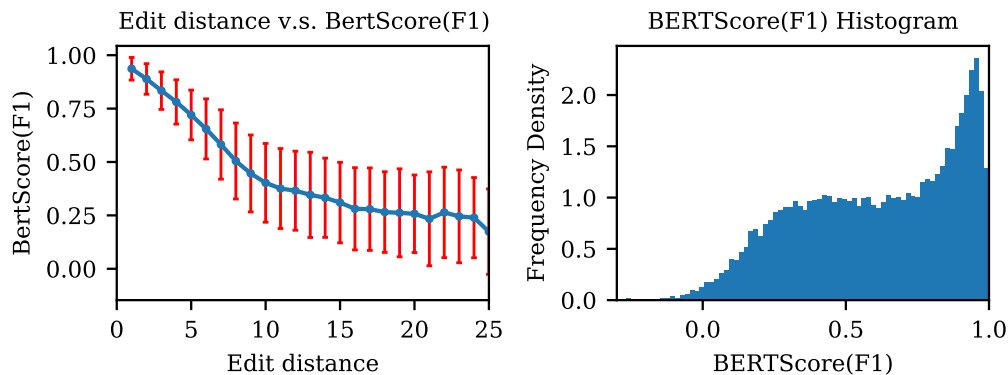


Figure 6.4: Figure (*left*): BERTScore decreases as more edits being applied until the pre/post-edit titles become irrelevant (BERTScore reaches to 0). Figure (*right*) shows that there is only few complete rewrite in news titles.

$$R = \frac{1}{|x|} \sum_{x_i \in x} \max_{\hat{x}_j \in \hat{x}} x_i \hat{x}_j; \quad P = \frac{1}{|\hat{x}|} \sum_{\hat{x}_j \in \hat{x}} \max_{x_i \in x} x_i \hat{x}_j$$

$$BERTScore_{F1} = 2 \frac{P * R}{R + P} \in [-1, 1],$$
(6.1)

where x_i, \hat{x}_i denote i^{th} token in two sentences x, \hat{x} .

Figure 7.6 (*right*) shows the distribution of BERTScore where the peak around 0.9 indicates that most edits do not change the semantic meaning of the headline, while the samples centered around 0 represent the post-publication edit completely changing the headline’s semantic meaning. We present examples associated with BERTScore in Table 6.9 of the appendix. Using a BERTScore threshold of 0.25, we find approximately 10% of the changed pairs in our dataset are significantly rewritten. We consider these headline changes to be the most damaging to readers as it is very likely that the message conveyed by the headline will change drastically after modification.

Table 6.2 shows the ordered list of news agencies by the average similarity score across all changed headlines. Generally, higher similarity indicates minor changes that do not alter the original semantic meaning. We find many well-regarded publishers (e.g., BBC, The Guardian, NYT) frequently modify headline semantics. This unexpected finding suggests that the popularity of a news outlet does not necessarily indicate greater restraint with post-publication headline changes. Contrastingly, we observe publishers such as The Epoch Times with an

Table 6.2: The statistics of semantic similarity (BERTScore) by agency (Ranked by the mean value). To clarify the similarity rankings from news reputation rankings, the ordered list does not reflect credibility. *Tracked* is the total number of tracked articles, *Mod. Ratio* is the percentage of the articles with at least one altered headline.

Agency	Mean	Median	Tracked	Mod.Ratio
Huffington Post	0.8292	0.8966	4,875	0.0357
The Epoch Times	0.8260	0.8908	4,765	0.1442
The Hill	0.8087	0.8644	5,676	0.0592
Fox News	0.7659	0.8645	11,003	0.0486
New York Post	0.7305	0.8174	13,881	0.0665
National Review	0.7268	0.8305	3,324	0.0126
The Blaze	0.7200	0.8145	4,401	0.0400
CNN	0.6888	0.7493	6,344	0.2030
Washington Post	0.6840	0.7916	6,076	0.1508
Newsmax	0.6733	0.7319	1,115	0.0233
Daily Beast	0.6584	0.7693	4,359	0.1308
MarketWatch	0.6551	0.7011	7,503	0.3453
BBC	0.6031	0.6260	5,854	0.2277
Yahoo News	0.5985	0.6160	227,246	0.0846
Daily Mail	0.5936	0.6348	75,118	0.0756
OAN	0.5830	0.5910	8,323	0.2616
The Guardian	0.5579	0.5826	6,916	0.1975
New York Times	0.5234	0.5595	9,746	0.1892
BuzzFeed	0.5085	0.4872	4,545	0.4438

Alexa rank of close to ten thousand modify headlines at a much lower rate than publishers with a much larger online presence.

Additionally, by noting the ratio of modified headlines with the average BERTScore for all modified headlines, we can deduce the expected consistency of a particular news outlet. For instance, we find that BuzzFeed modified the headlines of 44% of their articles during our data-collection period. Of those articles, we observe the headline changes produce the lowest average BERTScore (i.e. the modified headlines depart significantly from the original ones). Contrastingly, during our data collection period, The Huffington Post only modified the headlines of 3% of observed articles; achieving the highest average BERTScore with those changes. We can therefore conclude that, in terms of headline modifications, The Huffington Post is a more consistent news outlet compared to BuzzFeed. We note however, that this consistency of headlines does not necessarily imply accuracy of headlines.

6.4.2 Categorization of News Title Changes

Table 6.3: Examples of the altered titles sampled from our dataset by the modification category. The example of the label "Other" involves out-of-vocabulary words (J.&J) and changes in tone. The example of "Concision" removes the specific person, while the "Elaboration" example expands the original title with an attributive clause. "Forward-Reference" adds a question mark and "Personalization" substitute reader into the title, which both trigger curiosity from the readers. The "Neutralize" example remove "*long*" from the original title, making it less subjectivity. While "Emotional" example adds "*tease, big*", which makes the title more inflammatory.

Before	After	BERT-F1	Label
One Dose of J.&J. Vaccine Is Ineffective Against Delta...	J.&J. Vaccine May Be Less Effective Against Delta ...	0.6830	Other
Senator Capito says Republicans plan new US infrastructure offer	U.S. Senate Republicans prepare new infrastructure offer	0.5434	Concision
Raul Castro confirms he's resigning, ending long era in Cuba	Raul Castro resigns as Communist chief, ending era in Cuba	0.7310	Neutralize
Fourth stimulus check update: Your next payment could be these	Fourth stimulus check? These payments are already in the pipeline	0.4479	Forward Ref.
The Latest: UN: 38,000 Palestinians displaced in Gaza	The Latest: Biden expresses 'support' for Gaza cease-fire	0.4043	Dyn. Update
MAGA 2.0	"A new bargain": Biden's 2024 tease bets big on nostalgia	0.0257	Emotional
23 Amazing Jokes From Hot Fuzz	23 Jokes From "Hot Fuzz" That Humans Will Laugh At For The Next 10,000 Years	0.4715	Elaboration
Watch Jeff Bezos' 'Blue Origin' launch into space live today	Everything you need to know as Jeff Bezos' 'Blue Origin' launches into space today	0.6179	Personalize
Afghan guard killed: Firefight leaves at least one dead and others injured at Kabul airport	'It would be better to die under Taliban rule than face airport crush', say US embassy's 'betrayed' Afghan staff	0.0656	Citation

To discover trends in article headline changes, and the behaviors of the publishers responsible, we create a nine-class taxonomy of editing types based on journalism knowledge (e.g. Emotionalism, etc.), existing taxonomies for Wikipedia edits[42, 184], and the most common edits from our observations (e.g., Paraphrase, Dynamic update, etc.) . We design our taxonomy as follows:

- **Paraphrase:** We assign the label *Paraphrase* if the changed pairs have a similarity score (BERTScore-F1) greater than 0.8.
- **Dynamic Update:** If both old and new title contain keywords such as *Monday brief, update, live, stream, etc.* The keywords were manually selected.

- **Emotionalism[99]:** if only the news title contains any of words in the subjective dictionary.
- **Neutralization:** if only the old title contains subjective words mentioned above.
- **Forward Reference:** Forward Reference[21, 99] is a common feature in news titles, piquing reader curiosity. We assign this label only if the changed title contains the keywords such as *why, when, which, how, etc.*
- **Personalization[99]:** Personalization is used to retain audiences and make the readers feel involved in the news. We assign this label only if the new title contains keywords such as *you, we, s/he, your, etc.*
- **Citation:** Citation is a common technique in news headlines that make them look more reliable. We assign this label only if the new title contains keywords like *said, says, told, etc.*
- **Concision:** If the new title removes some text, and the remaining text aligns with the old title ($P < 0.6, R > 0.5$). BERT-Score Precision/Recall is defined in Eq.6.1
- **Elaboration:** If the new title adds text, and is semantically aligned with the old title: $P > 0.6, R < 0.5$).

These nine categories allow us to better understand headline modifications by classifying them into groups corresponding to their perceived purpose. With the combination of BERTScore, Stanza Pipeline [131], word sentiment dictionary [136], and hand-crafted rules, we are able to automatically assign labels using our proposed NLP pipeline. We empirically determined the thresholds to use by finding those that made the most sense with manual inspection. Table 6.9 of the appendix present more examples of each of these categories.

Figure 6.5 (*right*) shows the resulting label coverage. Our proposed categorization rules cover approximately 70% of news title changes (the changed pair has at least one assigned category). Among the 30% of modifications not covered by our pipeline, we find that the missing cases usually have a BERTScore of less than 0.8, involve more complex sentence structure changes (double negation), or out-of-vocabulary words (most of them are COVID-related “COVID-19, J.&J., AstraZenec”, which debuted after the release of the pre-trained model). We listed several examples in Table 6.3 and more examples in Table 6.9 in the Appendix.

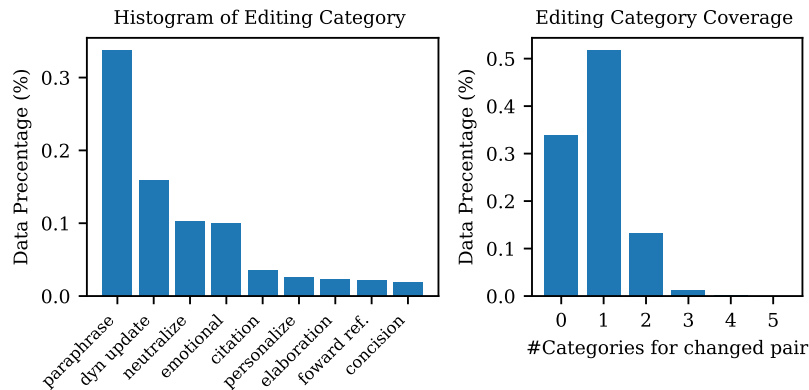


Figure 6.5: Assigned category statistics. Figure (*left*) shows the majority change types are paraphrase and dynamic update. Figure (*right*) shows that approx. 70% of samples have at least one category assigned. 50.3% modifications associate with benign edit categories (paraphrase, updates, elaboration, concision), while 23.13% modifications are linked with the other less benign edits.

We also find that the most common changes belong to the “Paraphrase” and “Dynamic Update” categories (44.24%), which do not significantly change the semantic meaning of the headlines. Changes in these categories typically correspond to updates of ongoing events and grammatical/spelling corrections. However, we note that all other categories in our taxonomy may contain headline changes that can be perceived as harmful to at least some readers.

Over the course of our data collection period, we observed an equal distribution of “Emotionalism” and “Neutralization” headline changes, suggesting that publishers are just as likely to add emotional words to attract more readers after initial publication as they are to remove them. However, since both of these categories transition the headline from a provocative to non-provocative state, or vice-versa, these two groups can have the same effect on different groups of readers. In the case of “Emotionalism” changes, readers who view a headline after it has been modified, will likely have a more emotional response to the subject-matter, while “Neutralization” changes will have the same effect on readers who view a headline pre-modification. Together, these two groups make up 20.13% of all headline changes in our dataset.

Table 6.4 shows the percentage of articles by each publisher belonging to each of the nine categories in our taxonomy. Since it reflects the explanation of headline changes, the percentage does not reflect the general media bias, which may be

Table 6.4: The breakdown of edit types per news agency. Each headline modification may belong to multiple labels. We highlight the top one in each column.

Agency	Paraphrase	Dynamic Update	Elaboration	Concision	Emotional	Neutralize	Forward Refer.	Personalize	Citation
BBC	0.3196	0.3848	0.0278	0.0113	0.1043	0.0818	0.0180	0.0188	0.0540
BuzzFeed	0.1587	0.0203	0.0312	0.1101	0.1026	0.1894	0.0709	0.0699	0.0238
CNN	0.4262	0.0916	0.0404	0.0148	0.0699	0.0738	0.0171	0.0342	0.0435
Daily Beast	0.4754	0.1035	0.0246	0.0175	0.1123	0.0912	0.0386	0.0351	0.0298
Daily Mail	0.2801	0.1158	0.0357	0.0144	0.0993	0.1218	0.0241	0.0521	0.0422
Fox News	0.6056	0.1925	0.0187	0.0093	0.0710	0.0617	0.0168	0.0224	0.0262
Huffington Post	0.7356	0.0690	0.0000	0.0000	0.0345	0.0632	0.0000	0.0345	0.0230
MarketWatch	0.3867	0.0872	0.0413	0.0178	0.0965	0.0799	0.0363	0.0154	0.0247
National Review	0.5476	0.3810	0.0476	0.0000	0.0714	0.0476	0.0000	0.0238	0.0000
New York Post	0.5211	0.0997	0.0336	0.0076	0.0715	0.0618	0.0336	0.0293	0.0141
New York Times	0.2923	0.1171	0.0108	0.0108	0.1123	0.1432	0.0380	0.0184	0.0331
Newsmax	0.3846	0.3077	0.0385	0.0000	0.0000	0.0769	0.0000	0.0000	0.0385
OAN	0.2692	0.0156	0.0280	0.0184	0.1029	0.0988	0.0032	0.0023	0.0271
The Blaze	0.5341	0.3239	0.0625	0.0227	0.0682	0.0398	0.0227	0.0398	0.0455
The Epoch Times	0.6856	0.1659	0.0146	0.0204	0.0277	0.0422	0.0044	0.0087	0.0364
The Guardian	0.2950	0.4100	0.0271	0.0124	0.1215	0.1164	0.0190	0.0190	0.0688
The Hill	0.6637	0.2024	0.0268	0.0327	0.0208	0.0446	0.0089	0.0060	0.0179
Washington Post	0.4891	0.2205	0.0186	0.0109	0.0884	0.0797	0.0207	0.0437	0.0371
Yahoo News	0.3256	0.1846	0.0150	0.0126	0.1047	0.0977	0.0156	0.0161	0.0340

embedded in the static news headlines. We observe that over 70% of the articles published by the Huffington Post, The Epoch Times and The Hill belong to either the “Paraphrase” or “Dynamic Update” categories, demonstrating that their headlines will typically not change in ways which will lead to drastically different opinions among readers. We also notice that *BuzzFeed* leads in three change categories, including the categories most closely related to click-bait: “Forward Reference”, and “Personalization”.

By observing the categorizations of each publisher, a model can be developed on their overall headline-modification strategies. For instance, the “Citation” category of our taxonomy allows us to deduce that *The Guardian* is the most likely to include witness or expert testimony in headlines post-publication, with 6.8% of their articles falling into that category. Conversely, we find that the publisher National Review is very unlikely to make such a headline change as we did not observe any instances of modification by either publisher during our data collection period. These observations quantify the regularity with which publishers modify their headlines, and can be used as a supplementary feature for future research on digital journalism and public trust in news.

6.4.3 News Propagation over Twitter

In recent years, social media services have emerged as a vital tool for news publishers to quickly share stories with the public. Due to the ability of users to share and “repost” links to articles with others connected to them online, information can spread faster than ever before. Because of this user-assisted amplification, false or misleading information in article headlines can propagate to exponentially many readers before headline changes occur, magnifying the negative repercussions of unanticipated headline changes.

We track the reachability of news on Twitter in terms of user engagement. As mentioned in Section 6.3, our data-collection infrastructure records the number of likes and retweets of tweets associated with news articles with modified headlines from the accounts of each publisher. In total, we detect 5,384 tweets corresponding to articles with modified headlines during our data collection period. We note that these tweets correspond to the original article headlines, with their immutability preventing publishers from simply editing their contents to reflect headline changes. Rather, publishers must first delete the original, outdated tweet, and replace it with a new tweet. Alarming however, we find that only 0.15% of all such tweets were deleted subsequent to a headline change in the corresponding article. Moreover, we find that these tweets on average garner 39 retweets and 137 favorites. This means that the vast majority of tweets associated with outdated and potentially misleading information remain online indefinitely, and receive considerable attention from users who then spread this information to others.

Figure 6.6 shows the distribution of time in which tweets associated with headline changes were “retweeted” and “favorited” by users. We observe a clear trend that news stories gradually lose popularity on social networks as they become less novel. People usually share (retweet) tweets associated with news stories within the first ten hours and react (favorite) within first five hours. Based on the observations in Figure 6.3, we found that almost 80% title changes happened within the first five hours after publishing. These findings are alarming as they show that many headline changes occur *after* most social media activity regarding the particular article ceases. This means that social media users are currently either spreading false or misleading information before the publisher can remedy it by modifying the headline, or sharing articles that will portray an entirely different emotional response when their followers view it at a later point in time. Both of these scenarios can lead to situations where different readers of the same article or headline will come to different conclusions depending on when they encountered it.

URL Preview Cards A popular feature of Twitter is the rendering of cards

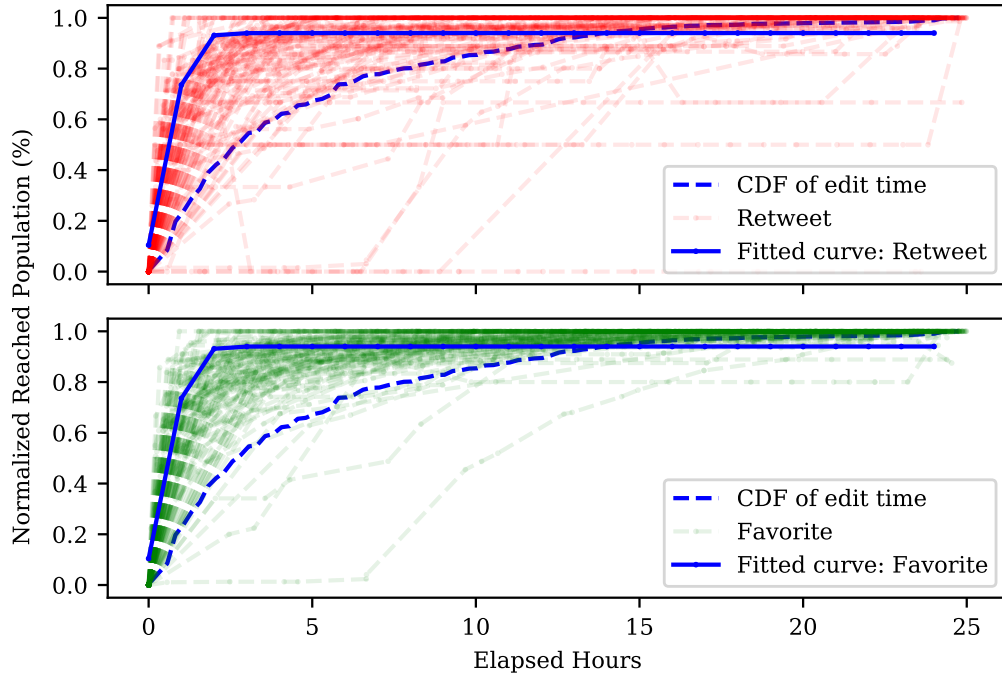


Figure 6.6: The normalized retweets (top) and favorites (bottom) V.S. news published time. The solid blue curve is the fitted curve $y = a \cdot (1 + e^{-b(x-c)})^{-1}$, approximating how quick the news achieves its max influence.

that preview the content located at the URL linked in a tweet. These cards work by parsing and rendering the Open Graph [3] metadata from the HTML source of the linked webpage directly below the tweet text. Typically, a webpage thumbnail, title, and description are rendered. This metadata is cached for each particular URL for approximately one week; only updating when the URL is modified [5]. This caching behavior can amplify the negative repercussions of post-publication headline changes as any tweet containing the URL of an article that was published prior to a headline change will display the outdated headline for at least one week. This is a behavior we have observed on the Twitter accounts of popular news publishers. Figure 6.7 demonstrates an example of this behavior with a headline change from the BBC, along with a tweet containing a link to the article posted by the official BBC Twitter account. Twitter users who only read the headline and description located on the rendered card will consume outdated information on the situation, as opposed to those who click through to the article webpage.



Figure 6.7: Twitter URL preview of article posted by BBC Politics. Article headline outdated on Twitter due to caching behavior of URL cards.

6.5 Conclusion

In 2022, trust in the media is at an all-time low. In this paper, we explored one dimension that we argue has the potential to further reduce the public’s trust in news outlets: post-publication headline changes. By monitoring over 411K articles for seven months across tens of news outlets, we discovered that 7.5% of titles changed at least once after they were published. This rate of headline modifications is anything but uniform, with certain popular outlets changing almost half of their headlines *after* publication. We used the BERTScore metric and devised a taxonomy to automatically characterize the type of post-publication change. We find that 49.7% of changes go beyond benign corrections and updates, with 23.13% corresponding to categories such as emotionalism, neutralization, and personalization. We also characterized the effects of post-publication headline changes in relation to social media. Among others, we discovered that maximal spread of news on Twitter happens within ten hours after publication and therefore a delayed headline correction will come *after* users have consumed and amplified inaccurate headlines. Finally, we discussed the issue of content caching in social networks and how it can further exacerbate the propagation of stale headlines.

Acknowledgements: This work was supported by the National Science Foundation (NSF) under grants CMMI-1842020, CNS-1941617, CNS-2126654, IIS-

1926781, IIS-1927227, IIS-1546113 and OAC-1919752.

Availability To assist in the understanding of the spread of misinformation on the web, we are open-sourcing our news headline dataset: <https://scripta-volant.github.io/>

6.6 Discussion

Headline Changes. The Internet has dramatically decreased the time between newsworthy events, and the consumption of information regarding those events by the public. This, along with the propensity of people to simply skim headlines rather than read full articles [6], has fostered an environment where post-publication changes to article headlines can lead to diverging world-views among readers. In this work, we studied the behavior of news publishers and developed a taxonomy of article headline modifications. We find that popular news publishers regularly make post-publication changes to their headlines, with some modifying almost half of them.

Additionally, we categorize these changes into well-defined groups, allowing us to quantify the behaviors of each publisher. We find that the majority of headline changes correspond to updates of ongoing events. Alarmingly however, 20.13% of headline changes are made to either increase or decrease the provocativeness of the headline, presenting a distorted view of the subject-matter to different groups of readers. Using this taxonomy, we are able to quantify the different headline update strategies of each news outlet studied, discovering a divergence in the perceived motives between publishers.

While the news outlets presented in this study do not appear to have outright malicious intentions, their actions contribute to the overall decrease in integrity of information consumed by millions of people. In order to slow the spread of misinformation in society, news outlets should limit the rate in which their article headlines are modified. With the speed in which news travels, headline changes can have devastating effects to reader understanding. We argue that, if a headline must be changed, the new headline should maintain high lexical similarity to the original headline, only adding new information to enhance reader understanding.

Information Travel on Social Media. The rapid propagation of information through shares and retweets on social media has only exasperated the negative ramifications of news article headline modifications. By observing the engagement of tweets associated with news articles with modified headlines, we determined that the majority of favorites and retweets occur within ten hours of a tweet's

publication. Due to the caching of article metadata and previews on Twitter, most article shares will contain a different headline than what is active on the publisher’s website. While it is infeasible for social media platforms to constantly monitor each and every webpage linked to from all posts, decreasing the caching of content can help reduce the spread of misinformation online. Moreover, it would be worthwhile to explore ideas around the penalization of aggressive headline changes. That is, if an article received 10K retweets *before* a significant headline change, is it appropriate for that article to keep all the clout that the previous title generated? Penalizing large changes has the potential to act as a deterrent of unwanted publishing behavior and encourage publishers to be more considerate about their content choices *before* an article is published.

6.7 Appendix

Table 6.5: Numerical difference between pre/post-edits in changed news titles: Most of them concern news dynamic updates of injuries and competition scores. High *BERTScore* shows that numerical changes does not alter the meaning.

Diff.	Number	Before	After	BERTScore
1.0	116	louisiana floods lead to 6 deaths	louisiana floods lead to 7 deaths	0.99
2.0	45	yankees lead astros 1-0 in game 1: live score and updates	yankees lead astros 3-0 in game 1: live score and updates	0.96
-1.0	31	ransomware attack hits 23 texas towns, authorities say	ransomware attack hits 22 texas towns, authorities say	0.99
3.0	24	super bowl 2020 live: chiefs lead the 49ers, 7-3	super bowl 2020 live: chiefs lead the 49ers, 10-3	0.93
4.0	17	iraq: suicide bombing kills at least 18 in baghdad	iraq: suicide bombing kills at least 22 in baghdad	0.98
5.0	14	albania earthquake kills at least 8	albania earthquake kills at least 13	0.97
100.0	6	iran-iraq earthquake kills more than 300	iran-iraq earthquake kills more than 400	0.98

Table 6.6: Breakdown of changed nouns. One pair may belong to more than one category

Category	Total	%	Examples (Before, After, #)	Description
Share lemma	132	15.33%	(report, reports, 4); (riots, riot, 3)	The change noun shares the lemma.
Synonym	65	7.54%	(advisor, adviser, 3); (investigate, probe,2)	The change noun is synonym.
Minor	109	12.65%	(protestors, protesters, 5); (reelection, re-election,4)	Only one character is changed (excluding same lemma pairs)
Hyponymn	33	3.83%	(housing, home, 3); (semiconductor, chip, 2), (official, officer, 2); (supporter, believer, 1)	Become more specific
Hypernymn	41	4.76%	(snaps, photos, 5);(budget, plan, 2)	Become more general
Others	481	55.86%	(demo, democrats, 7); (4th, fourth, 4) (live, close, 4); (valuation, value, 3)	All other noun changes
All	861	100%	-	All detected noun substitutions

Table 6.7: Breakdown of changed verbs. One pair may belong to more than one category

Category	Total	%	Examples (Before, After, #)	Description
Share lemma	135	23.56%	(cancelled, canceled, 7); (shuts, shut, 2)	The change noun shares the lemma.
Synonym	59	10.29%	(rise, climb, 2); (blew, botched, 2)	The change noun is synonym.
Minor	35	6.10%	(eying, eyeing, 2); (targetting, targeting, 2)	Only one character is changed (excluding same lemma pairs)
Hyponym	38	6.63%	(drops, tumbles, 3); (pull, drag, 2) (mulls, considers, 2); (rejects, rebuffs, 2)	Become more specific
Hypernym	46	8.02%	(passes, advances, 3); (linger, remain, 3) (breaking, damaging, 2); (reveals, shows, 1)	Become more general
Others	260	45.37%	(drop, slip, 3); (reveals, says, 3)	All other noun changes
All	573	100%	-	All detected verb substitutions

Table 6.8: *Top:* The tracked news categories per agency. *Bottom:* The headline modification ratio in each news category

Domain	Politics	Business	Entertainment	Technology	Top Stories	Total
BBC	1973	1562	1495	824	0	5854
BuzzFeed	330	92	3928	195	0	4545
CNN	4548	1	1166	629	0	6344
Daily Beast	0	0	0	0	4359	4359
Daily Mail	0	3670	36312	1263	33873	75118
Fox News	6307	108	4273	315	0	11003
Huffington Post	2909	57	1902	7	0	4875
MarketWatch	0	0	0	0	7503	7503
National Review	0	0	0	0	3324	3324
New York Post	0	1458	2018	514	9891	13881
New York Times	2374	2983	3851	538	0	9746
Newsmax	897	25	155	38	0	1115
OAN	2922	3545	528	1328	0	8323
The Blaze	0	0	0	0	4401	4401
The Epoch Times	3179	1077	193	316	0	4765
The Guardian	3456	627	1874	959	0	6916
The Hill	0	0	0	0	5676	5676
Washington Post	2126	2014	1458	478	0	6076
Yahoo News	11074	183653	7	32512	0	227246

Domain	Politics	Business	Entertainment	Technology	Top Stories	Total
BBC	0.3082	0.2855	0.1371	0.0898	0.0000	0.2277
BuzzFeed	0.2576	0.0000	0.4812	0.2154	0.0000	0.4438
CNN	0.2419	0.0000	0.1612	0.0000	0.0000	0.2030
Daily Beast	0.0000	0.0000	0.0000	0.0000	0.1308	0.1308
Daily Mail	0.0000	0.0515	0.0592	0.0451	0.0970	0.0756
Fox News	0.0591	0.0926	0.0314	0.0571	0.0000	0.0486
Huffington Post	0.0399	0.0877	0.0273	0.1429	0.0000	0.0357
MarketWatch	0.0000	0.0000	0.0000	0.0000	0.3453	0.3453
National Review	0.0000	0.0000	0.0000	0.0000	0.0126	0.0126
New York Post	0.0000	0.0638	0.0852	0.0292	0.0650	0.0665
New York Times	0.2784	0.3144	0.0444	0.1375	0.0000	0.1892
Newsmax	0.0268	0.0400	0.0065	0.0000	0.0000	0.0233
OAN	0.0404	0.4886	0.0890	0.2108	0.0000	0.2616
The Blaze	0.0000	0.0000	0.0000	0.0000	0.0400	0.0400
The Epoch Times	0.1787	0.0706	0.0259	0.1203	0.0000	0.1442
The Guardian	0.2922	0.3142	0.0326	0.1022	0.0000	0.1975
The Hill	0.0000	0.0000	0.0000	0.0000	0.0592	0.0592
Washington Post	0.2413	0.1226	0.0501	0.1736	0.0000	0.1508
Yahoo News	0.2390	0.0713	0.0000	0.1073	0.0000	0.0846

Table 6.9: Examples of altered headlines. Separated by the double line, the first part is the manually selected modifications. The second part is sampled from our dataset by type

Before	After	BERT-F1	Type
One Dose of J.&J. Vaccine Is Ineffective Against Delta, Study Suggests	J.&J. Vaccine May Be Less Effective Against Delta, Study Suggests	0.6830	other
Malawi burns thousands of Covid-19 vaccine doses	Malawi burns thousands of expired AstraZeneca Covid-19 vaccine doses	0.7217	other
Biden to huddle with Senate Democrats on Covid relief ahead of push for passage	Biden urges Senate Democrats to reject poison pills that could sink relief plan ahead of push for passage	0.3777	other
Australia to investigate two deaths for possible links to COVID-19 vaccine	Australia says two deaths not likely to be linked to COVID-19 vaccine	0.7236	citation
Canada adds blood clot warning to AstraZeneca's COVID-19 vaccine	Canada says AstraZeneca COVID-19 vaccine safe, but adds blood clot warning	0.7546	citation
China's Zhurong rover will land on Mars TONIGHT	China's Zhurong rover will land on Mars 'in the next five days	0.7234	other
Nike chief executive says firm is 'of China and for China'	Nike boss defends firm's business in China	0.4559	other
MAGA 2.0	"A new bargain": Biden's 2024 tease bets big on nostalgia	0.0257	emotional
At Least Eight People Died In A School Shooting In Russia	At Least Nine People Died In A School Shooting In Russia	0.9866	paraphrase
India sees cases officially drop below 300,000 a day but now country threatened by killer cyclone	India cases officially drop below 300,000 a day but now country threatened by killer cyclone	0.9034	paraphrase
The Latest: UN: 38,000 Palestinians displaced in Gaza	The Latest: Biden expresses 'support' for Gaza cease-fire	0.4043	dyn update
August 5 at 2PM ET: Join Engine Media CEO and Executive Chairman Fireside Chat	August 5 at 2PM ET: Join Engine Media CEO and Executive Chairman in Fireside Chat	0.9393	dyn update
23 Amazing Jokes From Hot Fuzz	23 Jokes From "Hot Fuzz" That Humans Will Laugh At For The Next 10,000 Years	0.4715	elaboration
Official: Haiti President Jovenel Moise assassinated at home	Haiti President Jovenel Moise assassinated at home; Biden calls it 'very worrisome'	0.5179	elaboration
Senator Capito says Republicans plan new U.S. infrastructure offer	U.S. Senate Republicans prepare new infrastructure offer	0.5434	concision
U.S. second-quarter economic growth revised slightly higher; weekly jobless claims rise	U.S. second-quarter growth raised; corporate profits surge	0.5540	concision
Undercover police officers spied on Peter Hain over 25 years	Peter Hain accuses undercover police of lying over reports on apartheid campaign	0.2465	emotional
Suspect arrested following series of Arizona traffic shootings	Arizona gunman goes on traffic shooting rampage, leaving one dead, 12 injured	0.2247	emotional
Raul Castro confirms he's resigning, ending long era in Cuba	Raul Castro resigns as Communist chief, ending era in Cuba	0.7310	neutralize
Nikki Grahame's life will be celebrated in a new Channel 4 documentary four months on from her death	Nikki Grahame to be commemorated in a new Channel 4 documentary	0.6698	neutralize
Fourth stimulus check update: Your next payment could be one of these	Fourth stimulus check? These payments are already in the pipeline	0.4479	foward ref.
12 Movie Opinions You Might Agree With	Here Are 12 More Movie Opinions I Strongly Believe, But Do You Agree With Me?	0.4246	foward ref.
Watch Jeff Bezos' 'Blue Origin' launch into space live today	Everything you need to know as Jeff Bezos' 'Blue Origin' launches into space today	0.6179	personalize
The "Degrassi: TNG" Cast Is Reuniting In Honor Of The Show's 20th Anniversary	The "Degrassi" Cast Is Reuniting And I Am So Excited To Relive My Teen Years	0.4838	personalize
Stimulus Update: States Give Out Thousands of Bonus \$1,000 Checks To School Employees	Stimulus Update: States Give Out Thousands of Bonus \$1,000 Checks – Will You Get One?	0.7416	personalize
Kendall Jenner Has Some Pretty Strong Thoughts About The Kardashian Curse	Kendall Jenner Talked About The Kardashian Curse And Said "The Men Need To Take Responsibility"	0.5229	citation
Afghan guard killed: Firefight leaves at least one dead and others injured at Kabul airport	'It would be better to die under Taliban rule than face airport crush', say US embassy's 'betrayed' Afghan staff	0.0656	citation
Apple beats sales expectations on iPhone, services, China strength	Apple says chip shortage reaches iPhone, growth forecast slows	0.2611	citation

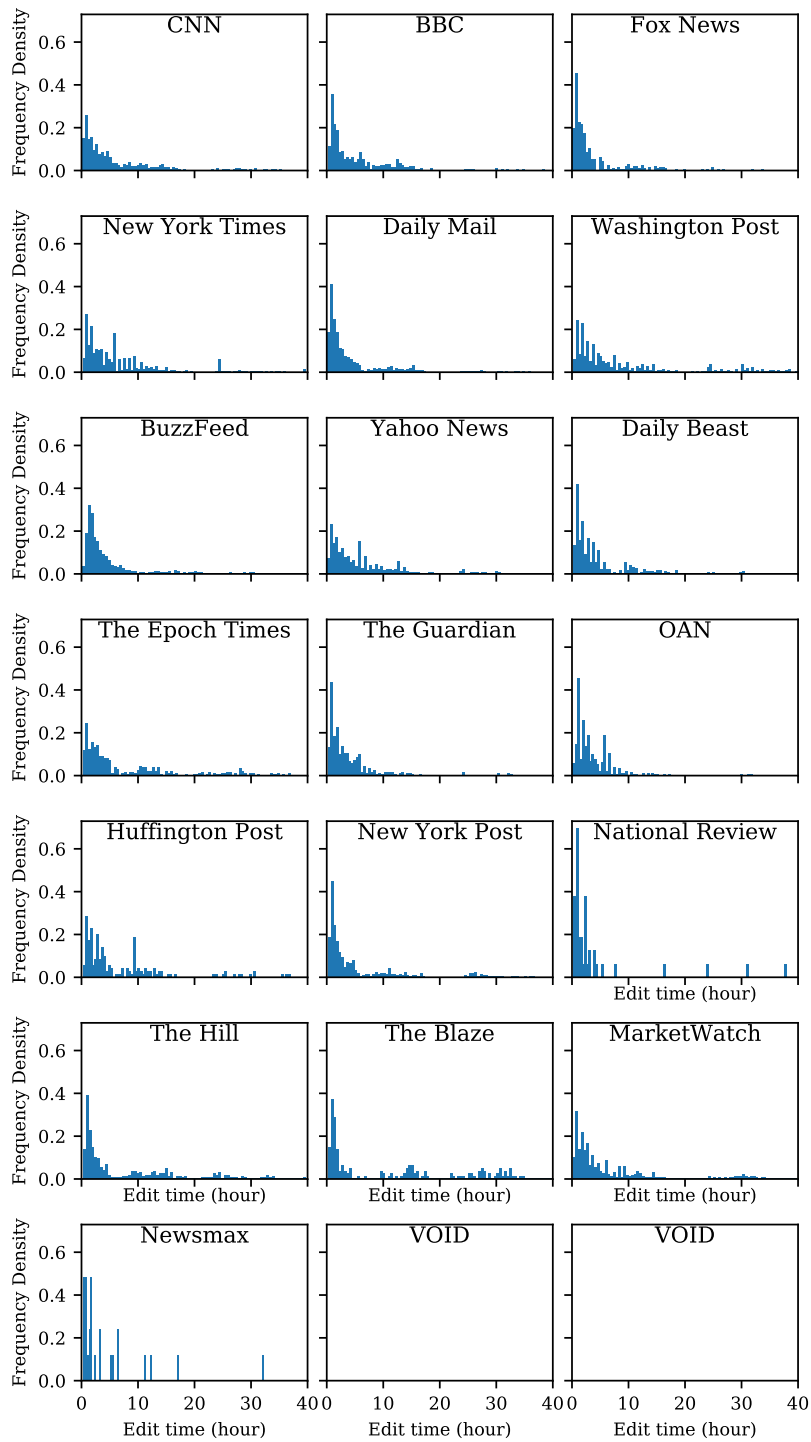


Figure 6.8: The post-publication edit time per news publisher.

Chapter 7

Information and Evolution of Personal Biographies ¹

7.1 Introduction

Self-identity is a concept of *who we think we are* that directs us how "to behave in a certain way" [167]. The formation of self-identity is rooted in people's autobiography memory, often cultivated from personal life experiences. Occupational work is arguably the life domain to which we devote the greatest part of our time awake, thus, it is an essential part of our experience, embedding itself into our motivation, life goals and personal sense of identity. "*One life-long objective is work per se*"; as Butler [26] suggested "Every man's work .. is always a portrait of himself."; However, not every person will develop a primary occupational identity (*e.g.*, "*I think of myself as a mother, rather than a bank clerk.*"). Likewise, not every job ultimately leads to the establishment of occupational identity (*e.g.*, "*I do not define myself as a deliverer, although I do it for living.*").

In this paper, we consider the question of *what factors contribute to the formation and transition of occupational identity?* However, research into personal identity is difficult because self-identity is not directly observable. Although an individual's employment status is explicitly stated in tax records and other datasets, an individual's occupational identity is an internal and invisible presentation of "*who I am*", and generally not publicly available.

But recent research [137] has proposed a new methodology, using Twitter

¹Guo, Xingzhi, Dakota Handzlik, Jason J. Jones, and Steven Skiena. Biographies and Their Evolution: Occupational Identities over Twitter. In Submission.

and other social media biographies as the proxy for self-identity. The concise (on Twitter, at most 160 character) personal biography is a feature of many social media platforms, and provides an outlet for users to report their current self-identity. On Twitter, this biography string is part of every user’s public profile, and research has explored the various and changing aspects of identity that users elect to associate themselves with [137, 146].

Although users differ in what they disclose, many social media biographies express relational identity (*e.g. father/mother of, alumni of*), demographics, occupations and political affiliations. Semertzidis et al. [146] further categorized biography content in terms of average word fraction: Occupation (7.5%), Interests/Preferences/Hobbies(4.6%), Personal Info (2.6%), etc. For example, the biography:

25. black man. student. Films. "We are guardians of the image & that’s how I see our role as DP’s"

contains information about age (*25-year old*), occupation (*student*), ethnicity (*black*), gender (*man*) and interests (*films*).

Longitudinal changes in a subject’s self-reported biography allows analysis of changing self-conception over the full life course. For example, the aforementioned biography is likely to updated to reflect age and career path (*e.g., 25 → 26, student → cameraman*). This would record an occupational identity change from *student* to *cameraman* upon graduation. Our dataset records 435.7 million twitter biography edits, and extracts more than 287,000 job transitions between over 25,000 distinct job titles. We present examples of the frequent job transitions in Table 7.1.

Our large-scale dataset of public biographies gives researchers a new opportunity to study the self-presented identities and their evolution among Twitter users. Previous studies involve much smaller datasets, and lack the longitudinal element enabling us to track changes in the self-identity of individuals over time. Pathak et al. [125] extracted a set of words from biographies as personal identifiers for future social identities studies. Other studies [152] use automatic tools to profile Twitter users, and observe that jobs in the creative sector (*e.g., writer, artist*) are over-represented in UK Twitter users. However, they only report population biases in Twitter users (*e.g., over-represented occupational jobs*), but do not further investigate the reasons behind them. Meanwhile, these studies generally analyze the population at one fixed time point, and ignore the evolution in each individual over time.

In our study, we collect and analyze a multimillion-subject scale temporal Twitter biographies dataset, and systematically explore self-authored occupational identities. We present our quantifiable findings to better understand how people consider occupations as a part of self-identity. To further clarify our motivation,

this paper focuses on the self-disclosed *occupational identity*, instead of the mere employment status over the Twitter population.

The primary contributions of this paper include:

- *A Temporal Self-Description Data Set* – We have assembled a longitudinal corpus of self-reported biographies as they evolve annually over the period from 2015-2021, with 1.35 million distinct users whose biographies are written in English. However, we are legally only able to share the word embeddings of bios due to privacy and terms-of-service concerns. We will also release an occupational transition graph with 25,033 unique jobs and 287,425 unique edges. Our dataset provides a unique resource for studying changes in self-identity, and will be made available on publication.
- *Identifying the Reasons Behind Occupational Identity* – With this rich dataset, we present a large-scale case study of occupational identities among Twitter users. Further, we quantify which occupations are over-represented in self-biographies relative to the number of people holding such positions. We show that 74.04% of over-represented jobs are above the overall median occupational prestige score, versus only 39.48% for under-represented jobs. We demonstrate that over-representation is highly correlated with job prestige, with a Spearman correlation of $\rho = 0.4858$. The correlation of over-representation with prestige is stronger than that with income, where $\rho = 0.3961$.
- *The Evolution of Identity* – We present a temporal analysis explaining how and why self-descriptions change, distinguishing life events (e.g. job promotion, graduation, etc) from lateral moves. In our study of occupation identity transitions, we discover that there is an inherent directionality towards increased occupational prestige with most transitions (e.g., from *assistant professor* to *associate professor*). Moreover, we also present an intriguing case study, reflecting changes in observed occupational identity amid COVID-19 and its aftermath.

This paper is organized as follows. Section 7.2 describes previous work in analysis of self-identity, particularly for social media. Section 7.3 describes our Twitter biography data set, followed by a discussion of research ethics in Section 7.4. Section 7.5 presents our observations concerning occupational identities on Twitter, and its relation to job prestige and income. We study the changes in user biographies over time and present the case study in Section 7.6. Finally, we present our conclusions and future work in Section 7.7.

7.2 Background and Related Work

Self-identity is a concept of *who we are* and directs us how to "behave in certain way" [167], fostered in our autobiographical memory [22]. Self-identity can be realized as a knowledge representation [98] of the past events with personal experience, often characterized as personal life story. However, due to the nature of its inobservability in practice, it is notoriously challenging to conduct quantitative research of self-identity on a large scale. Recently, [92, 137] proposed a new methodology to discover quantifiable insights of political identities from millions of Twitter biographies, leveraging them as a directly observable source of self-identities. Such research methodology makes it possible to study self-identity in a large-scale and computational manner.

In this section, we describe self-identity related theories, methods and insights from the existing research of psychology and computational social science.

Self-identity in theory: Generally speaking, there are two kinds of self-identity: 1) *Personal identity* describes how an individual defines him/her-self as a unique human-being; 2) *Social identity* represents how an individual feels belonging to certain groups as a member. Occupational identity lies somewhere in between (e.g., a unique self belonging to a work group). [34] first connected occupation to identity, suggesting that occupation contributes to identity shaping (e.g., *I am a sociologist*), and occupation provides a context for creating meaningful life, which promotes well-being and life-satisfaction. To understand the work-related identity, the current studies [11] aim to answer these key questions: 1). *What is work-related identity?*; 2). *Why does identity matters?*; 3). *How does identity evolve?* To address such questions, Kielhofner [97] proposed the term "*Occupational Identity*" and defined it as "a composite sense of who one is and wishes to become as an occupational being".

Establishment of occupational identity: Kielhofner [97] further argued that the occupation which are satisfying and recognized within one's environment are more likely to become meaningful and central to one's life, sustaining to self-identity. According to social identification theory [47, 88, 164], a healthy self and social identity tend to thrive toward positive self-evaluation and link to a positive social group identity. As emphasized in occupational identity research, social approval is also key to the identity establishment. For example, key occupational identity theorists suggest that [33, 127] "identities are fostered when individuals perceive that their chosen occupations win approval from the greater society". One quantitative measure of social approval is perceived occupation prestige [80, 85, 158], derived from job-specific factors like income and education levels. Specifically,

Hout et al. [85] released occupational prestige scores based on the interviews with 1,001 individuals during 2012. These ratings range from 0 (bottom) to 100 (top), covering 860 occupational titles or 539 job categories in the 2010 Standard Occupational Classification (SOC) [46]. This unique resource enables us to quantitatively measure the correlation between the occupations in identity and its social approval.

Self-identity in Twitter biographies: Social media users often present their self-identities in bios. Semertzidis et al. [146] investigated how people express themselves in Twitter biographies and discovered that the most common content in biographies are occupations. Pathak et al. [125] extracted several clusters of personal identifiers from Twitter biographies by matching text pattern, and suggest it as a resource for future social identity studies. Similarly, Sloan et al. [152] extracted job titles within the bios of UK Twitter users, and found that the jobs in creative sector (e.g., artist, writer) are over-represented. They explained this observation by the fact that Twitter is used by people who work in the creative industries as a promotional tool, and perhaps as a technical artifact from mis-classifying hobbies and occupations (e.g., leisure or professional writer). Other researchers [117] studied the demographic distribution of the Twitter population by analyzing self-reported user names and biographies, enabling large-scale social studies involving demographic characteristics. Note that self-identity researchers focus on how people self-present themselves, rather than working to improve the accuracy of user profiling algorithms [124, 130].

Self-identity transitions over time: Personal biographies are dynamic, reflecting the life or mind changes in a person over time. Shima et al. [148] analyzed the timing and reasons for Twitter bio changes and found that English users most frequently make changes on their birthdays. Rogers and Jones [137] discovered that Americans defined themselves more politically by integrating more political words in their Twitter bios over recent years. In our temporal analysis, we examine the reasons behind these modifications and discover interesting bio transitions for graduation, anniversaries and job transitions. To our best knowledge, this is also the largest resource available for studying dynamics in occupational identities.

7.3 Biography Dataset Collection and Pre-processing

We conducted a study on longitudinal occupational identity by extracting self-reported job titles from the biographies of Twitter users over six years, and further mapping the job titles to Standard Occupational Classification (SOC) ²

²The U.S. SOC: <https://www.bls.gov/soc/>

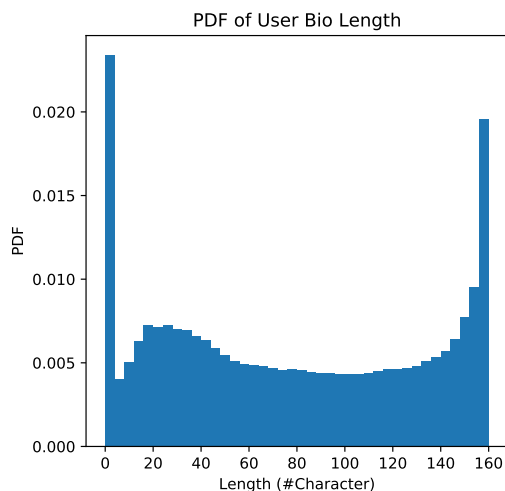


Figure 7.1: The statistics of sampled biography length. The two peaks indicate that people tend to either skip or write complete bios. More than $\sim 80\%$ users have bios longer than 25 characters.

for specific job category information (e.g., average salary, job prestige scores, etc). We provide a thorough description of our data processing procedures below.

Collecting longitudinal Twitter biographies: We collect the Twitter user biography associated with each of 51.18 million English-language³ re/tweets, from Feb. 2015 to July 2021 using Twitter API. We have been pulling 1% of all tweets from the Twitter stream on a daily basis over this period, and been recording personal biographies with each tweet’s observed timestamp. Our analysis detects 435.70 million biography changes over this corpus. Figure 7.1 shows the bio length distribution, demonstrating that more than 80% of users take advantage of the biography field to report a substantial self-description.

Large-scale demographics estimation from user names: Arguably, a human’s name serves as the very first identity. English user names reveal a lot of demographic information. For example, first names (e.g., *Jack*, *Rose*) may encode the gender, while last names (e.g., *Smith*, *Yao*) may indicate ethnicity. As a common practice for large-scale social media analysis [117], we estimate the ground truth from users’ self-reported names. To reduce the noise introduced by the non-genuine names (e.g., *Skies-of-Glory*, *Uber-Man*, *Morning Brew*, ...), we exclude most of the non-human-like names by matching the first/last names

³We use the FastText language identification tool [93, 94] to filter out non-English bios.

based on the 2000 U.S. Census Data ⁴, then manually inspect the first 500 most common first/last names to avoid systematic false positive errors. In total, we found 7,529,400 unique genuine names associated with 12,907,860 users (or 25.22% of the users in the raw data).

Similar to methods used in [117, 130, 180], we employ name embedding-based classifiers [153, 185, 186] to infer ethnicity and gender ⁵ purely from names. To properly handle the estimation uncertainty, instead of using a single label (e.g. male vs female), we represent the demographics attributes in a probabilistic manner. For example, The first name *Kellen* may have a probability of 80% male, 20% female. Ethnicity attributes are also presented probabilistically in four coarse ethnicity groups (White/African-American/Hispanic/Asian).

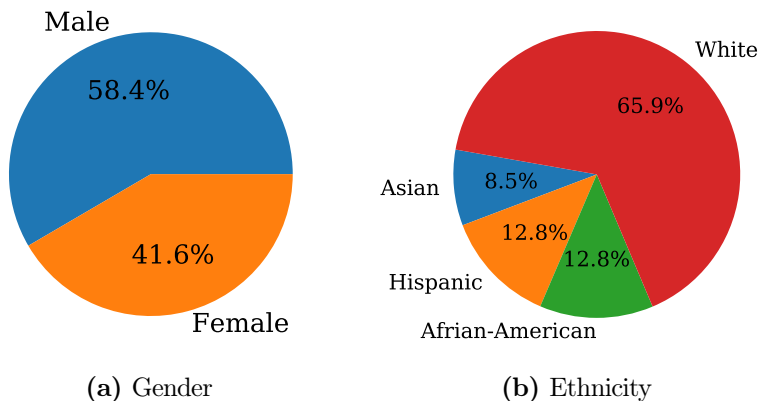


Figure 7.2: The overall estimated demographics distribution among 12.91M users. According to Statista, the gender ratio of Twitter users worldwide is 56.4% v.s. 43.6%. Since English Twitter users are dominated by U.S, the ethnicity distribution is similar to its in the U.S.

Extracting occupation identities from biographies: Biographies contain rich occupational information [146]. To demonstrate the usefulness of our dataset, we extract⁶ and analyze self-reported job titles on a large scale. From biographies sampled over a six year period (2015-2021), we detected 25,033 unique occupational titles from 6,028,581 Twitter users, which covers 11.78% of whole

⁴2000 U.S. Census Data contains 92,600 first name and 151,671 last names. <https://github.com/rossgoodwin/american-names>

⁵Gender detector: <https://github.com/kensk8er/chicksexer>

⁶Job title extractor: https://github.com/fluquid/find_job_titles

population in our dataset. Subjects often report multiple job titles over this period, reflecting promotion or career changes, as will be addressed in Section 7.6.

Mapping job titles to Standardized Occupational Codes (SOCs) with job prestige scores: Note that the detected job titles are pure text and unstructured. In order to gain richer insights about each job title (e.g., salary, popularity, ...), we organized them according to the U.S. Standard Occupational Classification (SOC), enriching with supplementary data (e.g., employment and income distribution).⁷ and job prestige data [85] (which estimates the occupation prestige in SOC-indexed work categories).⁸ We first use exact matching to map all Twitter job titles to *SOC(2018) Direct Match Title*, which exhaustively lists 6,593 job title examples in all SOC occupational categories. Then, we use the ROUGE score [107], which is based on text overlap, to *softly* match each job title to the examples provided in the Standard Occupational Classification (SOC). The SOC category of the example with the highest match score is then assigned to the job title. To ensure the precision of job category mapping, we consider the job title unmatched if the ROUGE-F1 score is lower than 0.8. For those filtered unmatched titles, we exclude them in the analysis to avoid noise. Since the job prestige is surveyed based on OCC(2010) format, we convert SOC(2018) to OCC(2010) via the official mappings, resulting in 1,834 unique job titles associated with high precision occupational prestige scores. We present several alignment examples with associated prestige scores in Table 7.2.

7.4 Ethical Considerations

Although Twitter data is public and often falls under public data exemptions in IRB consideration, sensitive information such as user’s gender, ethnicity, health, political affiliation or beliefs must be used with caution. Inference on the individual level is restricted use case per the Twitter Developer Agreement, however:⁹

Aggregate analysis of Twitter content that does not store any personal data (for example, user IDs, usernames, and other identifiers) is permitted, ...

All of our results are presented at an aggregate level, so that no individual identifier

⁷<https://www.bls.gov/soc/2018/home.htm>

⁸http://gss.norc.org/Documents/other/PRESTG10SEI10_supplement.xls

⁹More about restricted uses of the Twitter APIs: <https://developer.twitter.com/en/developer-terms/more-on-restricted-use-cases>

Table 7.2: Twitter job title mappings and job prestige estimates, ranked by match score and frequency of mention. Note that multiple job titles may map to the same SOC category. For example, both the *ceo*, *coo* titles fall into the category *Chief executives*, and share the same occupation prestige score. Match score is ROUGE-based with the range [0.0,1.0], where 1.0 indicates an exact match. We assign the occupation prestige score to those titles with the match score greater than 0.8 to avoid noise from job mapping noise.

Job Title (Bios)	Occupation Category (SOC)	Match Score	Mention Freq.	Occupation Prestige
ceo	Chief executives	1.00	325261	71.58
civil engineer	Civil engineers	1.00	46412	65.33
coo	Chief executives	1.00	41722	71.58
mechanical engineer	Mechanical engineers	1.00	38117	70.31
accountant	Accountants and auditors	1.00	36614	59.72
web developer	Web developers	1.00	32202	55.43
web designer	Web developers	1.00	16653	55.43
community manager	Public relations and fundraising managers	1.00	15279	51.64
general manager	General and operations managers	1.00	14309	49.64
registered nurse	Registered nurses	1.00	14116	64.43
...
tamping machine operator	Paving, surfacing, and tamping equipment operators	0.86	1	34.12
appliance service technician	Home appliance repairers	0.86	1	35.00
sheet metal worker apprentice	Sheet metal workers	0.86	1	34.52
software engineer web application	Software developers, applications and systems software	0.86	1	60.12
chief juvenile probation officer	Probation officers and correctional treatment specialists	0.86	1	46.71
director, religious education	Directors, religious activities and education	0.86	1	37.36
business service representative	Sales representatives, services, all other	0.86	1	43.18
assistant food service director	Food service managers	0.86	1	39.43
medical and health service manager	Medical and health services managers	0.80	2	64.06
waste water treatment plant operator	Water and wastewater treatment plant and system operators	0.80	1	38.87

or original content can be traced back or reconstructed from our results. All potentially identifiable examples given in our results have been artificially modified to enforce the privacy protection. The IRB of our institution has affirmed that the use of public information does not constitute human subjects research, in accordance with regulations from the US Department of Health and Human Services.

Opportunities and limitations in our dataset: To our best knowledge, our dataset is the first and largest resource for both 1). conducting temporal analysis of biographies 2). studying occupational identities on Twitter. It also provides a big picture of the Twitter population composition in multiple socioeconomic views. However, we also note several potential limitations in our current approach: 1). The difference in self-disclosure may cause the result biased towards the population who are more willing to reveal themselves. 2). The job title mapping are not perfect. Although we manually validate part of the results, how to accurately annotate users on a large scale is still a challenging problem in both computer and social science studies. 3). All real-world data (job prestige, occupation distribution, standard occupation category) is based on the U.S. Among the subset of users with a non-empty Twitter location field it was observed that over 99% of them are classified as being within the U.S. using a regex-based location parser, making the results not generalizable to other regions. 4). To protect user privacy, we can only share word embeddings of biography text and the full job transition graph.

7.5 Occupational Identities Reflected Through Twitter Biographies

Work is an essential event in our daily life, which contributes to our self-identity. Sociologists and occupational scientists have proposed several theories about the establishment of occupational identity. One fundamental factor is the quest for social approval [38, 97, 156] (e.g., job prestige, income). Although we have a wide variety of public labor statistics (e.g., employment by sector), Twitter biographies provide a unique and directly observable view of how users define *themselves* by occupation, displaying whether the users feel their current work reflects an important part of their *self-identity*. After filtering out the potential organizational and bot accounts¹⁰, we obtain a total of 23,267 distinct self-reported job titles. In addition, we match the job titles to Standard Occupation Code and associated

¹⁰For this analysis, we only include the users who report human-like names which can be matched to US Census data.

job prestige scores, as illustrated in Table 7.2.

In the following subsections, we first walk through a few extracted occupation examples from Twitter biographies. Then, we propose to use the *Occupation Over-Represented Ratio* (κ) statistic to describe the relative difference in the frequency of occupations in Twitter biographies compared to actual real-world presence, which captures people’s sense that the occupation as a part of self-identity. Finally, we analyze the job prestige variables with respect to the establishment of occupational identity.

7.5.1 Over/Under-represented Occupations in Twitter Biographies

The distribution of self-mentioned occupations in Twitter biographies is significantly different from that as occurs in the U.S. population at large¹¹. The most/least frequently mentioned jobs in Table 7.3 seem contradictory to our sense of the labor market in terms of volume and socioeconomic distribution: for example, we expect more workers than executives. Prestigious occupations appear much more likely to be included as part of occupational identity, and are thus over-represented in our data. We can quantify this observation through data on the relative prestige of jobs/titles. We present our findings below.

Table 7.3: The most/least popular self-reported jobs in biographies.

#	Occupation	(%)	#	Occupation	(%)
1	student	12.91	23248	restaurant busser	<0.01
2	founder	6.08	23252	track sweeper	<0.01
3	director	6.06	23257	referral clerk	<0.01
4	owner	5.37	23262	soil expert	<0.01
5	ceo	4.55	23264	grocery deliverer	<0.01
6	president	4.52	23266	culinary worker	<0.01

The salary of the self-reported occupations is significantly higher:

It is known that the average income of Twitter users is higher than that of the general population [20, 179]. We further find that the difference in self-reported occupations in biographies makes this gap even more significant. By matching the self-reported job titles to their incomes, Figure 7.3 presents the histogram of the salary of the occupations in bios, showing that most users have higher salary

¹¹We use the employment statistics from U.S. Labor Department

than the median income¹². This finding provides a clue that a job’s overall salary impacts its role in developing occupational identity.

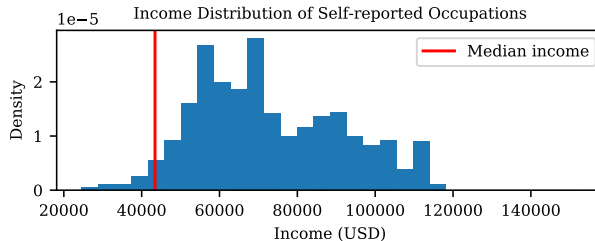


Figure 7.3: The salaries of self-reported jobs are significantly higher than the overall median (\$43,431 USD) in New York, US. We use New York’s job income statistics as standard to avoid salary discrepancy across regions.

Identifying over-represented occupations in Twitter biographies: Titles can be aspirational: being CEO of Ford Motor Company means something different than CEO of a one-person startup. One interesting observation is that more people define themselves as CEOs (#5) on Twitter than Grocery Deliverers (#23264), despite the fact that there are raw fewer CEOs in the general population. This difference can be explained by the fact that: 1) grocery delivers may be less likely have Twitter accounts, and/or 2) grocery delivers do not consider the job as part of their self-identity and exclude it from personal biographies. In our analysis, it is the latter possibility that reveals insights about the job-specific factors toward occupational identity.

To quantify over-represented occupational families in Twitter biographies, we use the *ver-representation atio* κ to measure how each self-mentioned occupation exceeds the expected frequency according to the real-world workforce percentage. Specifically, κ is defined by:

$$\kappa = \frac{P(\text{Occupation}|\text{Twitter})}{P(\text{Occupation}|\text{Real-World})} \begin{cases} > 1.0 & \text{,Over-represented} \\ = 1.0 & \text{,Balanced} \\ < 1.0 & \text{,Under-represented} \end{cases}$$

¹²We use Rouge-L F1 score to softly align reported occupations to New York median income list. resulting in 21,946 job titles (out of 25,033) from 3,408,916 users associated with their occupation income. To avoid the income discrepancy in different regions, we use New York’s job income list as the standard. Data source: <https://catalog.data.gov/dataset/occupational-employment-statistics>

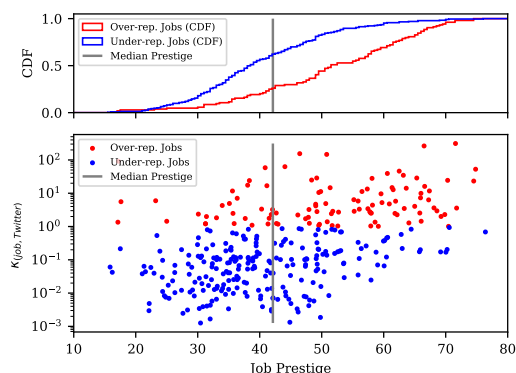


Figure 7.4: *Bottom:* Job prestige scores measure the socioeconomic status of an occupation according to its salary and public perception. κ measures the ratio of how an occupation is over-represented on Twitter compared to its real-world labor distribution. Prestige and κ correlate with Spearman’s correlation $\rho=0.4858$. Over-represented jobs (red) generally have higher than the median prestige. *Upper:* The prestige distribution between over/under-represented jobs are statistically different with K-S test $d=0.4284$ and p-value $\approx 2.07 \times 10^{-12}$.

In an extreme case, if one occupational family was never mentioned in all biographies, then $\kappa=0.0$, indicating a completely under-represented occupational category (e.g., *track sweeper*, *restaurant busser*, *grocery deliverer*). In contrast, $\kappa \gg 1.0$ indicates a highly over-represented category on Twitter (e.g., *CEO*, *COO*, ... *Chief Executive* category). Note that the biases in Twitter’s user population (e.g., having generally higher education and salary) can only amplify the over/under-representativeness, thus not it is a direct concern regarding to our goal. We emphasize that our proposal is **not** to uncover the real-world labor statistics from Twitter but to discover which occupations are more likely to form a part of a user’s self-identity (over-represented). Then, we quantitatively investigate its correlation to other hypothesized factors like social approval.

7.5.2 Social Approval and Demographics in Occupational Identity Establishment

The construction of occupational identity is a complex process involving personal variables and social approval. Based on the observable evidence in Twitter bios, we seek to answer the question: *Are high-prestige jobs more likely to be embedded into occupational identity?*

Table 7.4: The breakdown of the percentage of users who disclosed occupational identities by gender and ethnicity. Overall, males are 32.27% more likely to mention jobs than females do.

	Asian	Hispanic	Black	White	All Race
Female	15.01%	10.28%	16.20%	16.89%	15.80%
Male	23.19%	16.77%	21.07%	22.27%	21.69%
All gender	20.70%	13.64%	18.78%	20.05%	19.25%

Men are more likely to be embedded with occupational identity than women: Men are general more into career and power than women, as reported in [64]. Table 7.4 presents the percentage of the Twitter users who disclosed occupational identity in biographies, breaking down by ethnicity and gender. Across all races, we discover a consistent pattern that relatively 32.27% more males would mention jobs in the bios than females do. This finding is consistent to the hypothesis that men are more job-oriented than women.

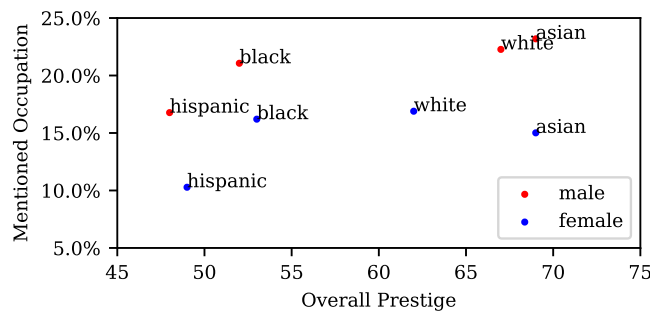


Figure 7.5: Men are more career-oriented regardless of ethnicity. The group with more prestigious jobs are more likely to mention occupations.

Separate ethnicity group shows different occupation disclosure rate, probably, due to disparate occupation prestige: Table 7.4 reports that significantly lower percentages in Hispanic community mention their occupations in both the fe/male cohorts, compared to other ethnicity. In a stratification lens, Jennings et al. [89] recently revealed that the occupational prestige in Hispanics is lower than other groups. This observation coincides with our findings in Figure 7.5. Given the disparity of job prestige in Hispanic community, they tend to not to identify with occupation as frequently as other groups do.

Self-reported jobs reflect the occupational concentration of demographics Table 7.5 and 7.6 shows the most over/under-represented occupations in each gender or ethnicity group based on the biased ratio $\kappa_{(\text{job}, \text{ethnicity})}$ defined as following:

$$\kappa_{(\text{job}, \text{ethnicity})} = \frac{P(\text{ethnicity} | \text{job})}{P(\text{ethnicity})} \begin{cases} > 1.0 & \text{,Over-represented} \\ = 1.0 & \text{,Balanced} \\ < 1.0 & \text{,Under-represented} \end{cases}$$

Note that if there is no ethnicity bias in job, $p(\text{ethnicity}|\text{job}) = p(\text{ethnicity})$, making $\kappa_{(\text{job}, \text{ethnicity})} = 1$. The similar measurement is also applied to job-gender bias.

Table 7.5: The top gender biased occupations in real world and Twitter

Real world	κ_{male}	Twitter	κ_{male}
Female-biased Occupations			
Skincare specialists	0.03	doula	0.27
kindergarten teachers	0.06	esthetician	0.29
Executive secretaries	0.06	kindergarten teacher	0.31
Dental hygienists	0.09	registered dietitian	0.32
Speech pathologists	0.09	makeup artist	0.34
Medical secretaries	0.09	early childhood	0.34
Childcare workers	0.10	independent consul.	0.36
Cosmetologists	0.14	yoga teacher	0.39
Male-biased Occupations			
Concrete finishers	1.89	asst. baseball coach	1.65
Power-line installers	1.87	asst. football coach	1.64
Crane operators	1.87	basketball coach	1.64
Heavy vehicle technician	1.86	offensive coordinator	1.64
Bus and truck mechanics	1.86	baseball player	1.63
Heating, AC technician	1.86	lead pastor	1.60
Electricians	1.85	software architect	1.60
Plumbers	1.85	golf professional	1.57

Table 7.5 presents the gender bias discovered from the real-world occupation survey and our Twitter data side-by-side. We found that females prevail in cosmetics, health and general education domain, which is consistent with the real-world

survey results. Males are closely related to sports, politics and technology, while the real-world data shows different but still reasonable results, and we will discuss the reasons behind this difference later.

Similarly, Table 7.6 presents that certain ethnicity groups participate more in sports, academic, technology and art industry (Table 7.14 in Appendix presents more samples). These results are demonstrative that our dataset captures complex aspects of society, and could be useful for quantitative social studies.

Prestigious jobs are more likely to be embedded into self-identity: The anecdotal evidence of Table 7.3, suggests that *prestigious* jobs (e.g. *CEO, COO, ...*) tend to be mentioned more frequently in personal biographies. This coincides with the hypothesis about social approval, that is, the social status of the job (including salary, perceived prestige) is an important factor contributing to the occupational identity establishment. In Figure 7.4, we plot the over/under-represented groups as red/blue dots against the job prestige scores. The result demonstrates that the job prestige score is highly correlated with κ of Spearman correlation $\rho = 0.4858$. It also shows that 74.04% of over-represented jobs are above the overall median prestige score, versus 39.48% for under-represented jobs. Specifically, the prestige distributions of over/under-represented jobs are significantly different with K-S test $D = 0.4284$ and p-value $\approx 2.07 \times 10^{-12}$.

Interestingly, we find that the correlation of over-representation to annual income ($\rho = 0.3961$) is weaker than it is to prestige, implying that social approval is more important than pure material return. For example, *Legislators, Clergy* and *Firefighters* share high prestige score (with percentile $> 80\%$ in prestige), although their income percentiles are only 22.55%, 55.93% and 57.27%, respectively. But they are all over-represented with $\kappa > 1$ based on our observations. This evidence that more prestigious jobs appear to be included more frequently in Twitter biographies as a part of one’s identity.

7.6 Occupational Identity Evolution

If Twitter biographies capture the notions of self-identity, then changes in biographies reflect changes in self-identify. Our dataset captures identity changes for millions of people over the six years from 2015-2021. In this section, we first characterize and analyze the general biography edits, then focus quantitatively on issues of occupational identity transitions.

We randomly sample 1,353,325 of our 51.18M individuals and acquire a subset of 2,597,550 consecutive changed pairs whose word edit distance is within 30

Table 7.6: The examples of over/under-represented occupations in each ethnicity group. We normalize the raw count for each ethnicity and occupation group. The column *Ratio* measures how many time the calculated value exceeds the expected value based on population prior. If ethnicity distribution of an occupation meets the prior distribution, the ratio value is 1.

White	κ	Asian	κ	Hispanic	κ	African-American	κ
Over-represented							
golf professional	2.12	research scholar	6.60	industrial engineer	3.48	performing artist	1.82
golf coach	2.10	chartered accountant	5.76	volleyball player	2.30	forex trader	1.81
pitching coach	2.09	political analyst	4.08	industrial engineering	2.18	motivational speaker	1.79
assistant superintendent	2.07	social worker	3.82	soccer player	2.14	radio personality	1.75
social studies teacher	2.07	electronics engineer	3.49	medical assistant	1.74	music artist	1.73
Under-represented							
research scholar	0.84	softball coach	0.17	golf professional	0.25	research scholar	0.74
chartered accountant	0.98	assistant football coach	0.18	support worker	0.29	industrial engineer	0.76
industrial engineer	1.07	assistant baseball coach	0.18	asst. basketball coach	0.30	software architect	0.77
electronics engineer	1.12	baseball coach	0.19	men's basketball coach	0.31	assistant professor	0.81
android developer	1.17	athletic director	0.20	golf coach	0.33	postdoctoral fellow	0.83

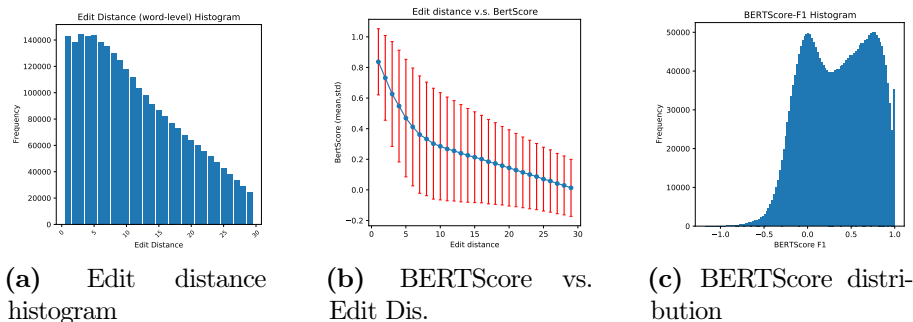


Figure 7.6: Left: Small bio changes are more common than complete rewrite. **Middle & Right:** Semantic similarity between changed bio pairs. Two peaks in 7.6c shows that the most common changes are minor updates and completely rewrite.

characters. Figure 7.6a shows that most people update their bios by 1-5 words at a time. But character differences do not completely reflect semantic differences: an "artist" transformed in a "painter" represents a smaller change than the edit distance suggests. To better capture semantic similarity, we extend this analysis to all changed pairs with $BERTScore_{F1} \in [-1, 1]$ ([199]) as the semantic similarity measure. Figure 7.6b shows the BERTScore against word-level Levenshtein distance. As expected, semantic similarity decreases as more edits are applied. Figure 7.6c shows the distribution of BERTScore, where the hump centered at 0 implies that a significant fraction of people completely rewrite their biographies with each transition, while the hump at 0.8 shows another large group of people making minor edits to their bios (e.g: age or job title updates).

Table 7.7: The top part-of-speech changes: The most popular change is between numbers, reflecting age updates on birthdays or anniversaries. X is not recognized, e.g.: Emoji or unrecognized abbreviation. Total number of replaced pairs is 89,838.

POS change (before, after)	Count
(NUM, NUM)	23,335
(NOUN, NOUN)	15,850
(X, X)	12,889

7.6.1 Minor Edits in Biographies

To understand the nature of the edits distribution, we look into the changed biography pairs where only single words have been substituted (89,838 pairs), and discover many occupational transitions over time. First, we present the top part-of-speech (POS) changes in Table 7.7. These changes usually share the same POS tag, indicating the alternation of word choices.

Breakdown of Nouns: To better understand the reasons behind word replacement, we organize interpretable relations between changed nouns in Table 7.8. We assign five categories of noun changes based on syntactic features (e.g: same lemma). Besides *Others* group, most of them are minor changes (with single character change), reflecting job promotion (e.g. *vp* to *svp*) or age updates. In addition, we observed many career transitions (e.g., from *manager* to *director*) in all categories, which will be addressed in Section 7.6.2.

Table 7.8: Breakdown of changed nouns in biography edits. One pair may belong to more than one category. Some of them are related to the change of occupational identity (e.g., (*vp* -> *svp*, *coordinate* -> *manager*)).

Category	Total	%	Examples (Before, After, #)
Share lemma	693	4.54%	(alumni, alumnus, 60); (dog, dogs, 31)
Synonym	669	4.38%	(alumni, alum, 46); (manager, director, 41)
One Token Change	2327	15.89%	(vp, svp, 20); (22yrs, 23yrs, 14)
Hyponymn	335	2.19%	(student, graduate, 46); (student, grad, 25) (student, alum, 15); (father, dad, 9)
Hypernymn	266	1.17%	(teacher, educator, 17); (journalist, writer, 8); (actress, actor, 7);
Others	10898	71.36%	(student, candidate, 104); (sophomore, junior, 68); (coordinate, manager, 28)
All	15272	100%	-

7.6.2 Transitions Between Occupational Identities

To better understand the changes of occupational identities, we extract and analyze those biography pairs in which any occupational title has been added or removed.

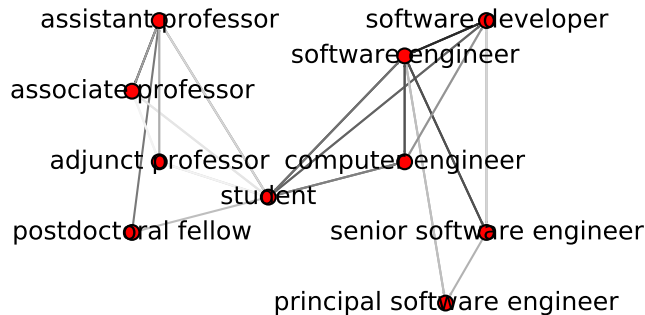


Figure 7.7: Examples of job transitions in the graph. Darker edges represent more frequently observed transitions.

Represent occupational transitions as a graph: We formulate occupational transitions as a directed weighted graph $G(V,E)$, where V contains all unique job titles as vertices, E contains all job title transitions $e_{i,j} = (v_i, v_j, w_{i,j})$, where edge weight $w_{i,j}$ represents the total number of the observed transitions from i to j . For example, a biography changed from "*Student, Volunteer*" to "*Software Engineer, Volunteer*" increases the edge weight of *Student* \rightarrow *Software Engineer*. Our final graph contains 25,033 nodes and 287,425 unique edges, consisting of seven weakly-connected components. The largest component contains 25,021 nodes (99.95% of all). We illustrate a subgraph in Figure 7.7.

Community of Occupational Identity Transitions: The job transition graph has an appealing property of clusteriness, which reflects the proximity between occupational titles. For example, in the rooted clusters from *Student* in Figure 7.7, the roles of academia are naturally clustered on the left-hand side (the source), while IT industrial roles are intertwined on the right-hand side (the sink), but well-separated from the academic counterpart.

Graph partitioning [35] is well studied for community detection. We partition the simple job graph (unweighted, undirected) based on modularity, discovering densely intra-connected communities. Table 7.9 shows that the related job titles generally fall into the same cluster. Some of these share common text patterns (e.g., "*hadoop developer*" and "*hadoop architect*"), while others are inherently related but without significant text overlap (e.g., "*highway maintenance worker*" and "*bridge inspector*"). These detected transitions and clusters can provide more context to better understand personal social dynamics. The full graph can serve as a unique resource for better job title clustering, which we will release upon publication.

Table 7.9: Each cluster (row) contains several highly-related job titles derived from our occupational transition graph.

Sampled Self-reported Titles in Each Clusters
health information director, health information technician
consumer lending manager, secondary market manager
loader operator, front end loader operator
highway maintenance worker, bridge inspector, toll collector, highway inspector
hadoop developer, hadoop architect, linux architect, windows server administrator, web systems developer, mainframe systems administrator
occupational safety specialist, safety and health manager, safety trainer, professor of early childhood education, peer educator, speech language pathologist assistant,
clinical assistant, clinic assistant, clinical associate, psychiatric assistant
communication instructor, language specialist, public speaking teacher
customer logistics manager, import manager, export sales manager, export specialist

Most importantly, this clusterness demonstrates that mobility in occupational identity is usually limited to the same job category, partially because occupational identity directs us to behave as a member of particular group. For example, a Professor in Computer Science rarely becomes a software engineer even though s/he may be able to do so for greater material return.

Directionality in Self-reported Job Transitions: We identify the most common title transitions (changing from Job- i to Job- j in either direction) in Table 7.10 (top), and find that the most frequent transitions relate to title revisions (e.g., *vice president* to *vp*). Furthermore, we define the transition *directionality*, the fraction of directed transitions from v_i to v_j , as :

$$dir_{i,j} = \frac{w_{i,j}}{w_{i,j} + w_{j,i}} \in [0,1], \quad (7.1)$$

We sort the transitions by $dir_{i,j}$ in Table 7.10 (middle), showing that the most directed transitions are related to job promotion and reflect a significant role change (eg., "*student to nurse*", "*postdoc to professor*"). Meanwhile, among the *less directed transitions*, most of the job titles are interchangeable with subtle difference in specificity (*scientist to neuroscientist*). The discovery of this directionality better quantifies the relationships between jobs, and is helpful for understanding job mobility.

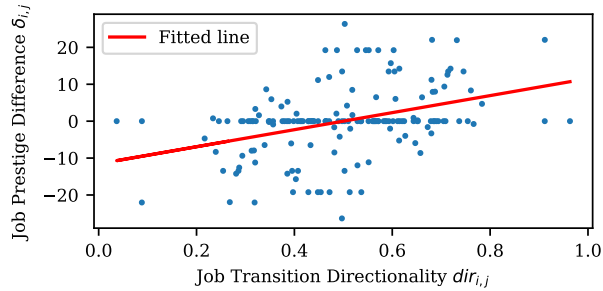


Figure 7.8: Highly-directed job transitions generally tend towards more prestigious positions. Some prestige scores do not change because of the limited granularity of the job prestige data (e.g., *assistant prof.* and *associate prof.* have the same job category and prestige).

Directionality Correlates with Job Prestige: One possible hypothesis is that job updates always reflect increases of job prestige. We calculate the prestige difference $\delta_{(i,j)}$ within each job transition pair, and plot against the transition directionality in Figure 7.8, where we observed a clear positive correlation with Pearson's $\rho = 0.3686$. This finding supports that "*we strive for positive work-related allegiances, enhance well-being ... and promote career development*", as suggested by Gecas [55] and echoed in [12, 30, 86].

7.6.3 Case Study: Transitions in/out Occupational Identities Space amid COVID-19

We performed a case study to qualify how users move in and out of occupational identity space. In order to cover the complete pandemic period, we augmented our dataset with full year data for 2022. With regards to the graph structure, the goal was to identify which jobs are most overrepresented in (none->job) and (job->none) transitions. Table 7.11 shows the breakdown of these transitions by type. Among 13,980,687 unique U.S. users there were 1,602,731 (~11.5%) who listed a recognizable job title in their bio at some point during the observation period.

Table 7.12 shows that jobs share the highest entry/exit counts, revealing that the top occupations in each category are the same, and even follow the same ranking order. Combined with the average number of transitions per user being just over two, this indicates that a large portion of these transitions consist of "flip-flops", where a user changes their bio away from a listed occupation, perhaps for something seasonal or topical, and then returns to their original bio by the next observation. For the purposes of this analysis such flip-flops are strictly a source of noise: to compensate for this, raw counts were abandoned in favor of net changes as defined in equation 7.2. Overrepresented job titles were only considered if they appeared in more than 1/10000 occupational identities.

$$\delta_{net}(Job) = \#(None \rightarrow Job) - \#(Job \rightarrow None) \quad (7.2)$$

Personal care and service jobs are rising: Table 7.13 presents the most overrepresented entry/exit jobs over the full observation period. Half of the top 10 entry jobs fall under the category of personal care and service occupations, including esthetician, licensed esthetician, doula, health advocate, and tattoo artist. According to the U.S. Bureau of Labor and Statistics this group of jobs is projected to grow 14% from 2021 to 2031, nearly double the growth rate of the job market overall ¹³. Other titles within this list (dominatrix, forex trader) correspond to more recent growth trends, particularly during the pandemic ¹⁴ ¹⁵.

Aspirational identities are easier to be abandoned: The top 10 exit jobs largely correspond to media positions (multimedia journalist, editor-in-chief), sports positions (soccer player, snowboarder), and entertainment (song writer,

¹³<https://www.bls.gov/ooh/personal-care-and-service/home.htm>

¹⁴<https://www.nytimes.com/2021/04/10/style/findom-kink.html>

¹⁵<https://financialit.net/news/people-moves/ironfx-hires-200-employees-after-massive-rise-forex-accounts-amid-covid-19>

Youtuber). These reflect a category which can be described as "aspirational jobs"; careers with low barriers to entry and title adoption but higher barriers for conversion to a long-term professional vocation. These aspirational jobs are also congruent with the most desired jobs among both children and teens according to several surveys^{16 17 18} Aspirational jobs are clearly over-represented on Twitter with respect to self-presented occupational identity. Other titles on the list, such as student, represent a position traditionally intended to be temporary. In these contexts it matches expectations to see users dropping these titles at a higher rate than more conventional long-term occupations.

Certain types of entry jobs significantly declined amid COVID-19: Figure 7 shows the changes in entry/exit job pool sizes over time. When considering unique job titles, the pool of possible entry jobs is consistently larger than the pool of possible exit jobs. Put another way, there are more unique ways to enter into occupational identity space than there are to leave it. This relationship holds true across the full observation period, but during the course of the COVID-19 pandemic the pool sizes draw significantly closer together, with the relationship nearly reversing during peak unemployment¹⁹. COVID-19 exacerbated trends which have not yet recovered.

Occupational Identity Rates During COVID-19: Figure 7.10 shows the proportions of valid job titles among the users who exhibit at least one transition (minimum two observations) and listed an occupational identity at least once within the observation period. Users with occupational identities show a greater sensitivity to actual employment rates, an effect which disappears in the total user cohort. Although in this paper our main goal is not to conduct real-world job market research using Twitter data, these aforementioned case study results demonstrate that our proposed dataset is a reliable and useful resource for the future work-related studies.

¹⁶<https://arstechnica.com/science/2019/07/american-kids-would-much-rather-be-youtubers-than-astronauts/>

¹⁷<https://www.thesun.co.uk/news/3617062/children-turn-backs-on-traditional-careers-in-favour-of-internet-fame-study-finds/>

¹⁸<https://today.yougov.com/topics/technology/articles-reports/2021/12/14/influencer-dream-jobs-among-us-teens>

¹⁹as reported by the U.S. Bureau of Labor and Statistics, <https://www.bls.gov/charts/employment-situation/civilian-unemployment-rate.htm>

7.7 Conclusions and Future Work

We have presented a study of occupational identities and their evolution in Twitter biographies from 2015 to 2021, and beyond. First, we described a new temporal self-identity dataset, consisting of extracted job titles with associated metadata (e.g., income, prestige score), and will release the occupation transition graph and the embeddings of biographies on publication. Secondly, we have quantitatively demonstrated that the high prestige jobs are more likely to be embedded into self-identity, and that occupational transitions are biased towards more prestigious jobs. In addition, we presented an interesting case study about how work identities changed during COVID-19, and demonstrated that our dataset captures intriguing real-world phenomenon. To our knowledge, this is the most comprehensive study of social media biography dynamics to date. We envision future work building on our results in several directions: 1). Deriving job title embeddings from the occupational graph, to better describe relations among job titles even without any textual similarity, as shown in Table 7.9. 2). Studying the persistence of self-identities over time. We are curious about which identities are ephemeral/eternal and the mechanisms behind self-description revisions. Occupational identities may change more frequently compared to other identities (e.g., *Father/Mom,...*).

7.8 Appendix

Table 7.1: Job transition pairs observed in Twitter biographies. These transitions reflect personal career advancement (e.g., from *assistant professor* to *associate professor*), graduation (e.g., from *student* to *engineer*) or work-status change (e.g, from *designer* to *freelance designer*). In this paper, we investigate why people self-present with such occupational identities.

Title A	Title B	# (A↔B)
co-founder	founder	10149
ceo	founder	8577
director	executive director	2351
assistant professor	associate professor	2154
graphic designer	freelance graphic designer	1975
software engineer	senior software engineer	1043
student	nursing student	770
accountant	chartered accountant	661
student	mechanical engineer	575

Table 7.10: The detected occupation transition pairs: generally the transition reflects career changes, graduation (e.g., *student* to *nurse*) or just rephrasing (e.g., *vice president* to *vp*). The directionality indicates the transition is biased toward one way, which usually indicates a positive movement (e.g., being promoted from *manager* to *director*.)

Title i	Title j	#	$dir_{i,j}$
Top Mentioned Transitions			
co-founder	founder	10149	0.54
ceo	founder	8577	0.57
owner	founder	7384	0.59
owner	ceo	5917	0.53
director	founder	2987	0.57
vice president	vp	2734	0.66
vice president	president	2545	0.76
Highly Directed Transitions			
student nurse	staff nurse	109	0.99
nursing student	registered nurse	217	0.98
assistant professor	associate professor	2154	0.97
postdoctoral fellow	assistant professor	136	0.96
account manager	account director	163	0.96
Sr. account manager	account director	105	0.96
editorial assistant	assistant editor	163	0.94
instructional coach	assistant principal	154	0.94
associate editor	senior editor	174	0.92
Sr. account exec.	account manager	102	0.91
Less Directed Transitions			
director	business director	142	0.50
scientist	neuroscientist	126	0.50
assistant coach	asst. basketball coach	110	0.50
graphic designer	video editor	110	0.50
cto	owner	110	0.50
software developer	ios developer	102	0.50
digital marketer	digital marketing spec.	102	0.50

Table 7.11: Transition Types. job->none and none->job transitions share nearly equal proportions of total transitions.

Type	Counts	Proportion
job->job	847,412	0.23
job->none	1,402,957	0.38
none->job	1,446,278	0.39

ht

Table 7.12: Top entry/exit jobs by raw counts. All job titles follow the same ranking in both categories.

Rank	Entry Jobs	Counts	Exit Jobs	Counts
1	Student	84,489	Student	95,848
2	Owner	65,162	Owner	60,284
3	President	58,465	President	57,441
4	Founder	51,650	Founder	49,124
5	CEO	49,004	CEO	43,527

Table 7.13: Top 10 Overrepresented entry/exit jobs. Positive net change $\delta_{net}(Job) > 0$: we observed more people establishing these work identities than giving them up.

Rank	Entry Jobs	Exit Jobs
1	Esthetician	Soccer Player
2	Licensed Esthetician	Multimedia Journalist
3	Assistant Baseball Coach	Editor-in-Chief
4	First Responder	Independent Consultant
5	Doula	Public Relations
6	Health Advocate	Snowboarder
7	Tattoo Artist	Student
8	Dominatrix	Song Writer
9	Assistant Professor	YouTuber
10	Forex Trader	Associate Professor

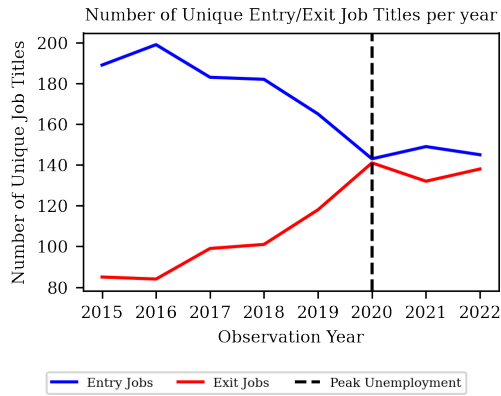


Figure 7.9: The number of unique entry job titles is consistently larger than the number of unique exit job titles. However, this relationship begins to falter during the COVID-19 pandemic, indicating that people were removing a wider variety of jobs from their occupational identities during the many employment disruptions surrounding the pandemic and associated lockdowns.

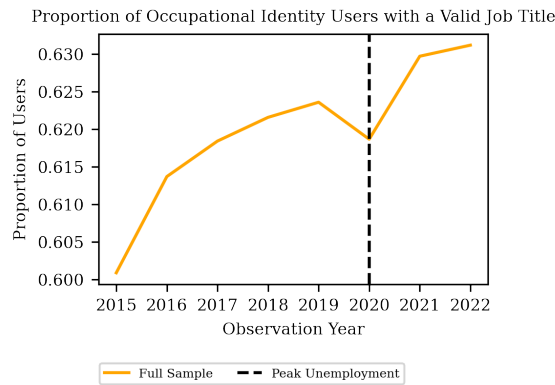


Figure 7.10: Among the cohort who have historically included an occupational identity there is a clear local minimum corresponding to the peak U.S. unemployment rate at the beginning of the COVID-19 pandemic. This indicates that the reported status of people who already subscribed to an occupational identity does share some correlation with actual employment status.

White	Ratio	Asian	Ratio	Hispanic	Ratio	African-American	Ratio
Over-represented							
golf professional	2.12	research scholar	6.60	industrial engineer	3.48	performing artist	1.82
golf coach	2.10	chartered accountant	5.76	volleyball player	2.30	forex trader	1.81
pitching coach	2.09	political analyst	4.08	industrial engineering	2.18	motivational speaker	1.79
assistant superintendent	2.07	social worker	3.82	soccer player	2.14	radio personality	1.75
social studies teacher	2.07	electronics engineer	3.49	medical assistant	1.74	music artist	1.73
athletic director	2.06	it engineer	3.43	full stack developer	1.67	recording artist	1.71
pe teacher	2.06	android developer	3.38	computer engineer	1.66	rap artist	1.71
baseball coach	2.05	it professional	3.21	flight attendant	1.64	song writer	1.70
assistant baseball coach	2.04	prime minister	3.18	systems engineer	1.63	event host	1.67
sports director	2.04	electrical engineer	2.94	medical doctor	1.57	college athlete	1.67
softball coach	2.03	mechanical engineer	2.92	mma fighter	1.54	event planner	1.65
volleyball coach	2.02	content writer	2.81	environmental engineer	1.51	basketball player	1.61
hockey player	2.01	secretary	2.78	community manager	1.50	sports analyst	1.61
director of comm.	2.00	growth hacker	2.78	fashion designer	1.49	fashion stylist	1.60
director of sales	2.00	civil engineer	2.76	networker	1.47	hip hop artist	1.58
Under-represented							
research scholar	0.84	softball coach	0.17	golf professional	0.25	research scholar	0.74
chartered accountant	0.98	assistant football coach	0.18	support worker	0.29	industrial engineer	0.76
industrial engineer	1.07	asst. baseball coach	0.18	asst. basketball coach	0.30	software architect	0.77
electronics engineer	1.12	baseball coach	0.19	men's basketball coach	0.31	assistant professor	0.81
android developer	1.17	athletic director	0.20	golf coach	0.33	postdoctoral fellow	0.83
political analyst	1.17	volleyball coach	0.21	development officer	0.33	senior director	0.83
it engineer	1.27	asst. basketball coach	0.21	primary teacher	0.34	assistant superintendent	0.83
medical doctor	1.29	offensive coordinator	0.22	athletic director	0.36	ios developer	0.83
computer engineer	1.29	assistant superintendent	0.22	recruitment consultant	0.37	pitching coach	0.84
social worker	1.30	golf coach	0.23	chief executive	0.37	sr. director	0.84
dominatrix	1.31	pitching coach	0.23	assistant football coach	0.38	associate professor	0.85
civil engineer	1.32	track coach	0.23	primary school teacher	0.38	senior software engineer	0.85
full stack developer	1.32	recruiting coordinator	0.23	tar heel	0.39	engineering manager	0.85
electrical engineer	1.34	golf professional	0.23	radio presenter	0.39	systems engineer	0.86
volleyball player	1.34	assistant principal	0.24	estate agent	0.40	senior vice president	0.87

Table 7.14: Top over/under-represented occupations in each ethnicity group (Occupation mentioned time < 60): The column *Ratio* measures how many times the calculated value exceeds the expected balanced value. We break ties by sorting occupation mentioned times in descending order.

Chapter 8

Conclusion and Future Work

In this thesis, we focus on the analysis of evolving graphs and texts. Specifically, we proposed a faster dynamic network embedding algorithm (*DynamicPPE*) based on approximate Personalized PageRank, which significantly improves running time by roughly 670 times in our subset node learning setting while maintaining comparable prediction accuracy.

Secondly, we investigate node-level anomaly tracking over dynamic graphs and propose an efficient framework (*DynAnom*) that utilizes PPR changes as anomaly signals and improves the anomaly detection accuracy by roughly 2 times while being approximately 2.3 times faster.

Third, we propose *GoPPE*, a framework that combines graph neural networks and PPR-based positional encoding for dynamic graphs. Thanks to recent studies on PPR-equivalent formulation, we can efficiently solve PPR up to ~ 6 times faster and provide robust node representation under noisy environment, achieving up to 3 times more accuracy than state-of-the-art (SOTA) baselines.

For the studies on text analysis, we collect and analyze the post-publication headline changes in major U.S. online news outlets. we discovered that 7.5% of titles changed at least once after they were published. We devised a taxonomy to automatically characterize the type of post-publication change and found that 49.7% of changes go beyond benign corrections and updates. Additionally, we find that the maximal spread of news on Twitter happens within 10 hours after publication and therefore a delayed headline correction will come after users have consumed and amplified inaccurate headlines.

Furthermore, we present a study of occupational identities and their evolution in Twitter biographies from 2015 to 2021 and beyond. We quantitatively demonstrate that high prestige jobs are more likely to be embedded into self-

identity, and that occupational transitions are biased towards more prestigious jobs. Additionally, we present an interesting case study about how work identities changed during COVID-19, and demonstrate that our dataset captures intriguing real-world phenomena.

There are three future directions based on our current works as described below:

- **Speeding up PPR approximation under optimization framework:** Local and efficient computation of PPR is fundamental to many downstream tasks and remains an open problem [51]. Recent research [29, 204] has pointed out that the ForwardPush algorithm is essentially a variant of the Gauss–Seidel method. One future direction is to further improve PPR calculation efficiency with its local property under PPR’s optimization formulation. The downstream applications include faster knowledge discovery [67] and efficient embeddings algorithms for real-time applications, such as Chatbot and online recommendation system [31, 56, 68, 108, 154].
- **Categorizing self-presented jobs over social network** Due to proprietary restrictions and technical difficulties in scraping people’s career data from the internet ¹, public longitudinal Twitter bios data provides a unique opportunity to study job titles. In particular, one future direction is to build a toolkit to classify arbitrary job titles according to the Standard Occupational Classification (SOC) categories. Many job-related statistics are surveyed based on the SOC category, which consists of about 800 classes. However, many people present their jobs in natural language instead of structured SOC categories.² The misalignment between the SOC category and job titles hinders large-scale computational social science studies about jobs. It is valuable to create a pipeline to classify arbitrary job titles into SOC categories based on our collected job title text and the job transition graph [74].
- **Text edit representation learning:** Building on our previous research on news headline changes, we propose a nine-class taxonomy to better understand modifications to titles. However, this categorization is currently based on a rule-based pipeline. Our goal is to represent edits in a neural way and utilize clustering algorithms to refine the taxonomy and improve classification accuracy. The downstream applications of this research include analyzing modifications to news articles, titles, and social media posts.

¹e.g., Law case of HiQ Labs v.s. LinkedIn about web scraping

²e.g., people would like to describe themselves as *Assistant Professor in CS* instead of *Computer Science Teachers, Postsecondary (25-1021)*

Chapter 9

Bibliography

- [1] Alexa top sites. <https://www.alexa.com/topsites>.
- [2] Media bias chart. <https://www.adfontesmedia.com/intro-to-the-media-bias-chart/>.
- [3] Open graph protocol. <https://ogp.me>.
- [4] Python newspaper library. <https://newspaper.readthedocs.io/en/latest/>.
- [5] Twitter card troubleshooting. <https://developer.twitter.com/en/docs/twitter-for-websites/cards/guides/troubleshooting-cards#outdated>.
- [6] How americans get their news. <https://www.americanpressinstitute.org/publications/reports/survey-research/how-americans-get-news/>, 2014.
- [7] Charu C Aggarwal, Yuchen Zhao, and S Yu Philip. Outlier detection in graph streams. In *ICDE*, pages 399–409. IEEE, 2011.
- [8] Leman Akoglu, Mary McGlohon, and Christos Faloutsos. Oddball: Spotting anomalies in weighted graphs. In *Pacific-Asia conference on knowledge discovery and data mining*, pages 410–421. Springer, 2010.
- [9] Reid Andersen, Fan Chung, and Kevin Lang. Local graph partitioning using pagerank vectors. In *2006 47th Annual IEEE Symposium on Foundations of Computer Science (FOCS'06)*, pages 475–486. IEEE, 2006.
- [10] Reid Andersen, Fan Chung, and Kevin Lang. Using pagerank to locally partition a graph. *Internet Mathematics*, 4(1):35–64, 2007.
- [11] Blake E Ashforth, Spencer H Harrison, and Kevin G Corley. Identification in organizations: An examination of four fundamental questions. *Journal of management*, 34(3):325–374, 2008.

- [12] Caroline Bartel and Jane Dutton. Ambiguous organizational memberships: Constructing organizational identities. *Social identity processes in organizational contexts*, pages 115–130, 2001.
- [13] Amir Beck and Marc Teboulle. A fast iterative shrinkage-thresholding algorithm for linear inverse problems. *SIAM journal on imaging sciences*, 2(1):183–202, 2009.
- [14] Tanya Y Berger-Wolf and Jared Saia. A framework for analysis of dynamic social networks. In *Proceedings of the 12th ACM SIGKDD international conference on Knowledge discovery and data mining*, pages 523–528, 2006.
- [15] Pavel Berkhin. Bookmark-coloring algorithm for personalized pagerank computing. *Internet Mathematics*, 3(1):41–62, 2006.
- [16] Alex Beutel, Wanhong Xu, Venkatesan Guruswami, Christopher Palow, and Christos Faloutsos. Copycatch: stopping group attacks by spotting lockstep behavior in social networks. In *WWW*, pages 119–130, 2013.
- [17] Siddharth Bhatia, Bryan Hooi, Minji Yoon, Kijung Shin, and Christos Faloutsos. Midas: Microcluster-based detector of anomalies in edge streams. In *Proceedings of the AAAI conference on artificial intelligence*, volume 34, pages 3242–3249, 2020.
- [18] Siddharth Bhatia, Arjit Jain, Pan Li, Ritesh Kumar, and Bryan Hooi. Mstream: Fast anomaly detection in multi-aspect streams. In *Proceedings of the Web Conference 2021*, pages 3371–3382, 2021.
- [19] Siddharth Bhatia, Mohit Wadhwa, Philip S Yu, and Bryan Hooi. Sketch-based streaming anomaly detection in dynamic graphs. *arXiv preprint arXiv:2106.04486*, 2021.
- [20] Grant Blank. The digital divide among twitter users and its implications for social research. *Social Science Computer Review*, 35(6):679–697, 2017.
- [21] Jonas Nygaard Blom and Kenneth Reinecke Hansen. Click bait: Forward-reference as lure in online news headlines. *Journal of Pragmatics*, 76:87–100, 2015.
- [22] Susan Bluck, Nicole Alea, Tilmann Habermas, and David C Rubin. A tale of three functions: The self-reported uses of autobiographical memory. *Social cognition*, 23(1): 91–117, 2005.
- [23] Aleksandar Bojchevski, Johannes Klicpera, Bryan Perozzi, Amol Kapoor, Martin Blais, Benedek Rózemberczki, Michal Lukasik, and Stephan Günnemann. Scaling graph neural networks with approximate pagerank. In *Proceedings of the 26th ACM SIGKDD International Conference on Knowledge Discovery & Data Mining*, pages 2464–2473, 2020.
- [24] Giorgian Borca-Tasciuc, Xingzhi Guo, Stanley Bak, and Steven Skiena. Provable fairness for neural network models using formal verification. *arXiv preprint arXiv:2212.08578*, 2022.

- [25] Matthew Brand. Incremental singular value decomposition of uncertain data with missing values. In *Computer Vision—ECCV 2002: 7th European Conference on Computer Vision Copenhagen, Denmark, May 28–31, 2002 Proceedings, Part I* 7, pages 707–720. Springer, 2002.
- [26] Samuel Butler. *The way of all flesh*. Number 118. Everyman’s Library, 1992.
- [27] Yen-Yu Chang, Pan Li, Rok Susic, MH Afifi, Marco Schweighauser, and Jure Leskovec. F-fade: Frequency factorization for anomaly detection in edge streams. In *WSDM*, pages 589–597, 2021.
- [28] Haochen Chen, Syed Fahad Sultan, Yingtao Tian, Muhao Chen, and Steven Skiena. Fast and accurate network embeddings via very sparse random projection. In *Proceedings of the 28th ACM International Conference on Information and Knowledge Management*, pages 399–408, 2019.
- [29] Zhen Chen, Xingzhi Guo, Baojian Zhou, Deqing Yang, and Steven Skiena. Accelerating personalized pagerank vector computation. In *Proceedings of the 29th ACM SIGKDD Conference on Knowledge Discovery and Data Mining*, pages 262–273, 2023.
- [30] Chi-Ying Cheng, Jeffrey Sanchez-Burks, and Fiona Lee. Connecting the dots within: Creative performance and identity integration. *Psychological Science*, 19(11):1178–1184, 2008.
- [31] Shu-Yin Chiang, Xingzhi Guo, and Hsien-Wen Hu. Real time self-localization of omni-vision robot by pattern match system. In *2014 International Conference on Advanced Robotics and Intelligent Systems (ARIS)*, pages 46–50. IEEE, 2014.
- [32] Eli Chien, Jianhao Peng, Pan Li, and Olga Milenkovic. Adaptive universal generalized pagerank graph neural network. *arXiv preprint arXiv:2006.07988*, 2020.
- [33] Charles Christiansen. Occupation and identity: Becoming who we are through what we do. *Introduction to occupation: The art and science of living*, pages 121–139, 2004.
- [34] Charles H Christiansen. Defining lives: Occupation as identity: An essay on competence, coherence, and the creation of meaning. *The American Journal of Occupational Therapy*, 53(6):547–558, 1999.
- [35] Aaron Clauset, Mark EJ Newman, and Cristopher Moore. Finding community structure in very large networks. *Physical review E*, 70(6):066111, 2004.
- [36] Colin B Clement, Matthew Bierbaum, Kevin P O’Keeffe, and Alexander A Alemi. On the use of arxiv as a dataset. *arXiv preprint arXiv:1905.00075*, 2019.
- [37] W.W. Cohen. Enron email dataset. <http://www.cs.cmu.edu/enron/>. Accessed in 2009.
- [38] Kaija Collin, Susanna Paloniemi, Anne Virtanen, and Anneli Eteläpelto. Constraints and challenges on learning and construction of identities at work. *Vocations and Learning*, 1(3):191–210, 2008.

- [39] Cristian Consonni, David Laniado, and Alberto Montresor. Wikilinkgraphs: A complete, longitudinal and multi-language dataset of the wikipedia link networks. In *Proceedings of the International AAAI Conference on Web and Social Media*, volume 13, pages 598–607, 2019.
- [40] Sanjoy Dasgupta and Anupam Gupta. An elementary proof of the johnson-lindenstrauss lemma. *International Computer Science Institute, Technical Report*, 22(1):1–5, 1999.
- [41] Ingrid Daubechies, Michel Defrise, and Christine De Mol. An iterative thresholding algorithm for linear inverse problems with a sparsity constraint. *Communications on Pure and Applied Mathematics: A Journal Issued by the Courant Institute of Mathematical Sciences*, 57(11):1413–1457, 2004.
- [42] Johannes Daxenberger and Iryna Gurevych. Automatically classifying edit categories in wikipedia revisions. In *Proceedings of the 2013 Conference on Empirical Methods in Natural Language Processing*, pages 578–589, 2013.
- [43] Sohan De Sarkar, Fan Yang, and Arjun Mukherjee. Attending sentences to detect satirical fake news. In *Proceedings of the 27th international conference on computational linguistics*, pages 3371–3380, 2018.
- [44] Daniel Dor. On newspaper headlines as relevance optimizers. *Journal of pragmatics*, 35(5):695–721, 2003.
- [45] Lun Du, Yun Wang, Guojie Song, Zhicong Lu, and Junshan Wang. Dynamic network embedding: An extended approach for skip-gram based network embedding. In *IJCAI*, volume 2018, pages 2086–2092, 2018.
- [46] Peter Elias, Margaret Birch, et al. Soc2010: revision of the standard occupational classification. *Economic & Labour Market Review*, 4(7):48–55, 2010.
- [47] Naomi Ellemers, Dick De Gilder, and S Alexander Haslam. Motivating individuals and groups at work: A social identity perspective on leadership and group performance. *Academy of Management review*, 29(3):459–478, 2004.
- [48] Dhivya Eswaran and Christos Faloutsos. Sedanspot: Detecting anomalies in edge streams. In *ICDM*, pages 953–958. IEEE, 2018.
- [49] Dhivya Eswaran, Christos Faloutsos, Sudipto Guha, and Nina Mishra. Spotlight: Detecting anomalies in streaming graphs. In *Proceedings of the 24th ACM SIGKDD Conference on Knowledge Discovery & Data Mining*, pages 1378–1386, 2018.
- [50] Lisa Fazio. Pausing to consider why a headline is true or false can help reduce the sharing of false news. *Harvard Kennedy School Misinformation Review*, 1(2), 2020.
- [51] Kimon Fountoulakis and Shenghao Yang. Open problem: Running time complexity of accelerated l-1 regularized pagerank. In *Conference on Learning Theory*, pages 5630–5632. PMLR, 2022.

- [52] Kimon Fountoulakis, Farbod Roosta-Khorasani, Julian Shun, Xiang Cheng, and Michael W Mahoney. Variational perspective on local graph clustering. *Mathematical Programming*, 174(1):553–573, 2019.
- [53] Dongqi Fu and Jingrui He. Sdg: a simplified and dynamic graph neural network. In *Proceedings of the 44th International ACM SIGIR Conference on Research and Development in Information Retrieval*, pages 2273–2277, 2021.
- [54] Johannes Gasteiger, Aleksandar Bojchevski, and Stephan Günnemann. Predict then propagate: Graph neural networks meet personalized pagerank. *arXiv preprint arXiv:1810.05997*, 2018.
- [55] Viktor Gecas. The self-concept. *Annual review of sociology*, pages 1–33, 1982.
- [56] Kellen Gillespie, Ioannis C Konstantakopoulos, Xingzhi Guo, Vishal Thanvantri Vasudevan, and Abhinav Sethy. Improving device directedness classification of utterances with semantic lexical features. In *ICASSP 2020-2020 IEEE International Conference on Acoustics, Speech and Signal Processing (ICASSP)*, pages 7859–7863. IEEE, 2020.
- [57] David F Gleich. Pagerank beyond the web. *Siam Review*, 57(3):321–363, 2015.
- [58] Jennifer Golbeck, Matthew Mauriello, Brooke Auxier, Keval H Bhanushali, Christopher Bonk, Mohamed Amine Bouzaghrane, Cody Buntain, Riya Chanduka, Paul Cheakalos, Jennine B Everett, et al. Fake news vs satire: A dataset and analysis. In *Proceedings of the 10th ACM Conference on Web Science*, pages 17–21, 2018.
- [59] Gene H Golub and Charles F Van Loan. *Matrix computations*. JHU press, 2013.
- [60] Simon Gottschalk and Elena Demidova. Eventkg: A multilingual event-centric temporal knowledge graph. In *Proceedings of the Extended Semantic Web Conference (ESWC 2018)*. Springer, 2018.
- [61] Simon Gottschalk and Elena Demidova. EventKG - the Hub of Event Knowledge on the Web - and Biographical Timeline Generation. volume 10, pages 1039–1070. IOS Press, 2019.
- [62] John C Gower. Generalized procrustes analysis. *Psychometrika*, 40(1):33–51, 1975.
- [63] Palash Goyal, Nitin Kamra, Xinran He, and Yan Liu. Dyngem: Deep embedding method for dynamic graphs. *arXiv preprint arXiv:1805.11273*, 2018.
- [64] Jeffrey H Greenhaus, Ann C Peng, and Tammy D Allen. Relations of work identity, family identity, situational demands, and sex with employee work hours. *Journal of Vocational Behavior*, 80(1):27–37, 2012.
- [65] Aditya Grover and Jure Leskovec. node2vec: Scalable feature learning for networks. In *Proceedings of the 22nd ACM SIGKDD international conference on Knowledge discovery and data mining*, pages 855–864, 2016.

- [66] Wentian Guo, Yuchen Li, Mo Sha, and Kian-Lee Tan. Parallel personalized pagerank on dynamic graphs. *Proceedings of the VLDB Endowment*, 11(1):93–106, 2017.
- [67] Xingzhi Guo and Steven Skiena. Hierarchies over vector space: Orienting word and graph embeddings. *arXiv preprint arXiv:2211.01430*, 2022.
- [68] Xingzhi Guo, Yu-Cian Huang, Edwinn Gamborino, Shih-Huan Tseng, Li-Chen Fu, and Su-Ling Yeh. Inferring human feelings and desires for human-robot trust promotion. In *International Conference on Human-Computer Interaction*, pages 365–375. Springer, 2019.
- [69] Xingzhi Guo, Baojian Zhou, and Steven Skiena. Subset node representation learning over large dynamic graphs. In *Proceedings of the 27th ACM SIGKDD Conference on Knowledge Discovery & Data Mining*, pages 516–526, 2021.
- [70] Xingzhi Guo, Baojian Zhou, and Steven Skiena. Subset node representation learning over large dynamic graphs. In *Proceedings of the 27th ACM SIGKDD Conference on Knowledge Discovery & Data Mining*, page 516–526, 2021.
- [71] Xingzhi Guo, Brian Kondracki, Nick Nikiforakis, and Steven Skiena. Verba volant, scripta volant: Understanding post-publication title changes in news outlets. In *Proceedings of the ACM Web Conference 2022*, pages 588–598, 2022.
- [72] Xingzhi Guo, Baojian Zhou, and Steven Skiena. Subset node anomaly tracking over large dynamic graphs. In *Proceedings of the 28th ACM SIGKDD Conference on Knowledge Discovery and Data Mining*, KDD '22, page 475–485, New York, NY, USA, 2022. Association for Computing Machinery. ISBN 9781450393850. doi: 10.1145/3534678.3539389. URL <https://doi.org/10.1145/3534678.3539389>.
- [73] Xingzhi Guo, Baojian Zhou, and Steven Skiena. Subset node anomaly tracking over large dynamic graphs. In *Proceedings of the 28th ACM SIGKDD Conference on Knowledge Discovery and Data Mining*, pages 475–485, 2022.
- [74] Xingzhi Guo, Dakota Handzlik, Jason J Jones, and Steven S Skiena. The evolution of occupational identity in twitter biographies. In *Proceedings of the International AAAI Conference on Web and Social Media*, volume 18, pages 502–514, 2024.
- [75] Nick Hagar and Nicholas Diakopoulos. Optimizing content with a/b headline testing: Changing newsroom practices. *Media and Communication*, 7(1):117–127, 2019.
- [76] Ehsan Hajiramezanali, Arman Hasanzadeh, Krishna Narayanan, Nick Duffield, Mingyuan Zhou, and Xiaoning Qian. Variational graph recurrent neural networks. *Advances in neural information processing systems*, 32, 2019.
- [77] Bronwyn H Hall, Adam B Jaffe, and Manuel Trajtenberg. The nber patent citation data file: Lessons, insights and methodological tools. Technical report, National Bureau of Economic Research, 2001.

- [78] Will Hamilton, Zhitao Ying, and Jure Leskovec. Inductive representation learning on large graphs. In *Advances in neural information processing systems*, pages 1024–1034, 2017.
- [79] William L Hamilton, Rex Ying, and Jure Leskovec. Representation learning on graphs: Methods and applications. *arXiv preprint arXiv:1709.05584*, 2017.
- [80] Robert W Hodge, Paul M Siegel, and Peter H Rossi. Occupational prestige in the united states, 1925-63. *American Journal of Sociology*, 70(3):286–302, 1964.
- [81] Peter Hoff. Modeling homophily and stochastic equivalence in symmetric relational data. *Advances in neural information processing systems*, 20:657–664, 2007.
- [82] Peter D Hoff, Adrian E Raftery, and Mark S Handcock. Latent space approaches to social network analysis. *Journal of the American Statistical Association*, 97(460):1090–1098, 2002.
- [83] Sungryong Hong, Bruno C Coutinho, Arjun Dey, Albert-L Barabási, Mark Vogelsberger, Lars Hernquist, and Karl Gebhardt. Discriminating topology in galaxy distributions using network analysis. *Monthly Notices of the Royal Astronomical Society*, 459(3):2690–2700, 2016.
- [84] Austin Hounsel, Jordan Holland, Ben Kaiser, Kevin Borgolte, Nick Feamster, and Jonathan Mayer. Identifying disinformation websites using infrastructure features. In *10th {USENIX} Workshop on Free and Open Communications on the Internet ({FOCI} 20)*, 2020.
- [85] Michael Hout, Tom W Smith, and Peter V Marsden. Prestige and socioeconomic scores for the 2010 census codes. *Methodological Report MR124, Chicago, NORC*. <http://gss.norc.org/get-documentation/methodological-reports>, 2015.
- [86] Herminia Ibarra. Provisional selves: Experimenting with image and identity in professional adaptation. *Administrative science quarterly*, 44(4):764–791, 1999.
- [87] Elly Ifantidou. Newspaper headlines and relevance: Ad hoc concepts in ad hoc contexts. *Journal of Pragmatics*, 41(4):699–720, 2009.
- [88] Jay W Jackson. Intergroup attitudes as a function of different dimensions of group identification and perceived intergroup conflict. *Self and identity*, 1(1):11–33, 2002.
- [89] Jacob Jennings, Jacqueline Strenio, and Iris Buder. Occupational prestige: American stratification. *Review of Evolutionary Political Economy*, pages 1–24, 2022.
- [90] Guoliang Ji, Shizhu He, Liheng Xu, Kang Liu, and Jun Zhao. Knowledge graph embedding via dynamic mapping matrix. In *Proceedings of the 53rd annual meeting of the association for computational linguistics and the 7th international joint conference on natural language processing (volume 1: Long papers)*, pages 687–696, 2015.
- [91] William B Johnson and Joram Lindenstrauss. Extensions of lipschitz mappings into a hilbert space. *Contemporary mathematics*, 26(189-206):1, 1984.

- [92] Jason Jeffrey Jones. A dataset for the study of identity at scale: Annual prevalence of american twitter users with specified token in their profile bio 2015–2020. *PloS one*, 16(11):e0260185, 2021.
- [93] Armand Joulin, Edouard Grave, Piotr Bojanowski, Matthijs Douze, Herve Jégou, and Tomas Mikolov. Fasttext.zip: Compressing text classification models. *arXiv preprint arXiv:1612.03651*, 2016.
- [94] Armand Joulin, Edouard Grave, Piotr Bojanowski, and Tomas Mikolov. Bag of tricks for efficient text classification. *arXiv preprint arXiv:1607.01759*, 2016.
- [95] Hamid Karimi, Proteek Roy, Sari Saba-Sadiya, and Jiliang Tang. Multi-source multi-class fake news detection. In *Proceedings of the 27th international conference on computational linguistics*, pages 1546–1557, 2018.
- [96] Seyed Mehran Kazemi and Rishab Goel. Representation learning for dynamic graphs: A survey. *Journal of Machine Learning Research*, 21(70):1–73, 2020.
- [97] Gary Kielhofner. *A model of human occupation: Theory and application*. Lippincott Williams & Wilkins, 2002.
- [98] John F Kihlstrom and Stanley B Klein. The self as a knowledge structure. *Handbook of social cognition*, 1:153–208, 1994.
- [99] Danielle K Kilgo and Vinicio Sinta. Six things you didn’t know about headline writing: Sensationalistic form in viral news content from traditional and digitally native news organizations. In *Research Journal of the International Symposium on Online Journalism*, volume 6, pages 111–130, 2016.
- [100] Dongkwan Kim and Alice Oh. How to find your friendly neighborhood: Graph attention design with self-supervision. *arXiv preprint arXiv:2204.04879*, 2022.
- [101] Thomas N Kipf and Max Welling. Semi-supervised classification with graph convolutional networks. *arXiv preprint arXiv:1609.02907*, 2016.
- [102] Thomas N. Kipf and Max Welling. Semi-supervised classification with graph convolutional networks. In *International Conference on Learning Representations (ICLR)*, 2017.
- [103] Jeffrey Kuiken, Anne Schuth, Martijn Spitters, and Maarten Marx. Effective headlines of newspaper articles in a digital environment. *Digital Journalism*, 5(10):1300–1314, 2017.
- [104] Srijan Kumar and Neil Shah. False information on web and social media: A survey. *arXiv preprint arXiv:1804.08559*, 2018.
- [105] Srijan Kumar, Xikun Zhang, and Jure Leskovec. Predicting dynamic embedding trajectory in temporal interaction networks. In *Proceedings of the 25th ACM SIGKDD International Conference on Knowledge Discovery & Data Mining*, pages 1269–1278, 2019.

- [106] TG Lei, CW Woo, JZ Liu, and F Zhang. On the schur complements of diagonally dominant matrices. 2003.
- [107] Chin-Yew Lin. Rouge: A package for automatic evaluation of summaries. In *Text summarization branches out*, pages 74–81, 2004.
- [108] Zhuoyi Lin, Lei Feng, Xingzhi Guo, Yu Zhang, Rui Yin, Chee Keong Kwoh, and Chi Xu. Comet: Convolutional dimension interaction for collaborative filtering. *ACM Transactions on Intelligent Systems and Technology*, 14(4):1–18, 2023.
- [109] Richard Lippmann, Joshua W Haines, David J Fried, Jonathan Korba, and Kumar Das. The 1999 darpa off-line intrusion detection evaluation. *Computer networks*, 34(4):579–595, 2000.
- [110] Xiaorui Liu, Jiayuan Ding, Wei Jin, Han Xu, Yao Ma, Zitao Liu, and Jiliang Tang. Graph neural networks with adaptive residual. *Advances in Neural Information Processing Systems*, 34:9720–9733, 2021.
- [111] Peter Lofgren. *Efficient Algorithms for Personalized PageRank*. PhD thesis, Stanford University, 2015.
- [112] Peter Lofgren, Siddhartha Banerjee, and Ashish Goel. Bidirectional pagerank estimation: From average-case to worst-case. In *Proceedings of the 12th International Workshop on Algorithms and Models for the Web Graph-Volume 9479*, pages 164–176, 2015.
- [113] Yuanfu Lu, Xiao Wang, Chuan Shi, Philip S Yu, and Yanfang Ye. Temporal network embedding with micro-and macro-dynamics. In *CIKM*, pages 469–478, 2019.
- [114] Edison Marrese-Taylor, Machel Reid, and Yutaka Matsuo. Variational inference for learning representations of natural language edits. *arXiv preprint arXiv:2004.09143*, 2020.
- [115] Miller McPherson, Lynn Smith-Lovin, and James M Cook. Birds of a feather: Homophily in social networks. *Annual review of sociology*, 27(1):415–444, 2001.
- [116] Tomas Mikolov, Ilya Sutskever, Kai Chen, Greg S Corrado, and Jeff Dean. Distributed representations of words and phrases and their compositionality. In *Advances in neural information processing systems*, pages 3111–3119, 2013.
- [117] Alan Mislove, Sune Lehmann, Yong-Yeol Ahn, Jukka-Pekka Onnela, and James Rosenquist. Understanding the demographics of twitter users. In *Proceedings of the International AAAI Conference on Web and Social Media*, volume 5, 2011.
- [118] Alexander Nazaryan. I Miss the Thrill of Trump. https://web.archive.org/web/20210211110734if_/https://www.theatlantic.com/ideas/archive/2021/02/i-miss-thrill-trump/617993/, 2021.
- [119] Alexander Nazaryan. I Was an Enemy of the People. https://web.archive.org/web/20210223004426if_/https://www.theatlantic.com/ideas/archive/2021/02/i-miss-thrill-trump/617993/, 2021.

- [120] Giang Hoang Nguyen, John Boaz Lee, Ryan A Rossi, Nesreen K Ahmed, Eunyee Koh, and Sungchul Kim. Continuous-time dynamic network embeddings. In *Companion Proceedings of the The Web Conference 2018*, pages 969–976, 2018.
- [121] Julie Nutini, Issam Laradji, and Mark Schmidt. Let’s make block coordinate descent converge faster: Faster greedy rules, message-passing, active-set complexity, and superlinear convergence. *arXiv preprint arXiv:1712.08859*, 2017.
- [122] Kenta Oono and Taiji Suzuki. Graph neural networks exponentially lose expressive power for node classification. In *International Conference on Learning Representations*, 2020. URL <https://openreview.net/forum?id=S1ldO2EFPr>.
- [123] Lawrence Page, Sergey Brin, Rajeev Motwani, and Terry Winograd. The pagerank citation ranking: Bringing order to the web. Technical report, Stanford InfoLab, 1999.
- [124] Jiaqi Pan, Rishabh Bhardwaj, Wei Lu, Hai Leong Chieu, Xinghao Pan, and Ni Yi Puay. Twitter homophily: Network based prediction of user’s occupation. In *Proceedings of the 57th Annual Meeting of the Association for Computational Linguistics*, pages 2633–2638, 2019.
- [125] Arjunil Pathak, Navid Madani, and Kenneth Joseph. A method to analyze multiple social identities in twitter bios. *Proceedings of the ACM on Human-Computer Interaction*, 5(CSCW2):1–35, 2021.
- [126] Bryan Perozzi, Rami Al-Rfou, and Steven Skiena. Deepwalk: Online learning of social representations. In *Proceedings of the 20th ACM SIGKDD international conference on Knowledge discovery and data mining*, pages 701–710, 2014.
- [127] Shanon Phelan and Elizabeth Anne Kinsella. Occupational identity: Engaging socio-cultural perspectives. *Journal of Occupational Science*, 16(2):85–91, 2009.
- [128] Ștefan Postăvaru, Anton Tsitsulin, Filipe Miguel Gonçalves de Almeida, Yingtao Tian, Silvio Lattanzi, and Bryan Perozzi. Instantembedding: Efficient local node representations. *arXiv preprint arXiv:2010.06992*, 2020.
- [129] Martin Potthast, Sebastian Köpsel, Benno Stein, and Matthias Hagen. Clickbait detection. In *European Conference on Information Retrieval*, pages 810–817. Springer, 2016.
- [130] Daniel Preoțiuc-Pietro, Vasileios Lamos, and Nikolaos Aletras. An analysis of the user occupational class through twitter content. In *Proceedings of the 53rd Annual Meeting of the Association for Computational Linguistics and the 7th International Joint Conference on Natural Language Processing (Volume 1: Long Papers)*, pages 1754–1764, 2015.
- [131] Peng Qi, Yuhao Zhang, Yuhui Zhang, Jason Bolton, and Christopher D Manning. Stanza: A python natural language processing toolkit for many human languages. *arXiv preprint arXiv:2003.07082*, 2020.

- [132] Jiezhong Qiu, Yuxiao Dong, Hao Ma, Jian Li, Chi Wang, Kuansan Wang, and Jie Tang. Netsmf: Large-scale network embedding as sparse matrix factorization. In *WWW*, pages 1509–1520, 2019.
- [133] Stephen Ranshous, Steve Harenberg, Kshitij Sharma, and Nagiza F Samatova. A scalable approach for outlier detection in edge streams using sketch-based approximations. In *IEEE International Conference on Data Mining (ICDM)*, pages 189–197. SIAM, 2016.
- [134] Julio CS Reis, André Correia, Fabrício Murai, Adriano Veloso, and Fabrício Benevenuto. Supervised learning for fake news detection. *IEEE Intelligent Systems*, 34(2):76–81, 2019.
- [135] Julio Rieis, Fabrício de Souza, Pedro Vaz de Melo, Raquel Prates, Haewoon Kwak, and Jisun An. Breaking the news: First impressions matter on online news. In *Proceedings of the International AAAI Conference on Web and Social Media*, volume 9, 2015.
- [136] Ellen Riloff and Janyce Wiebe. Learning extraction patterns for subjective expressions. In *Proceedings of the 2003 conference on Empirical methods in natural language processing*, pages 105–112, 2003.
- [137] Nick Rogers and Jason J Jones. Using twitter bios to measure changes in self-identity: Are americans defining themselves more politically over time? *Journal of Social Computing*, 2(1):1–13, 2021.
- [138] Emanuele Rossi, Ben Chamberlain, Fabrizio Frasca, Davide Eynard, Federico Monti, and Michael Bronstein. Temporal graph networks for deep learning on dynamic graphs. *arXiv preprint arXiv:2006.10637*, 2020.
- [139] Ryan A. Rossi and Nesreen K. Ahmed. The network data repository with interactive graph analytics and visualization. In *Proceedings of the AAAI conference on artificial intelligence*, 2015.
- [140] Ryan A Rossi, Brian Gallagher, Jennifer Neville, and Keith Henderson. Modeling dynamic behavior in large evolving graphs. In *Proceedings of the sixth ACM international conference on Web search and data mining*, pages 667–676, 2013.
- [141] Victoria L Rubin, Niall Conroy, Yimin Chen, and Sarah Cornwell. Fake news or truth? using satirical cues to detect potentially misleading news. In *Proceedings of the second workshop on computational approaches to deception detection*, pages 7–17, 2016.
- [142] Aravind Sankar, Yanhong Wu, Liang Gou, Wei Zhang, and Hao Yang. Dysat: Deep neural representation learning on dynamic graphs via self-attention networks. In *WSDM*, pages 519–527, 2020.
- [143] Purnamrita Sarkar and Andrew W Moore. Dynamic social network analysis using latent space models. *Acm Sigkdd Explorations Newsletter*, 7(2):31–40, 2005.

- [144] Purnamrita Sarkar and Andrew W Moore. Dynamic social network analysis using latent space models. In *Proceedings of the 18th International Conference on Neural Information Processing Systems*, pages 1145–1152, 2005.
- [145] Purnamrita Sarkar, Sajid M Siddiqi, and Geogrey J Gordon. A latent space approach to dynamic embedding of co-occurrence data. In *Artificial Intelligence and Statistics*, pages 420–427, 2007.
- [146] Konstantinos Semertzidis, Evaggelia Pitoura, and Panayiotis Tsaparas. How people describe themselves on twitter. In *Proceedings of the ACM SIGMOD Workshop on Databases and Social Networks*, pages 25–30, 2013.
- [147] Elisa Shearer. More than eight-in-ten americans get news from digital devices. <https://www.pewresearch.org/fact-tank/2021/01/12/more-than-eight-in-ten-americans-get-news-from-digital-devices/>, 2021.
- [148] Jinsei Shima, Mitsuo Yoshida, and Kyoji Umemura. When do users change their profile information on twitter? In *2017 IEEE International Conference on Big Data (Big Data)*, pages 3119–3122. IEEE, 2017.
- [149] Kijung Shin, Bryan Hooi, Jisu Kim, and Christos Faloutsos. Densealert: Incremental dense-subtensor detection in tensor streams. In *KDD*, pages 1057–1066, 2017.
- [150] Kai Shu, Amy Sliva, Suhang Wang, Jiliang Tang, and Huan Liu. Fake news detection on social media: A data mining perspective. *ACM SIGKDD explorations newsletter*, 19(1):22–36, 2017.
- [151] Arnab Sinha, Zhihong Shen, Yang Song, Hao Ma, Darrin Eide, Bo-June Hsu, and Kuansan Wang. An overview of microsoft academic service (mas) and applications. In *Proceedings of the 24th international conference on world wide web*, pages 243–246, 2015.
- [152] Luke Sloan, Jeffrey Morgan, Pete Burnap, and Matthew Williams. Who tweets? deriving the demographic characteristics of age, occupation and social class from twitter user meta-data. *PloS one*, 10(3):e0115545, 2015.
- [153] Gaurav Sood and Suriyan Laohaprapanon. Predicting race and ethnicity from the sequence of characters in a name. *arXiv preprint arXiv:1805.02109*, 2018.
- [154] Syed Fahad Sultan, Xingzhi Guo, and Steven Skiena. Low-dimensional genotype embeddings for predictive models. In *Proceedings of the 13th ACM International Conference on Bioinformatics, Computational Biology and Health Informatics*, pages 1–4, 2022.
- [155] Jie Tang, Jing Zhang, Limin Yao, Juanzi Li, Li Zhang, and Zhong Su. Arnetminer: extraction and mining of academic social networks. In *Proceedings of the 14th ACM SIGKDD international conference on Knowledge discovery and data mining*, pages 990–998, 2008.
- [156] RR Taylor, AW Pan, G Kielhofner, and RR Taylor. Doing and becoming: Occupational change and development. *Kielhofner’s model of human occupation*, pages 140–156, 2017.

- [157] Robert Tibshirani. Regression shrinkage and selection via the lasso. *Journal of the Royal Statistical Society: Series B (Methodological)*, 58(1):267–288, 1996.
- [158] Donald J Treiman. *Occupational prestige in comparative perspective*. Elsevier, 2013.
- [159] Rakshit Trivedi, Mehrdad Farajtabar, Prasenjeet Biswal, and Hongyuan Zha. Dyrep: Learning representations over dynamic graphs. In *International Conference on Learning Representations*, 2019.
- [160] Rakshit Trivedi, Mehrdad Farajtabar, Prasenjeet Biswal, and Hongyuan Zha. Dyrep: Learning representations over dynamic graphs. In *International Conference on Learning Representations*, 2019.
- [161] Anton Tsitsulin, Davide Mottin, Panagiotis Karras, and Emmanuel Müller. Verse: Versatile graph embeddings from similarity measures. In *Proceedings of the 2018 World Wide Web Conference*, pages 539–548, 2018.
- [162] Anton Tsitsulin, Marina Munkhoeva, Davide Mottin, Panagiotis Karras, Ivan Oseledets, and Emmanuel Müller. Frede: anytime graph embeddings. *VLDB Endowment*, 14(6): 1102–1110, 2021.
- [163] Laurens Van der Maaten and Geoffrey Hinton. Visualizing data using t-sne. *Journal of machine learning research*, 9(11), 2008.
- [164] Rolf Van Dick. My job is my castle: Identification in organizational contexts. *International review of industrial and organizational psychology*, 19:171–204, 2004.
- [165] Luis Vargas, Patrick Emami, and Patrick Traynor. On the detection of disinformation campaign activity with network analysis. In *Proceedings of the 2020 ACM SIGSAC Conference on Cloud Computing Security Workshop*, pages 133–146, 2020.
- [166] Ashish Vaswani, Noam Shazeer, Niki Parmar, Jakob Uszkoreit, Llion Jones, Aidan N Gomez, Łukasz Kaiser, and Illia Polosukhin. Attention is all you need. In *Advances in neural information processing systems*, pages 5998–6008, 2017.
- [167] Vivian L Vignoles, Claudia Manzi, Camillo Regalia, Simone Jemmolo, and Eugenia Scabini. Identity motives underlying desired and feared possible future selves. *Journal of personality*, 76(5):1165–1200, 2008.
- [168] Ulrike Von Luxburg, Agnes Radl, and Matthias Hein. Hitting and commute times in large random neighborhood graphs. *The Journal of Machine Learning Research*, 15(1): 1751–1798, 2014.
- [169] Chang Wang and Sridhar Mahadevan. Manifold alignment using procrustes analysis. In *International Conference on Machine Learning (ICML)*, pages 1120–1127, 2008.
- [170] Hanzhi Wang, Mingguo He, Zhewei Wei, Sibao Wang, Ye Yuan, Xiaoyong Du, and Ji-Rong Wen. Approximate graph propagation. In *Proceedings of the 27th ACM SIGKDD Conference on Knowledge Discovery & Data Mining*, pages 1686–1696, 2021.

- [171] Hanzhi Wang, Zhewei Wei, Junhao Gan, Ye Yuan, Xiaoyong Du, and Ji-Rong Wen. Edge-based local push for personalized pagerank. *arXiv preprint arXiv:2203.07937*, 2022.
- [172] Sibó Wang, Renchi Yang, Xiaokui Xiao, Zhewei Wei, and Yin Yang. Fora: simple and effective approximate single-source personalized pagerank. In *KDD*, pages 505–514, 2017.
- [173] Teng Wang, Chunsheng Fang, Derek Lin, and S Felix Wu. Localizing temporal anomalies in large evolving graphs. In *IEEE International Conference on Data Mining (ICDM)*, pages 927–935. SIAM, 2015.
- [174] Yuheng Wang, Giorgian Borca-Tasciuc, Nikhil Goel, Paul Fodor, and Michael Kifer. Knowledge authoring with factual english. *arXiv preprint arXiv:2208.03094*, 2022.
- [175] Yuheng Wang, Paul Fodor, and Michael Kifer. Knowledge authoring for rules and actions. *Theory and Practice of Logic Programming*, 23(4):797–811, 2023.
- [176] Zhewei Wei, Xiaodong He, Xiaokui Xiao, Sibó Wang, Shuo Shang, and Ji-Rong Wen. Topppr: top-k personalized pagerank queries with precision guarantees on large graphs. In *CIKM*, pages 441–456, 2018.
- [177] Kilian Weinberger, Anirban Dasgupta, John Langford, Alex Smola, and Josh Attenberg. Feature hashing for large scale multitask learning. In *Proceedings of the 26th annual international conference on machine learning*, pages 1113–1120, 2009.
- [178] Qianlong Wen, Zhongyu Ouyang, Jianfei Zhang, Yiyue Qian, Yanfang Ye, and Chuxu Zhang. Disentangled dynamic heterogeneous graph learning for opioid overdose prediction. In *Proceedings of the 28th ACM SIGKDD Conference on Knowledge Discovery and Data Mining*, pages 2009–2019, 2022.
- [179] Stefan Wojcik and Adam Hughes. Sizing up twitter users. *PEW research center*, 24, 2019.
- [180] Zach Wood-Doughty, Paiheng Xu, Xiao Liu, and Mark Dredze. Using noisy self-reports to predict twitter user demographics. *arXiv preprint arXiv:2005.00635*, 2020.
- [181] Felix Wu, Amauri Souza, Tianyi Zhang, Christopher Fifty, Tao Yu, and Kilian Weinberger. Simplifying graph convolutional networks. In *International conference on machine learning*, pages 6861–6871. PMLR, 2019.
- [182] Hao Wu, Junhao Gan, Zhewei Wei, and Rui Zhang. Unifying the global and local approaches: An efficient power iteration with forward push. In *Proceedings of the 2021 International Conference on Management of Data*, pages 1996–2008, 2021.
- [183] Da Xu, Chuanwei Ruan, Evren Korpeoglu, Sushant Kumar, and Kannan Achan. Inductive representation learning on temporal graphs. *arXiv preprint arXiv:2002.07962*, 2020.
- [184] Diyi Yang, Aaron Halfaker, Robert Kraut, and Eduard Hovy. Identifying semantic edit intentions from revisions in wikipedia. In *Proceedings of the 2017 Conference on Empirical Methods in Natural Language Processing*, pages 2000–2010, 2017.

- [185] Junting Ye and Steven Skiena. The secret lives of names? name embeddings from social media. In *Proceedings of the 25th ACM SIGKDD International Conference on Knowledge Discovery & Data Mining*, pages 3000–3008, 2019.
- [186] Junting Ye, Shuchu Han, Yifan Hu, Baris Coskun, Meizhu Liu, Hong Qin, and Steven Skiena. Nationality classification using name embeddings. In *Proceedings of the 2017 ACM on Conference on Information and Knowledge Management*, pages 1897–1906, 2017.
- [187] Pengcheng Yin, Graham Neubig, Miltiadis Allamanis, Marc Brockschmidt, and Alexander L Gaunt. Learning to represent edits. *arXiv preprint arXiv:1810.13337*, 2018.
- [188] Rex Ying, Ruining He, Kaifeng Chen, Pong Eksombatchai, William L Hamilton, and Jure Leskovec. Graph convolutional neural networks for web-scale recommender systems. In *Proceedings of the 24th ACM SIGKDD International Conference on Knowledge Discovery & Data Mining*, pages 974–983, 2018.
- [189] Minji Yoon, Woojeong Jin, and U Kang. Fast and accurate random walk with restart on dynamic graphs with guarantees. In *WWW*, pages 409–418, 2018.
- [190] Minji Yoon, Bryan Hooi, Kijung Shin, and Christos Faloutsos. Fast and accurate anomaly detection in dynamic graphs with a two-pronged approach. In *Proceedings of the 25th ACM SIGKDD Conference on Knowledge Discovery & Data Mining*, pages 647–657, 2019.
- [191] Wenchao Yu, Wei Cheng, Charu C Aggarwal, Kai Zhang, Haifeng Chen, and Wei Wang. Netwalk: A flexible deep embedding approach for anomaly detection in dynamic networks. In *Proceedings of the 24th ACM SIGKDD Conference on Knowledge Discovery & Data Mining*, pages 2672–2681, 2018.
- [192] Chengxi Zang and Fei Wang. Neural dynamics on complex networks. In *Proceedings of the 26th ACM SIGKDD International Conference on Knowledge Discovery & Data Mining*, pages 892–902, 2020.
- [193] Chi Zhang, Wenkai Xiang, Xingzhi Guo, Baojian Zhou, and Deqing Yang. Subanom: Efficient subgraph anomaly detection framework over dynamic graphs. In *2023 IEEE International Conference on Data Mining Workshops (ICDMW)*, pages 1178–1185. IEEE, 2023.
- [194] Hongyang Zhang, Peter Lofgren, and Ashish Goel. Approximate personalized pagerank on dynamic graphs. In *Proceedings of the 22nd ACM SIGKDD Conference on Knowledge Discovery & Data Mining*, pages 1315–1324, 2016.
- [195] Hongyang Zhang, Peter Lofgren, and Ashish Goel. Approximate personalized pagerank on dynamic graphs. *arXiv preprint arXiv:1603.07796*, 2016.
- [196] Junqi Zhang, Yuheng Wang, Cheng Wang, and Mengchu Zhou. Symmetrical hierarchical stochastic searching on the line in informative and deceptive environments. *IEEE transactions on cybernetics*, 47(3):626–635, 2016.

- [197] Junqi Zhang, Yuheng Wang, Cheng Wang, and MengChu Zhou. Fast variable structure stochastic automaton for discovering and tracking spatiotemporal event patterns. *IEEE transactions on cybernetics*, 48(3):890–903, 2017.
- [198] JunQi Zhang, YuHeng Wang, and MengChu Zhou. Fast adaptive search on the line in dual environments. In *2017 13th IEEE Conference on Automation Science and Engineering (CASE)*, pages 1540–1545. IEEE, 2017.
- [199] Tianyi Zhang, Varsha Kishore, Felix Wu, Kilian Q Weinberger, and Yoav Artzi. Bertscore: Evaluating text generation with bert. *arXiv preprint arXiv:1904.09675*, 2019.
- [200] Ziwei Zhang, Peng Cui, Haoyang Li, Xiao Wang, and Wenwu Zhu. Billion-scale network embedding with iterative random projection. In *2018 IEEE International Conference on Data Mining (ICDM)*, pages 787–796. IEEE, 2018.
- [201] Ziwei Zhang, Peng Cui, Jian Pei, Xiao Wang, and Wenwu Zhu. Timers: Error-bounded svd restart on dynamic networks. In *Proceedings of the 32nd AAAI Conference on Artificial Intelligence*. AAAI, 2018.
- [202] Yanping Zheng, Hanzhi Wang, Zhewei Wei, Jiajun Liu, and Sibao Wang. Instant graph neural networks for dynamic graphs. In *Proceedings of the 28th ACM SIGKDD Conference on Knowledge Discovery and Data Mining*, pages 2605–2615, 2022.
- [203] Baojian Zhou, Feng Chen, and Yiming Ying. Dual averaging method for online graph-structured sparsity. In *Proceedings of the 25th ACM SIGKDD International Conference on Knowledge Discovery & Data Mining*, pages 436–446, 2019.
- [204] Baojian Zhou, Yifan Sun, Reza Babanezhad Harikandeh, Xingzhi Guo, Deqing Yang, and Yanghua Xiao. Iterative methods via locally evolving set process. *arXiv preprint arXiv:2410.15020*, 2024.
- [205] Lekui Zhou, Yang Yang, Xiang Ren, Fei Wu, and Yueting Zhuang. Dynamic network embedding by modeling triadic closure process. In *Proceedings of the AAAI Conference on Artificial Intelligence*, volume 32, 2018.
- [206] Xinyi Zhou, Reza Zafarani, Kai Shu, and Huan Liu. Fake news: Fundamental theories, detection strategies and challenges. In *Proceedings of the twelfth ACM international conference on web search and data mining*, pages 836–837, 2019.
- [207] Linhong Zhu, Dong Guo, Junming Yin, Greg Ver Steeg, and Aram Galstyan. Scalable temporal latent space inference for link prediction in dynamic social networks. *IEEE Transactions on Knowledge and Data Engineering*, 28(10):2765–2777, 2016.